Structural and Functional Studies of Phosphoenolpyruvate Carboxykinase

A Thesis Submitted to the
College of Graduate Studies and Research
in Partial Fulfillment of the Requirements
for the Degree of Doctor of Philosophy
in the Department of Biochemistry
University of Saskatchewan
Saskatoon

By
Julien Joseph Hubert Cotelesage

Permission to Use

In presenting this thesis in partial fulfillment of the requirements for a Postgraduate degree from the University of Saskatchewan, I agree that the Libraries of this university may make it freely available for inspection. I further agree that permission for copying of this thesis in any manner, in whole or in part, for scholarly purposes may be granted by the professor or professors who supervised my thesis work or, in their absence, by the Head of the Department or the Dean of the College in which my thesis work was done. It is understood that any copying or publication use of this thesis or parts thereof for financial gain shall not be allowed without my written permission. It is also understood that due recognition shall be given to me and the University of Saskatchewan in any scholarly use which may be made of any material in my thesis.

Requests for permission to copy or to make use of materials in the thesis in whole or in part should be addressed to:

Head of the Department of Biochemistry
University of Saskatchewan
107 Wiggins Road
Saskatoon, Saskatchewan
S7N 5E5 CANADA

Abstract

ATP-dependent phosphoenolpyruvate carboxykinase (E. C. 4.1.1.49; PCK) is an enzyme that catalyses the reversible conversion of oxaloacetate and ATP into phosphoenolpyruvate, ADP and CO_2. PCK is made up of about 500 to 600 amino acid residues and is divided into two roughly equal domains. Upon binding of substrates, the two domains of PCK move towards each other. PCK is well known for its role in gluconeogenesis but in some species, it can have an anaplerotic role. In other species, PCK is important for metabolic steps involved in fermentation.

Presented in this thesis are five solved crystal structures of the ATP-dependent form of PCK. Three of the PCK crystal structures determined were from *Escherichia coli*; one was a complex of ATP, Mg^{2+} and CO_2, the second structure was an ATP, Mg^{2+}, Mn^{2+}, CO_2 and oxaloacetate complex and, the third *E. coli* structure was a Lys213Ser mutant complexed with ATP, $Mg^{2+}$and Mn^{2+}. Two *Anaerobiospirillum succiniciproducens* PCK crystal structures were also solved; one was in the native form and the other was an ATP-Mg^{2+}-Mn^{2+}-oxalate complex.

In the *E. coli*-PCK-ATP-Mg^{2+}-CO_2 crystal complex structure, the observed location of CO_2 was in agreement with a previously determined *E. coli* PCK-CO_2 crystal structure, which incorporated CO_2 into the structure by a different technique. The findings from the *E. coli* PCK-ATP-Mg^{2+}-CO_2 crystal structure allowed the reaction mechanism presented in this work to be proposed.

The PCK-ATP-Mg^{2+}-Mn^{2+}-CO_2-oxaloacetate structure is the first structure where oxaloacetate is observed bound to PCK. Surprisingly, the observed location of oxaloacetate in this structure is 5 Angstroms away from its expected

position near Mn^{2+}. Oxaloacetate is weakly bound to a non-catalytic region of the enzyme. It is proposed that when the domains of PCK move towards each other upon binding nucleotide, oxaloacetate experiences steric crowding which results in it being 'pushed' towards the active site to react.

Previous kinetic studies on the *E. coli* PCK mutant Lys213Ser have determined that Mn^{2+} is unexpectedly inhibitory. A crystal structure of K213S-PCK-ATP-Mg^{2+}-Mn^{2+} demonstrates that Mn^{2+} is tetrahedrally coordinated in the active site, not octahedrally as occurred in other structures. By having Mn^{2+} in the tetrahedral coordination state, substrate binding in the active site of PCK is altered in a way that does not allow catalysis to occur.

The two crystal structures of *A. succiniciproducens* PCK were useful in quantifying the substrate-induced domain movement. A surface active site lid made up of residues 385 to 405 that had never been observed in any of the previous PCK crystal structures was observed in the *A. succiniciproducens* PCK-ATP-Mg^{2+}-Mn^{2+}-oxalate crystal structure. Mutational studies of this lid have shown it to be essential for the function of PCK; however, its exact function is not certain. It has been proposed that the lid has multiple functions. One is to sequester the substrates from bulk solvent. Another function may be to assist in domain closure. The third function may be to assist in the proper positioning of substrates in the active site.

Acknowledgements

My mother, Joy, you have been there since day one, whether it has been packing a lunch, financial help or just encouraging me when I needed it. Thanks Mom. My wife, Melanie, you have helped me with so much; I do not know even where to start. I cannot go one day without noticing your positive influence in my life. It means a lot to have you by my side. I love you with all my heart. My two sons, Severin and Dion who often give me the strength to keep me going on, some days the only thing that stopped me from giving up and hiding under a rock was you two guys. My father, Hubert, thank you for teaching me to believe in myself. My stepfather Peter, and stepmother, Anna, thanks for all your help, whether it was lending me a printer or cooking me supper, it all means a lot to me. My brothers Gabriel, Joel, Louis and Chris, you all have been there for me, often when I did not deserve it, thanks. All my lifelong friends and the ones I have met over the years, you are too many to mention but all have somehow played a part in many of my successes, I hope I have helped you all out as much. To all the people who did not like me and told me I would not amount to anything – thanks, spite can sometimes be a good thing. So many people in the academic world were instrumental for my academic success. There are lots people to thank from the University of Manitoba who gave me the academic foundation to grow upon. Both Greg Zeikus and Maris Laivenieks from Michigan State University have done a lot for me, a lot of my experimental work would not have been possible without their contributions. Here at the University of Saskatchewan, many people need to be thanked. Margaret and Deanna if it was not for your help, the bureaucracy of graduate school would have eaten me up a long time ago. People in the Delbaere lab: Lata, Yvonne, Sanjukta,

Kurt, Jenny, Dipi, Eduardo and all the others from over the years, you have all done many many nice things for me. Thanks. The members of my committee: Mary, Ramji, Dave, Hughes, Rob and Lambert, you have all been very kind to me. Your patience and understanding have made graduate school a great experience for me. Thanks for encouraging and not intimidating. Every one else in the Biochemistry Department has been wonderful to me, sorry I cannot list everyone, you know who you are, thanks. Sammy from the Saskatchewan Structural Sciences Centre, thanks for making research a fun and creative endeavor, I swear we will get that paper published one day! The work Hughes Goldie from Microbiology has done for me has been critical for much of my research. Thanks Hughes, you have taught me lots. I also thank you for the many discussions that we have had. On more than one occasion, you have saved me from so much stress by pointing me in the right direction. Of course, all the encouragement in the world could not have gotten me to this point if it was not for my supervisor Louis Delbaere. Louis, I thank you for the giving me the chance to start graduate school, I am eternally grateful. You have given me the opportunity of a lifetime, which has given me the skills and confidence to succeed at whatever life has in store for me in the future. You have always been patient, understanding and kind to me. You have also let me do my research with an open mind and try ideas that most people would think are crazy. It means a lot that my opinion carries weight with you. The thing I want to thank you the most for is letting me put my family first, because of this I have been able to watch my children grow up and play a big part in their lives, that means the most to me. I can't thank you enough.

Dedication

This thesis is dedicated to my mother in-law Christa and father in-law Bert Lesage who both left us way too early. They should be here to see this and other important family milestones. We all miss them dearly.

Table of Contents

Permission to Use i
Abstract ii
Acknowledgements iv
Dedication vi
Table of Contents vii
List of Tables x
List of Figures xi
List of Abbreviations xiii

Chapter 1. INTRODUCTION 1

1.1 Overview 1
1.2 Introduction to Phosphoenolpyruvate Carboxykinase (PCK) 1
1.2.1 PCK and Gluconeogenesis 10
1.2.1.1 Gluconeogenesis in *E. coli* 10
1.2.1.2 Gluconeogenesis in Eukaryotes 12
1.3 Anaplerotic Role of PCK and Production of Krebs Cycle Intermediates 15
1.4 *E. coli* PCK 18
1.4.1 Structural Studies of *E. coli* PCK 20
1.4.1.1 Native *E. coli* PCK 20
1.4.1.2 *E. coli* PCK-ATP-Mg^{2+}-oxalate 23
1.4.1.3 *E. coli* PCK-AlF_3-Mg^{2+} 27
1.4.1.4 Proposed Reaction Mechanism of the Forward Reaction 28
1.5 Roles of PCK in Other Species 31
1.5.1 Plants 31
1.5.2 *Trypanosoma cruzi* PCK 33
1.6 PCK from Succinate-Producing Microbes 34
1.6.1 Overview of *Actinobacillus succinogenes* 39
1.6.2 *A. succiniciproducens* PCK 40
1.7 Summary 41

Chapter 2. MATERIALS AND METHODS 42

2.1 *A. succiniciproducens* PCK-ATP-Oxalate-Mg^{2+}-Mn^{2+} Complex 42
2.1.1 Source and Cloning of Genes 42
2.1.2 Expression and Purification of Protein 42
2.1.3 Crystallization Conditions 43
2.1.4 Diffraction, Data Collection and Processing 44
2.1.5 Phase Determination, Model Building and Refinement 44

2.1.6 Structure Validation and Protein Data Bank Accession Number 46
2.2 Substrate-Free *A. succiniciproducens* PCK Structure 46
2.2.1 Source and Cloning of Genes 46
2.2.2 Expression and Purification of Protein 46
2.2.3 Crystallization Conditions 46
2.2.4 Diffraction, Data Collection and Processing 47
2.2.5 Phase Determination, Model Building and Refinement 47
2.2.6 Structure Validation and Protein Data Bank Accession Number 48
2.3 *E. coli* PCK-ATP-Mg^{2+}-CO_2 structure 48
2.3.1 Source of PCK Gene, Cloning, Expression and Purification of Protein 48
2.3.2 Crystallization Conditions 49
2.3.3 Diffraction, Data Collection and Processing 49
2.3.4 Phase Determination, Model Building and Refinement 49
2.3.5 Structure Validation and Protein Data Bank Accession Number 50
2.4 *E. coli* PCK-ATP- Mg^{2+}-Mn^{2+}-CO_2-Oxaloacetate Structure 50
2.4.1 Source of Genes, Cloning, Expression and Purification of Protein 50
2.4.2 Crystallization Conditions 50
2.4.3 Diffraction, Data Collection and Processing 51
2.4.4 Phase Determination, Model Building and Refinement 51
2.4.5 Structure Validation and Protein Data Bank Accession Number 52
2.5 *E. coli* PCK mutant Lys213Ser 52
2.5.1 Source of genes, cloning, expression and purification of protein 52
2.5.2 Crystallization conditions 52
2.5.3 Diffraction, data collection and processing 53
2.5.4 Phase determination, model building and refinement 53
2.5.5 Structure validation and Protein Data Bank accession number 54
2.6 Production of *A. succiniciproducens* PCK Lid Deletion Mutant with Shortened, Δ2x2 54
2.7 Production of *A. succiniciproducens* PCK Mutant Arg65Ala and Kinetic Assay 55

Chapter 3. RESULTS 56

3.1 *A. succiniciproducens* PCK-ATP-oxalate-Mg^{2+}-Mn^{2+} Structure 56
3.1.1 Substrate Binding 58
3.1.2 Metal Binding 62
3.1.3 Domain Movement 63

3.1.4 Visualization of Previously Disordered Loop Region (383-395) 64
3.2 Native *A. succiniciproducens* PCK Structure 66
3.3 *E. coli*-ATP-Mg^{2+}-CO_2 structure 69
3.3.1 Binding of CO_2 71
3.3.2 Disordered Loop/Lid 73
3.4 *E. coli* –PCK- ATP- Mg^{2+}-Mn^{2+}-CO_2-OxaloacetateStructure 76
3.4.1 Oxaloacetate Binding 78
3.5 *E. coli* –K213S-PCK-ATP-Mg^{2+}-Mn^{2+} Structure 80
3.6 Kinetic Assay of *Anaerobiospirillum succiniciproducens* PCK Deletion Mutant Δ2x2 82
3.7 Kinetic Assay of the *Anaerobiospirillum succiniciproducens* PCK Mutant Arg65Ala 83

Chapter 4. DISCUSSION 84

4.1 Domain Movement of *A. succiniciproducens* PCK 84
4.2 *A. succiniciproducens* PCK-ATP-oxalate-Mg^{2+}-Mn^{2+} Structure 93
4.2.1 Active Site Lid 94
4.2.1.1 Truncation of the Active Site Lid 99
4.2.2 Potential Interactions Between the Active Site Lid and the C-Terminal Domain 102
4.3 *E. coli*-PCK-ATP-Mg^{2+}-CO_2 Structure 106
4.4 *E. coli* –PCK-ATP-oxaloacetate-CO_2-Mg^{2+}-Mn^{2+} 111
4.4.1 Location of Substrates 113
4.4.2 Conformation of Oxaloacetate 115
4.4.3 Role of Lid (residues 380-405) in Positioning Oxaloacetate 116
4.5 *E. coli* K213S PCK-ATP-Mg^{2+}-Mn^{2+} Structure 119
4.6 Survey of Ordered Water Molecules 126
4.6.1 Ordered Water Molecules in the Oxaloacetate Binding Site 132
4.7 Role of Helix Dipole (residues 209-227) in Carboxylation/Decarboxylation 133
4.8 Mechanism for Oxaloacetate Formation 136
4.8.1 Comparison to Other Carboxylases 139

Chapter 5. CONCLUSIONS AND FUTURE WORK 142

5.1 Lid Made by Residues 385-405 142
5.2 CO_2 Binding to PCK 143
5.3 Oxaloacetate, Lid and Non-catalytic Second Binding Site 144
5.4 K213S PCK Mutant 145

REFERENCES 146

List of Tables

Table 1.1 Kinetic Parameters of Mutational Study on *E. coli* PCK 20

Table 3.1. Refinement Statistics for *A. succiniciproducens* PCK-ATP-Mg^{2+}-Mn^{2+}- oxalate 57

Table 3.2. Refinement Statistics for Native *A. succiniciproducens* PCK 68

Table 3.3. Refinement Statistics for *E. coli* PCK-ATP-Mg^{2+}-CO_2 70

Table 3.4. Refinement Statistics for *E. coli* PCK-ATP-Mg^{2+}-Mn^{2+}-CO_2-oxaloaceatate 77

Table 3.5. Data collection and refinement statistics for PCK mutant K213S 81

Table 3.6. Kinetic Parameters for the Bicarbonate Ion in the Mutational Study on *A. succiniciproducens* PCK. 83

List of Figures

Figure 1.1. Synthesis of OAA in the coupled reverse assay from CO_2 and HCO_3^- by PCK 9
Figure 1.2. Some key metabolic steps involved in gluconeogenesis and glycolysis in E. coli grown under different carbon sources 11
Figure 1.3. Two metabolic pathways in a typical mammal cell that are associated with gluconeogenesis 13
Figure 1.4. Comparison of PCK-nucleotide binding fold to Classical nucleotide binding fold 21
Figure 1.5. The cracking and dissolving of native *E. coli* PCK crystals upon the addition of a 2 µl of a 10 mM ATP - 5 mM Mg^{2+} solution 24
Figure 1.6. Proposed reaction mechanism for PEP production 30
Figure 1.7. One of the pathways used by some types of C_4 plants to concentrate CO_2 in the bundle-sheath cells 32
Figure 1.8. Industrial and metabolic steps involved in ethanol production 35
Figure 1.9. Proposed metabolic pathway from succinate production in A. succinogenes, A. succiniciproducens and E. coli 37
Figure 3.1. Residues Pro476, Tyr477 and Phe478 in the γ-turn motif 58
Figure 3.2. Interactions between ATP with the active site residues of ATP 60
Figure 3.3. Stereo view of the hydrogen bonding network made between the phosphate groups of ATP and the P-loop, residues 249-255, of PCK 61
Figure 3.4. Mg^{2+} binding in active site 62
Figure 3.5. The coordination of the Mn^{2+} 63
Figure 3.6. Domain movement PCK undergoes upon substrate binding 64
Figure 3.7. A α-carbon trace of *A. succiniciproducens* PCK showing the surface loop made by residues 383 to 395 folding over active site 65
Figure 3.8. Hydrogen bonds between the peptide backbone of Arg65, nitrogen from the backbone of Arg396 and the carbonyl oxygen of Thr394 66
Figure 3.9. Difference electron density map ($|F_o|$-$|F_c|$) contoured at 4σ with a molecule of CO_2 modeled into the electron density. 72
Figure 3.10. The active site of the CO_2-containing crystal structure. 73
Figure 3.11. Crystal structure of *E. coli* PCK-ATP-Mg^{2+}-CO_2. 74
Figure 3.12. Interactions between the lid made by residues 385-405, with a symmetry related molecule 75
Figure 3.13. Oxaloacetate superimposed onto $|F_o|-|F_c|$ omit density map (contoured at 3.0σ) made from E. coli PCK-ATP-Mg^{2+}-Mn^{2+}-oxaloacetate data 79

Figure 3.14. The tetrahedral coordination of Mn^{2+} in the *E. coli* K213S-PCK-ATP-Mg^{2+}-Mn^{2+} structure 82
Figure 4.1. Ribbon diagram of *A. succiniciproducens* PCK illustrating the regions calculated by DynDom to be involved in domain movement 85
Figure 4.2. A. Interactions SO_4^{2-} makes with the P-loop of *Trypanosoma cruzi*. B. The interactions the β-phosphate group ATP makes with the P-loop in the A. succiniciproducens ATP-Mg^{2+}-Mn^{2+}-oxalate PCK complex 87
Figure 4.3. ATP induced movement of the P-loop in PCK 89
Figure 4.4. Stereo image of ATP-dependent *A. succiniciproducens* PCK (PDB accession number 1YTM), in red, aligned and superimposed with GTP-dependent chicken PCK (PDB accession number 2FAH), in blue. 92
Figure 4.5. Stereo image of aligned α-carbon trace of the lids from ATP-dependent *A. succiniciproducens* PCK (PDB accession number 1YTM), in red, and GTP-dependent chicken PCK (PDB accession number 2FAH), in blue. 98
Figure 4.6. Image of lid made by residues 385 to 405. Only the peptide backbone is shown for clarity. Residues deleted in the Δ2x2 mutant, Phe397 and Thr388 in red, Thr404 and Phe405 in green, are shown. 99
Figure 4.7. Native PAGE of *A. succiniciproducens* PCK 101
Figure 4.8. Lid made by residues 385-405 from *E. coli* PCK. The lid is pointing away from the N-terminal domain and adjacent to the C-terminal helix made up of residues 505 to 521. 103
Figure 4.9. The active sites of the PCK-ATP-Mg^{2+}- CO_2 crystal structure, PCK2 and PCK-ATP-Mg^{2+}-Mn^{2+}-CO_2 crystal structure, PCK1 superimposed 109
Figure 4.10. Torsion Bond Angles of Oxaloacetate Found in Protein Crystal 116
Figure 4.11. *E. coli* PCK-ATP-Mg^{2+}-Mn^{2+}-CO_2-oxaloacetate superimposed with *A. succiniciproducens* PCK-ATP-Mg^{2+}-Mn^{2+}-oxalate 117
Figure 4.12. Potential alternative binding sites for oxaloacetate in the K213S PCK mutant when Mn^{2+} is tetrahedrally coordinated. 125
Figure 4.13. . An example of three ordered water molecules that are conserved in *E. coli, T. cruzi* and *A. succiniciproducens* PCK. 127
Figure 4.14. An example of conserved ordered water molecules conserved in ATP-dependent PCK. 129
Figure 4.15. Stereogram of the PCK2 crystal structure from section 3.4 demonstrating the region around the α-helix made up by residues 209-227, shown in blue. 136
Figure 4.16. Proposed reaction mechanism for the conversion of PEP into oxaloacetate. 138

List of Abbreviations

ADP	Adenosine diphosphate
AMP	Adenosine monophosphate
ATP	Adenosine triphosphate
CAM	Crassulacean acid metabolism
CH2THF	10-methylene-5,6,7,8-tetrahydrofolate
DAOCS	Deacetoxycephalosporin C Synthase
dUMP	Deoxyuridine 5'-monophosphate
dTMP	Deoxythymidine 5'-monophosphate
E.C.	Enzyme commission number
EDTA	Ethylenediamine tetraacetate
GDP	Guanosine diphosphate
GTP	Guanosine triphosphate
IDP	Inosine diphosphate
ITP	Inosine triphosphate
NAD^+	Nicotinamide adenine dinucleotide (oxidized)
NADH	Nicotinamide adenine dinucleotide (reduced)
NSF	N-ethylmaleimide sensitive factor
NTS	Nitrilotriacetic acid
OAA	Oxaloacetate
PCK	Phosphoenolpyruvate carboxykinase
PCK-C	Cytoplasmic phosphoenolpyruvate carboxykinase
PCK-M	Mitochondrial phosphoenolpyruvate carboxykinase
PDB	Protein Data Bank
PEP	Phosphoenolpyruvate
PEPCK	Phosphoenolpyruvate carboxykinase
PFOR	Pyruvate:Ferredoxin Oxidoreductase
P_i	Inorganic phosphate(PO_4^{3-})
Rubisco	Ribulose-1,5-bisphosphate carboxylase
SAXS	Small angle X-ray scattering
TEMED	Tetramethylethylenediamine
Tris	2-amino-2-hydroxymethyl-1,3-propanediol
TS	Thymidylate synthase
UD	Uroporphyrinogen decarboxylase

Chapter 1. Introduction

1.1 Overview

The focus of the research presented in this thesis is to characterize the enzyme phosphoenolpyruvate carboxykinase (PCK, also abbreviated as PEPCK) from *Escherichia coli* and *Anaerobiospirillum succiniciproducens* by X-ray crystallography. In total, five crystal complexes of PCK have been solved. Three of the structures solved were from *E. coli*; one was an ATP, Mg^{2+} and CO_2 complex; the second structure was an ATP, Mg^{2+}, Mn^{2+}, CO_2 and oxaloacetate complex and the third *E. coli* structure was a Lys213Ser mutant complexed with ATP, $Mg^{2+}$and Mn^{2+}. Two *A. succiniciproducens* PCK structures were also determined, one was in the native (substrate and cofactor free) form and the other was an ATP-Mg^{2+}-Mn^{2+}-oxalate complex. The findings from the five crystal structures presented here offer valuable insight into the reaction mechanism of PCK. Some of the findings presented here also suggest an unusual mechanical component in its reaction mechanism.

1.2 Introduction to Phosphoenolpyruvate Carboxykinase (PCK)

Phosphoenolpyruvate carboxykinase (PCK) is found in essentially all species. PCK can vary significantly in amino acid sequence but even so, all forms catalyze the reversible conversion of oxaloacetate (OAA) into phosphoenolpyruvate (PEP) and carbon dioxide [1]. This reaction employs a phosphate from a nucleotide

triphosphate (usually ATP or GTP/ITP) and has a strict divalent metal ion requirement. The ATP-utilizing form is given the E.C. number 4.1.1.49 and the GTP/ITP-utilizing form is E.C. 4.1.1.32 (Utter and Kolenbrander 1972).

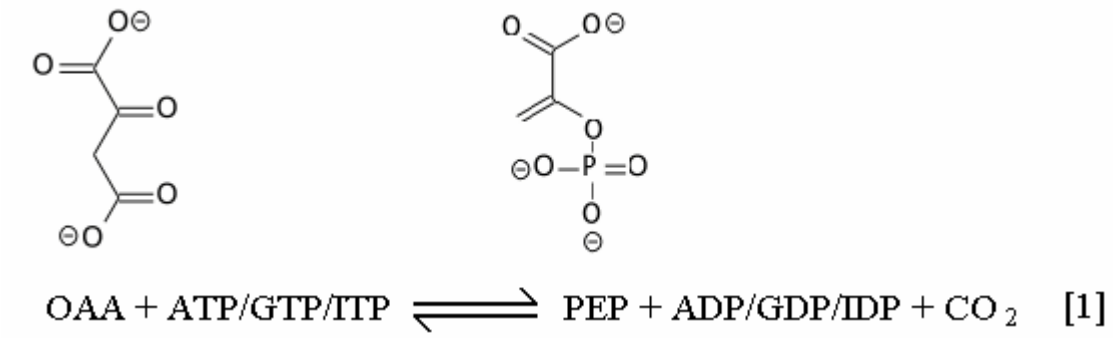

$$\text{OAA} + \text{ATP/GTP/ITP} \rightleftharpoons \text{PEP} + \text{ADP/GDP/IDP} + CO_2 \quad [1]$$

This thesis uses the convention that defines the reaction PCK catalyzes to produce PEP, ADP and CO_2 as the forward reaction. Conversely, the direction of reaction that produces OAA and ATP is defined as the reverse reaction. Another convention used in this thesis concerns the system of numbering of the amino acid positions in PCK. The numbering used to denote amino acid positions in PCK are based on the *Escherichia coli* amino acid sequence regardless of the species being discussed.

ATP-dependent PCK is mainly found in plants, bacteria and fungi. The GTP-dependent form is found in animals and archaebacteria (Tari *et al.* 1997; Utter and Kolenbrander 1972). There are exceptions though, for example, PCK from the bacterium *Corynebacterium glutamicum* has GTP-specific activity (Aich *et al.* 2003). In all species, PCK has a very strict conservation of active site residues, suggesting that the reaction mechanism for PCK is universal. Except for the active

site residues, the amino acid sequence of PCK can vary considerably between species (Aich *et al.* 2007; Dunten *et al.* 2002).

PCK was first discovered in chicken liver (Utter and Kurahashi 1953). It was initially thought that PCK was the enzyme responsible for carbon fixation in animals. After PCK was characterized kinetically, it was determined that it has a relatively high K_m for bicarbonate/CO_2. The K_m for bicarbonate was found to be two to four times higher than physiological cellular concentration of bicarbonate (5 to 8 mM) suggesting that PCK was not suitable for carbon fixation. Using the findings from kinetic studies it was initially concluded that *in vivo*, PCK effectively decarboxylates oxaloacetate irreversibly. Ten years later pyruvate carboxylase (E.C. 4.1.1.31) was discovered [2].

$$\text{pyruvate} + HCO_3^- + \text{ATP} \rightleftharpoons \text{OAA} + \text{ADP} + P_i + H^+ \qquad [2]$$

Further research determined that pyruvate carboxylase was a more suitable enzyme for carbon fixation since its K_m for bicarbonate is found to be in the range of 1 mM (Utter and Kolenbrander 1972). At around the same time that pyruvate carboxylase was discovered, it was reasoned that the main function of PCK was for gluconeogenesis. It has been demonstrated that, in tissues known to be involved in gluconeogenesis, the cellular concentration of PCK is higher. It was also found that

when gluconeogenesis-inducing substances such as alloxan or mannoheptulose were added to rat liver cells, levels of PCK increased (Utter and Kolenbrander 1972). Genetic studies have demonstrated that some types of PCK-deficient strains of bacteria cannot grow on minimal media consisting of substrates that would require the cell to rely on gluconeogenesis for sugar production (Utter and Kolenbrander 1972). Later studies found that when PCK from some species are assayed under physiological conditions, the reaction PCK catalyzes is close to equilibrium and therefore readily reversible (Rohrer *et al.* 1986; Trapani *et al.* 2001; Wiese *et al.* 1991).

There has been considerable scientific interest in PCK over the last fifty years; during this time PCK from a wide array of species has been studied by a wide range of fields in the biological sciences (Novakovski 2001; Utter and Kolenbrander 1972). The metabolic roles and genetic regulation of PCK have been investigated (Goldie 1984; Hansen and Patel 1994; Rohrer *et al.* 1986; Samuelov *et al.* 1991). Structural studies of PCK have contributed a significant amount of insight into the function and the mechanism of enzymatic catalysis. Chemical modification studies have been able to determine certain active site residues (Cheng and Nowak 1989), and fluorescent studies have been able to quantify that domain movement in PCK is occurring during catalysis (Encinas *et al.* 1993). By solving the structures of a number of PCK crystal complexes it was possible to propose a reaction mechanism for PCK (Matte *et al.* 1996; Sudom *et al.* 2001; Tari *et al.* 1996).

PCK from at least eighty species have been studied (Hansen and Patel 1994; Utter and Kolenbrander 1972). Since PCK is found in essentially all species,

it has been very useful for examining the evolutionary relationships between species (Aich *et al.* 2007; Friedlander *et al.* 1996). There is also interest within the succinate manufacturing industry to understand how PCK functions. PCK is believed to catalyze the rate limiting step of bacterial succinate production; by genetically altering PCK it may make it possible to increase the efficiency of succinate production (Zeikus *et al.* 1999).

When the amino acid sequences of PCK from a number of species are aligned, the sequences can vary considerably, especially between the ATP- and GTP-dependent forms (Aich *et al.* 2007). Despite the differences, there are motifs that both ATP- and GTP-dependent forms of PCK have that are strictly conserved. In the following sequences described, X represents any hydrophobic residue. There are two conserved regions that are found to be specific only to PCK, the first region consists of, 207-Y X G X X K K–213; this region is likely involved in the binding of PEP and oxaloacetate (Tari *et al.* 1996). The second PCK-specific sequence, 280-N X E X G X X X X-288, is indirectly involved in positioning some of the residues involved in metal binding (Leduc *et al.* 2005). There are two other motifs found in PCK that are encountered in other proteins. The first is the P-loop, also known as the *kinase-1a* or the Walker A motif, is made up of residues 250-S X X G K T-255. This region is where Mg^{2+} and the phosphate groups of ATP bind. The second motif is *kinase-2* or Walker B motif, 265-X X X D D-269, is involved in metal ion binding and substrate positioning (Tari *et al.* 1996; Traut 1994). The amino acid sequences responsible for nucleotide specificity are obviously different between ATP- and GTP-dependent PCKs; however, within these two groups of

PCK, amino acids not involved in catalysis can be highly conserved between species (Aich *et al.* 2007; Leduc *et al.* 2005).

In some C_4 and most Crassulacean Acid Metabolism (CAM) plant species there are additional conserved residues in the N-terminal region of PCK. The conserved sequence is made up of Q-K-K-R-S-T, which is a motif consistent with being a phosphorylation site. PCK with this motif is phosphorylated when the plant cells are under dark conditions (Walker and Leegood 1996). For example PCK from *Panicum maximum*, a C_4 plant, contains the abovementioned conserved N-terminal phosphorylation sequence. Research has found that when *P. maximum* PCK is phosphorylated, its activity is significantly reduced (Walker *et al.* 2002).

There are other species-specific amino acid sequences with additional functions that are observed in PCK. In *Trypanosoma brucei* there is a targeting sequence on the C-terminal end of the PCK that is responsible for the translocation of itself to the glycosomes (Sommer *et al.* 1994). The glycosome is an organelle that is analogous to the peroxisome. The function of the peroxisome is to segregate some of the toxic intermediates produced during the β-oxidation of fatty acids from the cell cytoplasm. Glycosomes instead contain the enzymes responsible for glycolysis. *T. brucei* uses glycolysis to derive most of its food energy, and because of this metabolic restriction, a large amount of glycolytic enzymes must be present. The high concentration of glycolytic metabolites can be toxic to the organism, so in a fashion similar to peroxisomes, glycosomes are used to prevent damage by keeping glycolytic enzymes sequestered from the rest of the cell (Guerra-Giraldez *et al.* 2002). Along with PCK there are at least three other enzymes found in the glycosome of *T. brucei* that have a known tripeptide targeting signal found on their

C-terminal ends. A mutational study examining the effects of deletions in the C-terminal region of PCK have on its translocation to the glycosome was performed. It was found that when the last 29 residues are removed, the amount of PCK delivered to the glycosome was reduced by 50%. When the last 47 residues are removed, no PCK was transported to the glycosomes (Sommer *et al.* 1994).

PCK from *T. cruzi* and *T. brucei* are homodimeric. In both species, there are two conserved sequences involved in dimer formation. Residues 10 to 32 and 280-293 make the interactions that bridge the two PCK molecules of the dimer. The interactions made between the molecules in the dimer consist of a number of hydrophobic contacts and one hydrogen bond (Trapani *et al.* 2001).

CO_2 and not bicarbonate is utilized by PCK during the carboxylation reaction. Evidence for CO_2 being the active species was found by assaying PCK from the photosynthetic bacterium *Rhodospirillum rubrum*, in the forward direction (Cooper *et al.* 1968). The assay was performed with and without carbonic anhydrase present in the assay conditions; during the assay the pressure of the reaction vessel was monitored with a manometer. When the reaction was assayed without carbonic anhydrase present, the pressure of the vessel increased. However, when the assay was performed in the presence of carbonic anhydrase [3], no pressure increase in the experimental setup was observed, implying that CO_2 is produced during the reaction. It is reasoned that when carbonic anhydrase is present in the assay conditions, CO_2 is converted to carbonic acid/bicarbonate, thus staying in solution (Cooper *et al.* 1968).

$$H^+ + HCO_3^- \rightleftharpoons CO_2 + H_2O \qquad [3]$$

Another kinetic study of PCK has also been able to demonstrate that CO_2 and not the bicarbonate ion is used by PCK (Cotelesage *et al.* 2007). The study assayed the reverse reaction of *E. coli* PCK. A series of assays were performed with varying starting carbon sources. One assay used CO_2, which is formed by combining equimolar amounts of HCl and sodium bicarbonate in the reaction mixture. Another assay used bicarbonate. For each of the abovementioned type of carbon source used, two more assays were performed by adding carbonic anhydrase to the reaction conditions. In total four assays were performed. It was found that when PCK is assayed in the presence of bicarbonate with carbonic anhydrase, bicarbonate without carbonic anhydrase, or CO_2 with carbonic anhydrase, the production of oxaloacetate was slow, Figure 1.1. To explain the observed rates in these three experiments, the first two assays suggest oxaloacetate production must be limited to the slow non-catalytic production of CO_2, In the case when CO_2 is present with carbonic anhydrase, CO_2 is converted to bicarbonate before it can be used by PCK. When PCK activity with CO_2 is assayed in the absence of carbonic anhydrase, the rate of oxaloacetate formation is much higher. In this situation, the formation of oxaloacetate by PCK appears to be limited by the concentration of CO_2 (Cotelesage *et al.* 2007).

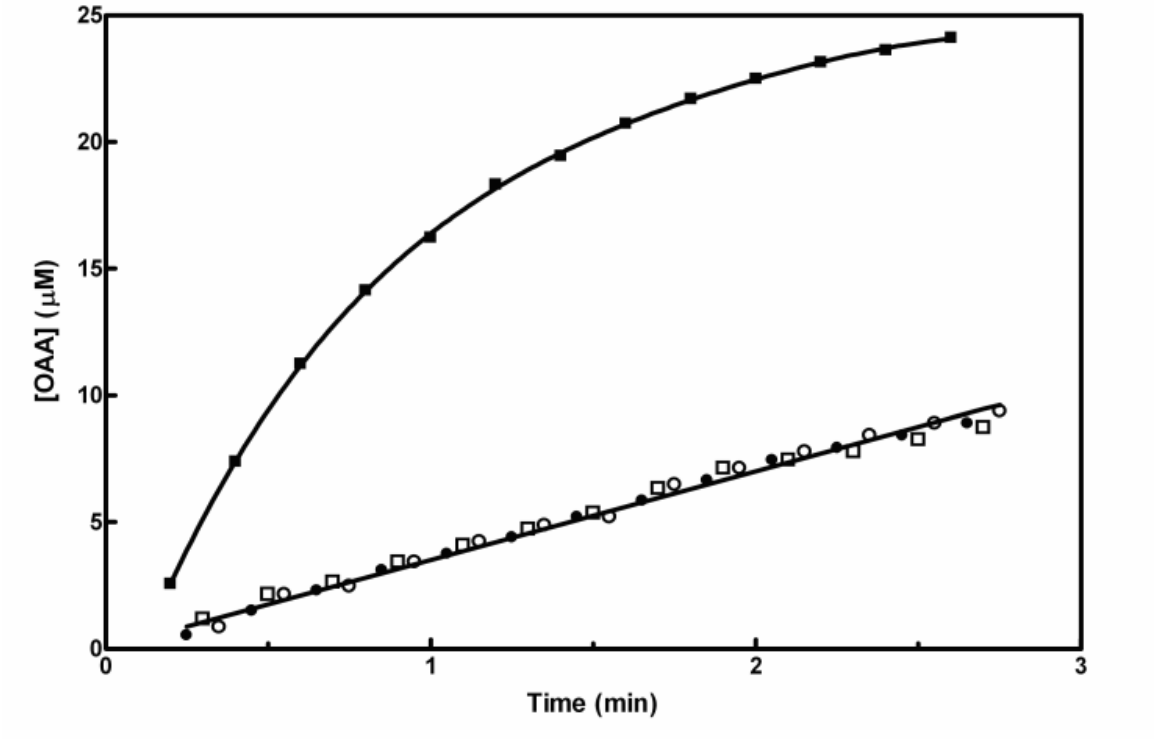

Figure 1.1 Synthesis of OAA in the coupled reverse assay from CO_2 (□ and ■) and from HCO_3^- (○ and ●) by PCK (5 μg/mL). Closed symbols represent the absence, and open symbols the presence, of carbonic anhydrase (20 μg/mL). Curves were fitted using linear or non-linear regression methods.

Other studies indicate PCK contains a binding site specific for CO_2, which is unusual because CO_2 binding sites in enzymes are not commonly observed (O'Leary 1992). Earlier studies have deduced a binding site for CO_2 in chicken liver PCK through chemical modification studies. By using the arginine-modifying chemicals phenylglyoxal, 2,3-butanedione, or 1,2-cyclohexanedione it was found that an active site arginine is protected from modification when CO_2 is present

(Cheng and Nowak 1989). Another study was also able to confirm that PCK contains a CO_2 binding site by determining the kinetic isotope effect of $^{14}CO_2$. The study concluded that the substrates, CO_2, ADP and PEP could bind PCK in any order. For the kinetic isotope effect to be observed for $^{14}CO_2$ when all the other substrates were varied means the reaction has a random kinetic mechanism. In order for an enzyme to have a random mechanism all the substrates involved must have a binding site, leading to the conclusion that CO_2 has a binding site on PCK (Arnelle and O'Leary 1992; O'Leary 1992).

1.2.1 PCK and Gluconeogenesis

1.2.1.1 Gluconeogenesis in *E. coli*

During glycolysis in *E. coli*, PEP is irreversibly dephosphorylated by pyruvate kinase to form pyruvate. Pyruvate can be directly converted to PEP by the enzyme PEP synthase [4] (Goldie and Sanwal 1980b).

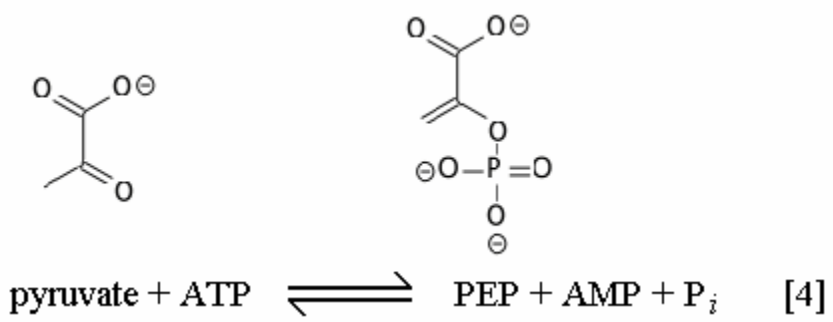

PCK is also a key gluconeogenic enzyme in *E. coli*. When *E. coli* is grown on succinate or oxaloacetate as the carbon source, PCK is responsible for the production of PEP (Liao *et al.* 1994).

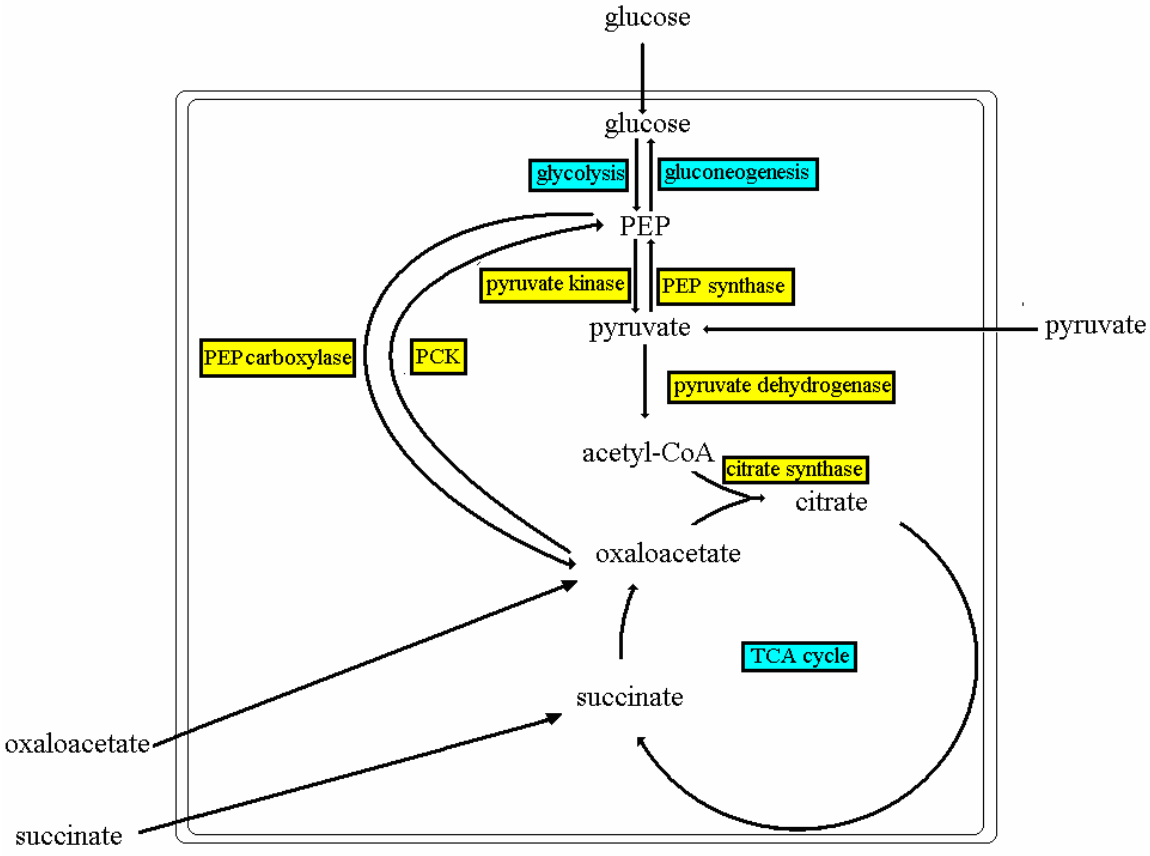

Figure 1.2. Some key metabolic steps involved in gluconeogenesis and glycolysis in *E. coli* grown under different carbon sources. Key enzymes are shown in yellow boxes.

1.2.1.2 Gluconeogenesis in Eukaryotes

In eukaryotic cells, two forms of PCK exist: the cytoplasmic form, PCK-C and the mitochondrial form, PCK-M. Both forms are used in gluconeogenesis but the two function under different metabolic situations. To synthesize glucose, the cell requires reducing power in the form of reduced nicotinamide adenine dinucleotide, NADH, in the cytoplasm in order to convert 1,3-bisphosphoglycerate into glyceraldehyde-3-phosphate via glyceraldehyde-3-phosphate dehydrogenase. Compared to mitochondria, the concentration of NADH is 10^5 times lower in the cytoplasm. Thus the oxidation state of the starting metabolite involved in gluconeogenesis will determine the metabolic strategy employed by the cell (Hansen and Patel 1994).

When pyruvate is the starting metabolite for gluconeogenesis, the strategy used in this metabolic situation requires the transfer of NADH from the mitochondria to the cytoplasm. Pyruvate is first imported into the mitochondria and converted to oxaloacetate by pyruvate carboxylase. Next, NADH reduces oxaloacetate to malate by mitochondrial malate dehydrogenase. Malate is transported out of the mitochondria and converted back to oxaloacetate and NADH by cytoplasmic malate dehydrogenase. Oxaloacetate can be converted to PEP by PCK-C and PEP can then continue along the gluconeogenic pathway, Figure 1.3 (Hansen and Patel 1994).

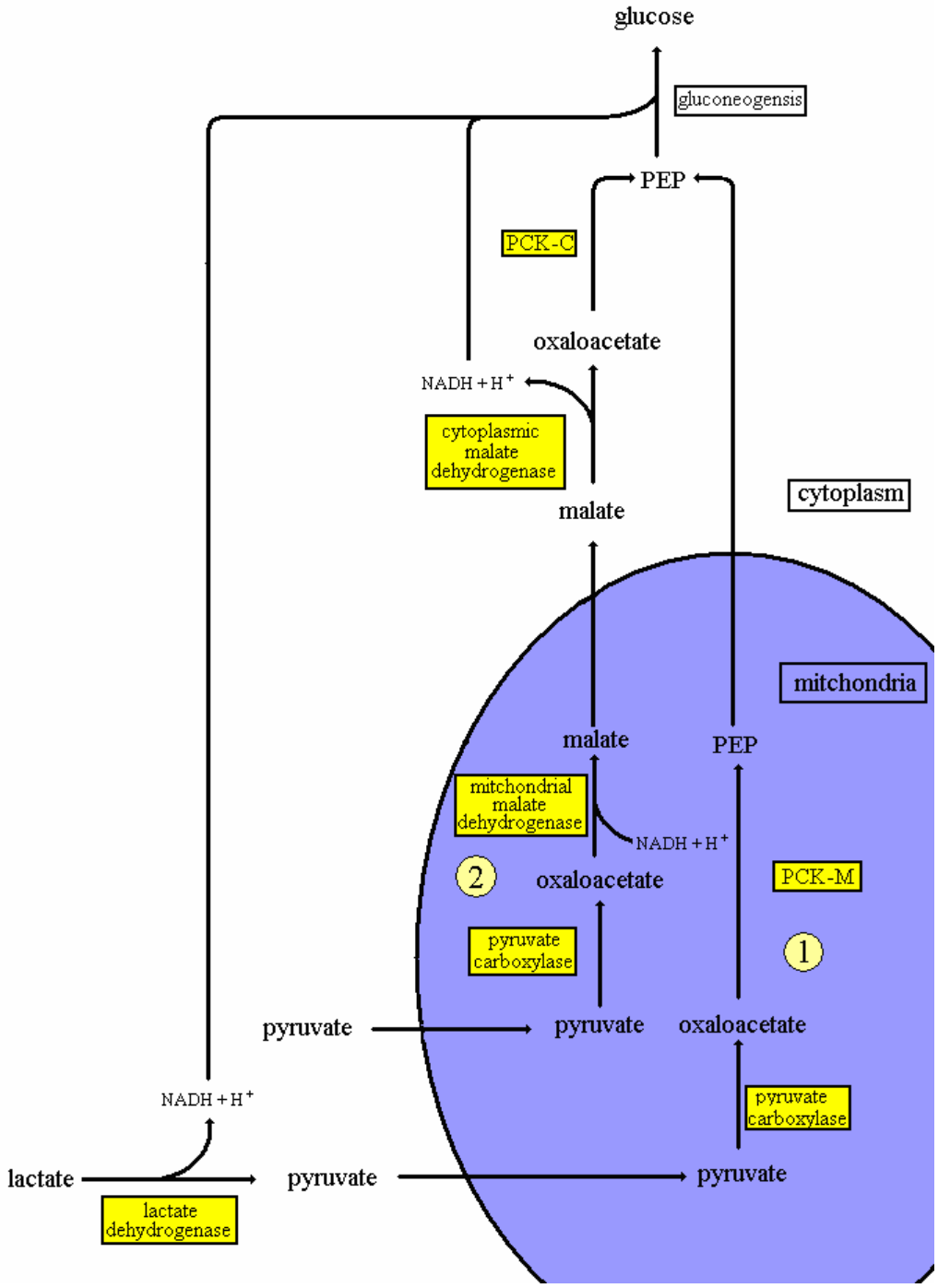

Figure 1.3. Two metabolic pathways in a typical mammal cell that are associated with gluconeogenesis. Enzymes are shown in yellow boxes. Pathway 1. Route taken if lactate is the starting metabolite of gluconeogenesis. Pathway 2. Direction taken when pyruvate is to be converted to glucose.

In the metabolic situation where the starting metabolite for gluconeogenesis is lactate, PCK-M is employed for gluconeogenesis. While still in the cytoplasm, lactate is oxidized to pyruvate by lactate dehydrogenase yielding NADH + H^+. Pyruvate is then imported into the mitochondria while NADH + H^+ remains in the cytoplasm. Once in the mitochondria, pyruvate is converted to oxaloacetate by pyruvate carboxylase. Oxaloacetate is then converted to PEP by PCK-M. Once synthesized, PEP is translocated from the mitochondria into the cytoplasm where gluconeogenesis can continue (Hansen and Patel 1994).

The PCK-C to PCK-M ratio can differ considerably between different tissue cell types, species and metabolic state. The ratios can often be indicative of what are the usual starting materials for glucose production for that cell. For example, in avian liver cells all the PCK present is in the mitochondrial form which can be explained because of the significant amounts of lactate produced during flight via the Cori cycle. About 90% of PCK found in rat liver is in the cytoplasmic form. The high PCK-C ratio is likely because many of the starting metabolites the rat uses for glucose production will be converted to pyruvate, and therefore reducing power in the form of NADH + H^+ must be imported into the cytoplasm. Pyruvate is converted to malate in the mitochondria and exported to the cytoplasm where gluconeogenesis can continue (Hansen and Patel 1994; Wiese *et al.* 1991).

PCK-M is constitutively expressed, although there is at least one known instance where it can be induced (Hansen and Patel 1994). During lactation in guinea pig mammary cells the activities of both PCK-M and PCK-C both increase by an order of magnitude. On the other hand, the activity of PCK-C is regulated throughout all species. The mechanisms that regulate PCK-C can be controlled by

elaborate means. The factors that regulating PCK-C depend on the species, tissue, changes in diet plus a number of other metabolic and hormonal factors. The rate at which the PCK-C gene is transcribed is often controlled. The promoter of the PCK-C gene is regulated by a wide range regulatory elements. There are at least a dozen regulatory proteins known to bind to the promoter. The rates of translation can also be controlled. Both cAMP and insulin levels affect transcription. The stability and translation of PCK-C mRNA also can be controlled to keep activity of PCK at the appropriate levels (Hansen and Patel 1994).

1.3 Anaplerotic Role of PCK and Production of Krebs Cycle Intermediates

In most situations, the primary function of PCK is for gluconeogenesis. However, it has been observed in some species such as *Ascaris suum*, and *T. cruzi* that PCK readily can function in both directions. Catalysis by PCK in the reverse direction serves as an anaplerotic function that replenishes Krebs cycle intermediates, which can be used for energy production or anabolic metabolism. By giving the organism a wider range of substrates it can metabolize, it has a greater chance to survive (Rohrer *et al.* 1986; Trapani *et al.* 2001). In species such as *Actinobacillus succinogenes, Anaerobiospirillum succiniciproducens* and *Manheimia succiniciproducens*, the primary function of PCK seems to be for production of Krebs cycle intermediates (Leduc *et al.* 2005; Lee *et al.* 2006; Podkovyrov and Zeikus 1993).

Many of the assumed metabolic roles of PCK are based on the results of kinetic assays that are not necessarily reflective of the biological conditions in

which it normally functions. Substrate and cofactor concentrations can be many magnitudes higher than biological conditions. Substrate analogues, activators and inhibitors that may be present *in vivo* are often missing in the assays, thus, the actual kinetic response that PCK will experience under true biological conditions may be different from what is observed under actual assay conditions. For example many of the kinetic assays and crystallographic studies performed on PCK used only Mn^{2+} at non-physiologically high concentrations (Chen *et al.* 2002; Holyoak *et al.* 2006; Jabalquinto *et al.* 2002a; Jabalquinto *et al.* 2002b; Rohrer *et al.* 1986).

The original assays of PCK from the C_4 plant *Panicum maximum* were performed under non-physiological conditions. The concentration of Mn^{2+} in the assays was in the millimolar range, but in the cells of *P. maximum* it is only in the low micromolar range (Urbina and Avilan 1989). The K_m for CO_2 was determined to be about 1.5 mM. This value was thought to be too high for the predicted carboxylation function of PCK in *P. maximum*, it was expected that the K_m PCK has for CO_2 should be closer to the K_m ribulose-1,5-bisphosphate carboxylase, rubisco, a CO_2-binding enzyme, in C_4 plants have for CO_2, 30 to 60 μM. More recently, assays of *P. maximum* PCK were performed under biological concentrations of Mg^{2+} and Mn^{2+} which are in the low millimolar and micromolar range, respectively (Chen *et al.* 2002). The assays determined that under physiological concentrations of Mg^{2+} and Mn^{2+}, the K_m for ATP increases up to twenty-fold, while a thirteen-fold decrease in K_m for CO_2 is observed. When PCK is assayed under cellular Mg^{2+}, Mn^{2+}, ATP and ADP concentrations, the K_m for CO_2 further decreases 50% to about 50 μM, concluding that when *P. maximum* PCK is assayed under appropriate

conditions, its kinetic parameters are in agreement the presumed metabolic function of PCK (Chen *et al.* 2002).

The original assays of PCK from *A. succiniciproducens* determined that the K_m for CO_2 is too high with respect to its preferred direction of catalysis (Podkovyrov and Zeikus 1993). The main function of *A. succiniciproducens* PCK is believed to be for oxaloacetate production, yet it has a K_m for CO_2 of about 30 mM, higher than what would be expected considering its preference for functioning in the reverse reaction. The main role of *Saccharomyces cerevisiae* PCK is thought to be for PEP production, therefore a higher K_m for CO_2 would encourage CO_2 to dissociate from the active site faster. A higher K_m for CO_2 decreases the likelihood CO_2 remains bound to PCK once formed, therefore the chance that CO_2 will be consumed in the reverse reaction is reduced. When *A. succiniciproducens* and *S. cerevisiae* PCK are assayed at physiological concentrations of metal ions, ATP and ADP, it is found that for both enzymes the K_m values for CO_2 are in ranges that are appropriate for their function. In the case of *A. succiniciproducens* PCK, the K_m for CO_2 is 8.4 mM when assayed with only 4 mM Mn^{2+} present. When the Mg^{2+} and Mn^{2+} concentrations are at physiological ratios, the K_m of CO_2 decreases about five-fold. When the [ATP]/[ADP] ratio is 4:1, the K_m for CO_2 can be further reduced by 50%, to 1.2 mM. When *A. succiniciproducens* PCK is assayed under the same conditions the K_m for CO_2 in *S. cerevisiae* PCK increases three-fold to 0.9 mM (Bazaes *et al.* 2007).

1.4 *E. coli* PCK

E. coli PCK is a monomeric soluble globular enzyme consisting of 540 amino acid residues (Matte *et al.* 1996). Some of the earlier kinetic studies of *E. coli* PCK were performed by Krebs and Bridger (Krebs and Bridger 1980). One distinguishing finding from the study worth noting is that the K_m for bicarbonate was up to twenty times higher than the K_m for the rest of the substrates, thus implying the main role of *E. coli* PCK is for gluconeogenesis. If TCA cycle intermediates are needed by the cell, the other anaplerotic enzymes, pyruvate carboxylase, malic enzyme and PEP carboxylase would be used to meet cellular demands instead (Liao *et al.* 1994). *E. coli* PCK has been intensely studied kinetically. A thorough site directed mutagenesis study investigating the forward reaction of *E. coli* PCK was performed. The importance of a number of presumed active site residues could be confirmed. Residues Arg65, Tyr207, Lys212, Lys213, His232, Lys254, Asp268 and Asp269 were all found to be interacting with substrates and cofactors of PCK, Table 1.1 (Novakovski 2001). The study also established that Cys233, which is located near the active site (Matte *et al.* 1997), does not have a catalytic role. There was interest in determining if there is a catalytic role for Cys233 in ATP-dependent PCK. In GTP-dependent PCK there is a reactive cysteine in the active site that has a role in catalysis (Holyoak *et al.* 2006).

The R65Q mutant demonstrates that Arg65 is very important for oxaloacetate binding, but not as important for catalysis. The K_m for oxaloacetate increases from 0.77 mM to 159 mM while k_{cat} drops from 26.5 to 14.8. Mn^{2+} does not appear to mediate the interaction between oxaloacetate and Arg65. When assays

are performed on R65Q without Mn^{2+}, the K_m for oxaloacetate is 156 mM; however, R65Q lowers the K_m for ATP from 0.26 mM to well under 0.01 mM (Novakovski 2001).

The K_m for oxaloacetate in K212S changes little with and without Mn^{2+} present. There is over a twenty-fold reduction in K_m for ATP while for Mn^{2+} the K_m increases over thirty-fold. The k_{cat} for K212S reduces to 0.67 min^{-1}. Similar results are observed with assays on K213S, except for an unexpected inhibition of activity when concentrations of Mn^{2+} are increased (Novakovski 2001).

In both H232Q and D269N, the K_m for Mn^{2+} increases over 7000- and 1000-fold respectively. Without Mn^{2+} present, the K_m for oxaloacetate increases 30- and 3.4-fold respectively for each mutant. The K_m for oxaloacetate in the presence of Mn^{2+} was determined for H232Q but could not be determined for D269N. It was questioned whether the value determined for H232Q in the presence of Mn^{2+} is relevant due to solubility issues with Mn^{2+} in the assays (Novakovski 2001).

The K254S mutation reduced k_{cat} seventeen-fold while the K_m for ATP increased seventy-two-fold. The K_ms for oxaloacetate with and without Mn^{2+} present are two and twelve-fold higher (Novakovski 2001).

With the exception of the activity of the K213S mutant enzyme being inhibited by Mn^{2+}, all the PCK mutants investigated behaved kinetically in a fashion that was predicted by previously determined crystal structures (Matte *et al.* 1997; Tari *et al.* 1997).

Table 1.1. Kinetic parameters of mutational study on *E. coli* PCK. Taken from Novakovski 2001.

Mutant	K_m				k_{cat} min $^{-1}$
	OAA (mM)		Mg^{2+} ATP	Mn^{2+}	
	with Mn^{2+}	without Mn^{2+}	mM	μM	
R65Q	159* ± 34	156*	<0.01	<0.01	14.8 ±2.0
K212S	1.24 ± 0.44	1.05 ±0.23	0.010±0.003	1.0 ±0.03	0.67 ±0.02
K213S	0.26 ±0.09	0.55 ±0.04	0.06 ±0.02	Inhibition	5.20 ±0.17
H232Q	23.7 ±5.9 [a]	66.2 ±0.9 [b]	0.08 ±0.01 [a]	222 ±16	1.84 ±0.06 [a]
C233S	1.31 ±0.33	0.32 ±0.04	0.20 ±0.05	0.09 ±0.02	18.9 ±1.8
K254S	1.78 ±0.39 [b]	6.72 ±1.65 [b]	18.0 ±2.0	0.09 ± 0.02 [b]	1.54 ±0.06 [b]
D269N	n.e.	122 ±15 [a]	0.42 ±0.02 [a]	32.1 ±3.7	1.69 ±0.08 [a]
Wild Type	0.77 ±0.17	0.51 ±0.10	0.26 ±0.07	0.03 ±0.01	26.5 ±1.2

* - extrapolated value
n.e - could not be evaluated (OAA inhibitory at high concentrations)
[a] - values determined at less than saturating concentrations of Mn^{2+}
[b] - values determined at less than saturating concentrations Mg^{2+} ATP
Errors are standard error

1.4.1 Structural Studies of *E. coli* PCK

1.4.1.1 Native *E. coli* PCK

The first crystal structure of PCK solved was of *E. coli* (Matte *et al.* 1996). The overall morphology of PCK can be described as two roughly equal-sized domains with a cleft between them. The tertiary structure of PCK is an open-faced protein with a mixed α/β topology. The manner that PCK was found to fold was unique. The fold shows some similarity to the classical nucleotide-binding fold, which consists of four parallel β-strands that are flanked by two α-helices above and below the β-sheet (Schulz *et al.* 1986). In contrast PCK is made up of six mixed β-strands that are flanked by two α-helices on each side of the β-sheet. Despite the

differences between the two motifs, the relative locations of the P-loop, *kinase 2* and adenine binding domain are the same, Figure 1.4 (Matte *et al.* 1996).

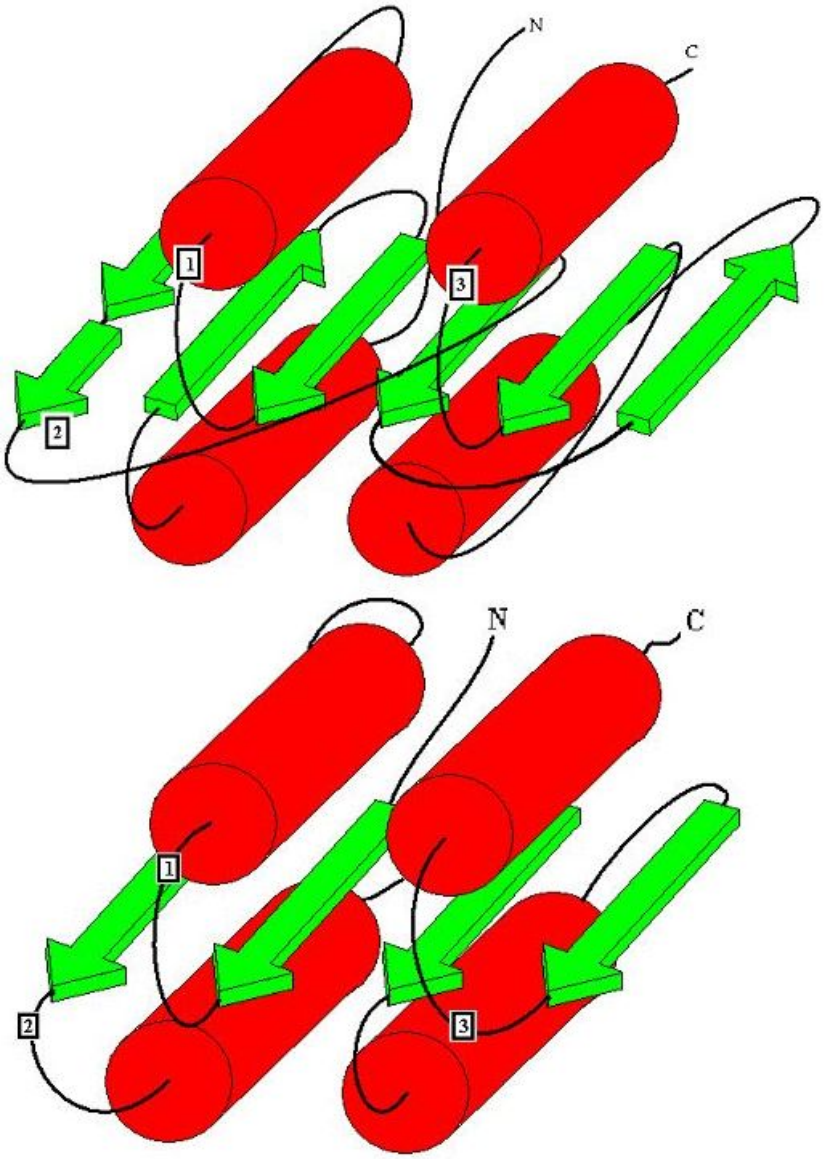

Figure 1.4. Comparison of PCK-nucleotide binding fold (top) to Classical nucleotide binding fold (below). **(1)** P-loop (*kinase 1a)* motif **(2)** *kinase 2* motif **(3)** adenine-binding region.

A study surveying almost 60,000 kinase sequences and 702 kinase crystal structures found that most kinases can be categorized in ten groups (Cheek *et al.* 2005). The ten groups can be further divided into twenty-five families. Twenty-two of the families represent 98.8 % of all the structures examined. The study classified PCK in the Rossmann-like fold group. The common structural feature of the Rossmann-like group is the layered α/β/α secondary structure, a motif consisting of a four to seven strand parallel β-sheet that has two α-helices above it and two α-helices below. Another distinguishing feature found in the Rossman-like fold group is that the polypeptide chain is made up of adjacent β-strands and α-helices repeated many times. All members of the Rossman-like fold group have their nucleotide-binding region near the C-terminal end of the central β-sheet. Also found in all members of this group is a positive charge from the N-terminal end of an α-helix dipole pointing at the phosphate groups of ATP (Cheek *et al.* 2005).

The Rossman-like fold group is further divided into eight families. PCK was assigned into the PEPCK family. The PEPCK family consists of the catabolite repression mediating protein HPr kinase/phosphatase, ATP- and GTP-dependent PCK (Cheek *et al.* 2005; Cheek *et al.* 2002). Some of the major differences between PCK and HPr kinase/phosphatase are the number of residues separating the P-loop and the *kinase-2* motifs; HPr kinase/phosphatase typically has about five more residues than PCK. Another difference between the two motifs concerns the two lysines found at positions 212 and 213 of ATP- and GTP-dependent PCK. In HPr kinase/phosphatase there are no equivalent residues interacting with Mn^{2+} (Galinier *et al.* 2002).

Within the Rossman-like fold group, the closest family related to the PEPCK family is the P-loop family. Like the PEPCK family, the P-loop family contains the P-loop and the *kinase-2* motifs. Also in common with PEPCK, the P-loop family has a divalent metal requirement for catalytic activity (Cheek *et al.* 2005; Cheek *et al.* 2002).

1.4.1.2 *E. coli* PCK-ATP-Mg^{2+}-oxalate

The first attempts to create a crystal of PCK complexed with substrates were done by soaking an ATP solution into a pre-made native crystal. It was found that immediately after the addition of ATP, the PCK crystal cracked and within thirty minutes it dissolved, Figure 1.5. The abrupt deterioration of the crystals was attributed to PCK undergoing a major substrate induced-conformation change (Matte 1996).

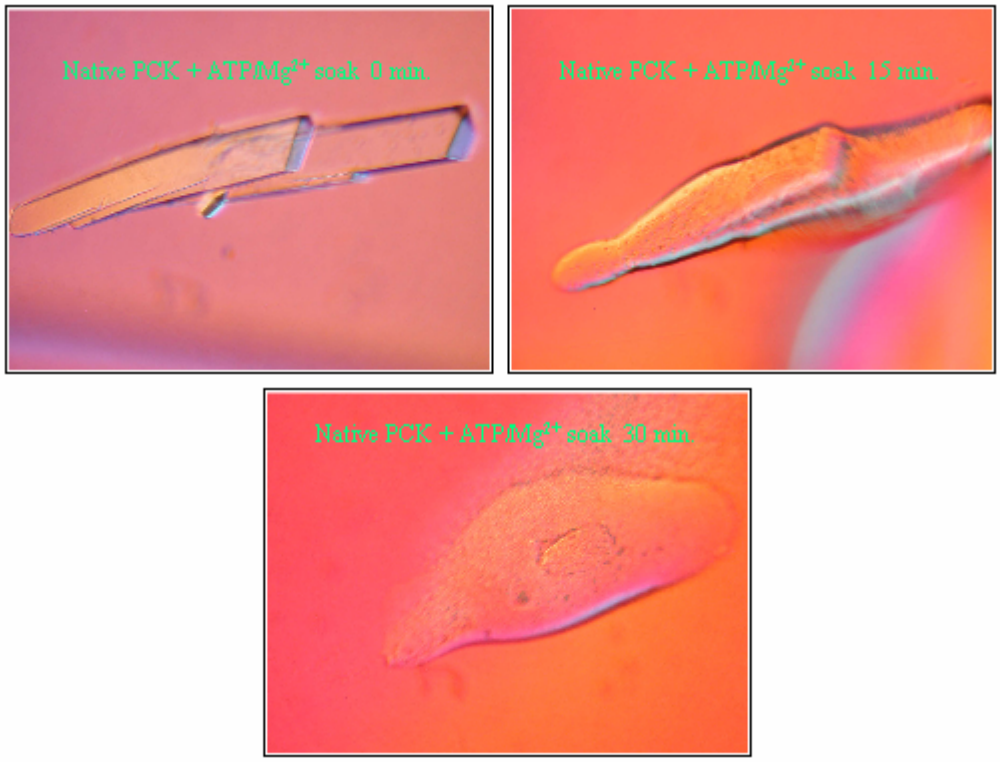

Figure 1.5. The cracking and dissolving of native *E. coli* PCK crystals upon the addition of a 2 µl of 10 mM ATP, 5 mM Mg^{2+} solution. The crystal was in a 10 µl drop of mother liquor. After the addition of the ATP/Mg^{2+} solution, cracking was instantly observed around the crystal and within minutes, the crystals began to lose its solid form and dissolve, after thirty minutes the crystal completely dissolved. Experiment performed by the author. Images taken by the author.

A number of *E. coli* PCK crystal structures complexed with various substrates, cofactors and analogues have been determined through co-crystallization (Delbaere *et al.* 2004; Sudom *et al.* 2003; Sudom *et al.* 2001; Tari *et al.* 1997). The first crystal structure of PCK complexed with substrates contained ATP, Mg^{2+}, and oxalate (Tari *et al.* 1996). The structure revealed that Mg^{2+} is coordinated in an octahedral fashion by a β- and a γ-oxygen atom of ATP, three water molecules and

a hydroxyl group from the side chain of Thr255. The role of Thr255 and Mg^{2+} is to draw electrons away from the phosphate groups of ATP, effectively reducing the negative charges on the phosphate groups. The reduction in negative charge lessens the repulsion the β- and γ-oxygen atoms of ATP have when in the eclipsed conformation. By remaining in the eclipsed conformation, the strain on the phosphate groups make ATP more reactive by making it energetically favourable to transfer its γ-phosphoryl group to oxaloacetate to form PEP.

A PCK- Mg^{2+}-Mn^{2+}-pyruvate-ATP crystal structure also demonstrated that Mn^{2+} is octahedrally coordinated; it is coordinated by the lone pair electrons from the ζ-nitrogen of Lys213, lone pair electrons from the ε-nitrogen of His232, one oxygen atom of the carboxyl group from the side chain Asp269, a γ-phosphoryl oxygen atom from ATP and two water molecules. Based on the location of the substrate analogue oxalate, the substrates PEP and oxaloacetate should also likely interact with Mn^{2+} (Tari *et al.* 1997).

When the native and complexed structures are compared by superimposing their atomic coordinates it was observed that when PCK binds substrates, the N-terminal and C-terminal domains move towards each other (Tari *et al.* 1996). The N-terminal domain was designated as the larger of the two domains at 272 residues and the C-terminal domain consists of 268 amino acid resides. The driving force of the domain movement is believed to be from two groups of interactions PCK makes with ATP. The first set of interactions involved in domain closure occurs between the phosphate groups of ATP and the P-loop, residues 249-255, of PCK. The second set is two hydrophobic interactions between the side chains of Ile452 and Arg449 and the adenine ring of ATP. It is thought that that

ATP first binds to PCK on the N-terminal domain forming the first set of interactions, the two domains then close towards each other to form the hydrophobic interactions with Ile452 and Arg449, which are part of the C-terminal domain (Tari *et al.* 1996). Evidence for this is seen in a native crystal structure of ATP-dependent PCK from *T. cruzi* (Trapani *et al.* 2001). PCK from *T. cruzi* is very similar in overall structure and amino acid sequence to *E. coli* PCK; between the two species there is a 42% sequence identity. Results from a small angle X-ray scattering, SAXS, experiment suggests that native *T. cruzi* PCK is in the open conformation similar to what is observed in the native *E. coli* PCK crystal structures. However, the crystal structure of *T. cruzi* PCK it is observed in the closed conformation. A sulfate ion was a located in the active site approximately where the β-phosphate of ATP/ADP would be found. The sulfate ion is interacting via hydrogen bonds and non-bonding contacts with residues from the P-loop on the C-terminal domain and indirectly with residues on the N-terminal domain. In light of the SAXS study it was concluded that the tri-phosphate group of ATP may also play a part in the domain movement of *T. cruzi* PCK (Trapani *et al.* 2001).

Another distinct feature of ATP-dependent PCK is that the χ-bond of ATP is in the high-energy *syn*-conformation. To compensate for the additional strain in ATP, the ribose sugar ring adopts the lower energy conformation of $C_{2'}$-endo. It is predicted that the bound *syn*-ATP is about 4 kJ/mol (1 kcal/mol) higher in energy than bound ATP in the *anti* conformation (Zhou *et al.* 2000). Despite being higher in energy, *syn*-ATP makes more optimal contacts with PCK than the *anti* conformation would (Tari *et al.* 1996). ATP in the *syn*-conformation is rarely observed in protein crystal structures. N-ethylmaleimide sensitive factor (NSF) is a

hexameric protein that is indirectly involved in membrane fusion events. ATP is in part bound to NSF through a P-loop motif. The χ angle of ATP puts the adenine ring in the *syn* conformation. To relieve some of the strain the sugar adopts $C_{2'}$-endo conformation (Yu *et al.* 1998). The crystal structure of *E. coli* dihydroxyacetone kinase also reveals ADP is bound in the *syn*-conformation. The pucker of the ribose ring assumes a conformation not seen in PCK or NSF. The ring is visibly strained in a conformation that is not in one of the preferred sugar puckering modes (Saenger 1984). Both C_2 and C_3 are in the *endo* position. However, the resolution of this crystal structure is only 2.6 Å, so it is difficult to say what conformation ribose is in with any degree of confidence (Oberholzer *et al.* 2006). The authors of both of these studies offer no suggestion for the reason the nucleotide would be bound in the *syn*-conformation.

1.4.1.3 *E. coli* PCK-AlF_3-Mg^{2+}

Crystal structures of *E. coli* PCK complexed with AlF_3 and relevant substrates suggest that the phosphate transfer occurs by an S_N2-like associative mechanism. In these structures, AlF_3 is observed in a region where the γ-phosphate group is believed to be during transfer (Sudom *et al.* 2001; Tari *et al.* 1997). AlF_3 is a useful transition state analogue that can mimic the geometry a phosphoryl group assumes when it is being transferred via an S_N2-like associative mechanism (Yu *et al.* 1998). The AlF_3 observed in the active site of two PCK crystal structures is isomorphic with the proposed transition state pentavalent phosphate group that would be bridging enol-pyruvate and ADP. All the fluorine atoms of AlF_3 are

interacting with positively charged atoms in the PCK complex. The residues and cofactor involved in binding the transition state complex are Lys213, Arg333 and Mg^{2+}. The PCK-AlF_3 structures reveal that there are three positive charges interacting with the transition state complex. The role of the three positive charges are presumed to be neutralizing the three negative charges on the predicted transition state phosphoryl group. It was reasoned that if the phosphate transfer step of the reaction proceeded by a S_N1-like dissociative mechanism, the residues in the immediate region around AlF_3 should only accommodate a charge of –1 made by the planar metaphosphate group that would transfer during catalysis (Sudom *et al.* 2001).

1.4.1.4 Proposed Reaction Mechanism of the Forward Reaction

Based on the findings from kinetic and crystallographic studies, a catalytic mechanism for the forward reaction catalyzed by ATP-dependent PCK was proposed (Tari *et al.* 1997; Tari *et al.* 1996). Due to the conserved active site residues between ATP- and GTP-dependent PCK, the reaction mechanism of GTP-dependent PCK is believed to be similar to the one proposed for ATP-dependent PCK. The forward reaction is divided into two steps with each step occurring in a distinct region in the active site.

In a random order ATP-Mg^{2+}, $Mn^{2+}$and oxaloacetate must first all bind to PCK (Krebs and Bridger 1980). The first step begins when oxaloacetate forms a number of interactions with PCK and Mn^{2+}, Figure 1.6. There is a hydrogen bond between one of the guanidinium nitrogen atoms from the Arg65 side chain and the

C1 carboxylate group of oxaloacetate/pyruvate, which is thought to be maintained throughout the reaction. The lone pair electrons from the keto hydroxyl group of C2 and the C1 carboxylate group of oxaloacetate are coordinating Mn^{2+} as a bidentate ligand. A hydrogen bond between the C_4 carboxylate group of oxaloacetate and the nearby hydroxyl group of Tyr207 is also made. The oxaloacetate-Tyr207 interaction stimulates oxaloacetate to decarboxylate to form pyruvate by polarizing its carboxylate group. By being polarized, the resonant form of the carboxylate group has its arrangement of delocalized electrons unfavourably altered, reducing its stability and therefore making it more likely to dissociate. The newly formed pyruvate is in the enolate form. The second step of the reaction then occurs because the deprotonated hydroxide group of the enolate form of pyruvate is correctly positioned for nucleophilic attack on the γ-phosphate of ATP.

Along with positioning oxaloacetate, Mn^{2+} is promoting catalysis by withdrawing electrons from the *γ*-gamma phosphate ATP, further polarizing the phosphorus-oxygen bond, thus making the *γ*-gamma phosphorus more electrophilic and therefore more susceptible to nucleophilic attack. Lys254 and Mg^{2+} are also withdrawing electrons from the β- and γ-phosphate groups to increase the reactivity of ATP. Combined, all these interactions make the phosphorus atom of the γ-phosphate sufficiently electrophilic so that the nearby lone pair of electrons of the deprotonated hydroxyl group from pyruvate can nucleophilicly attack it. A pentacoordinated phosphorus-containing transition state complex is formed, then the phosphoryl group can complete its transfer to form PEP and ADP, and the products can then dissociate from PCK, Figure 1.6 (Matte *et al.* 1998; Matte *et al.* 1997; Novakovski 2001; Tari *et al.* 1997).

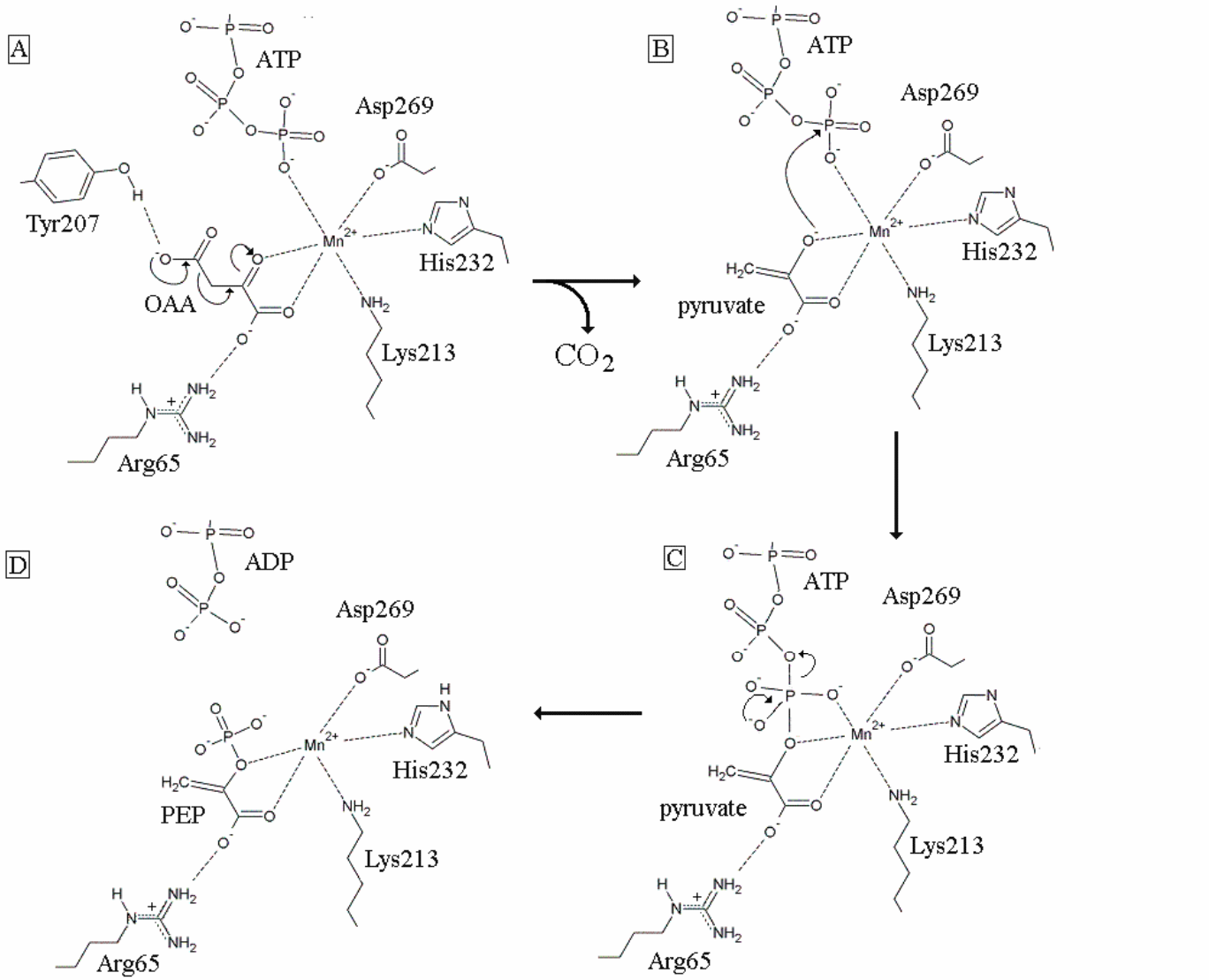

Figure 1.6. Proposed reaction mechanism for PEP production. Lys254 and Mg^{2+} are omitted from figure for clarity. **A.** Oxaloacetate decarboxylates to form the enolate form of pyruvate. **B.** A nucleophilic attack on the γ-phosphoryl group by the lone pair electrons of the hydroxide ion of pyruvate occurs. **C.** A pentacoordinated phosporus-containing transition state complex forms. **D.** The γ-phosphoryl group transfers to form PEP (Matte *et al.* 1998; Matte *et al.*1997;Novakovski 2001; Tari *et al.* 1997).

1.5 Roles of PCK in Other Species

1.5.1 Plants

Plants can utilize PCK for a metabolic role other than gluconeogenesis. In some forms of C_4 plant species such as *P. maximum* and *Zea mays,* PCK serves the function of concentrating CO_2 in the inner tissues of the plant to enhance photosynthesis. CO_2 enters the leaf where it becomes hydrated to carbonic acid, which can dissociate to a proton and bicarbonate ion. Once in the mesophyll cell, CO_2 is affixed to PEP by PEP carboxylase to form oxaloacetate. Oxaloacetate is transported into the bundle-sheath cells and is converted to PEP and CO_2 by PCK. CO_2 can then be fixed to ribulose-1,5-bisphosphate by ribulose-1,5-bisphosphate carboxylase (rubisco) to form two molecules of 3-phosphoglycerate, Figure 1.7. The reason for this indirect approach to bringing CO_2 to rubisco is due to the fact that when rubisco is subjected to higher temperatures it begins to fix oxygen to ribulose-1,5-bisphosphate forming 3-phosphoglycerate and phosphoglycolate in a process known as photorespiration. With a cost in terms of energy, phosphoglycolate must be salvaged and converted back into something usable to the cell. To minimize oxygen fixation in C_4 plants, the bundle-sheath cells, which contain rubisco, are kept from direct exposure to the atmosphere by residing under a layer of mesophyll cells, Figure 1.7. It should be noted that this is only an example of C_4 metabolism. Different metabolites and enzymes can be used to shuttle CO_2 to rubisco (Walker *et al.* 2002; Wingler *et al.* 1999).

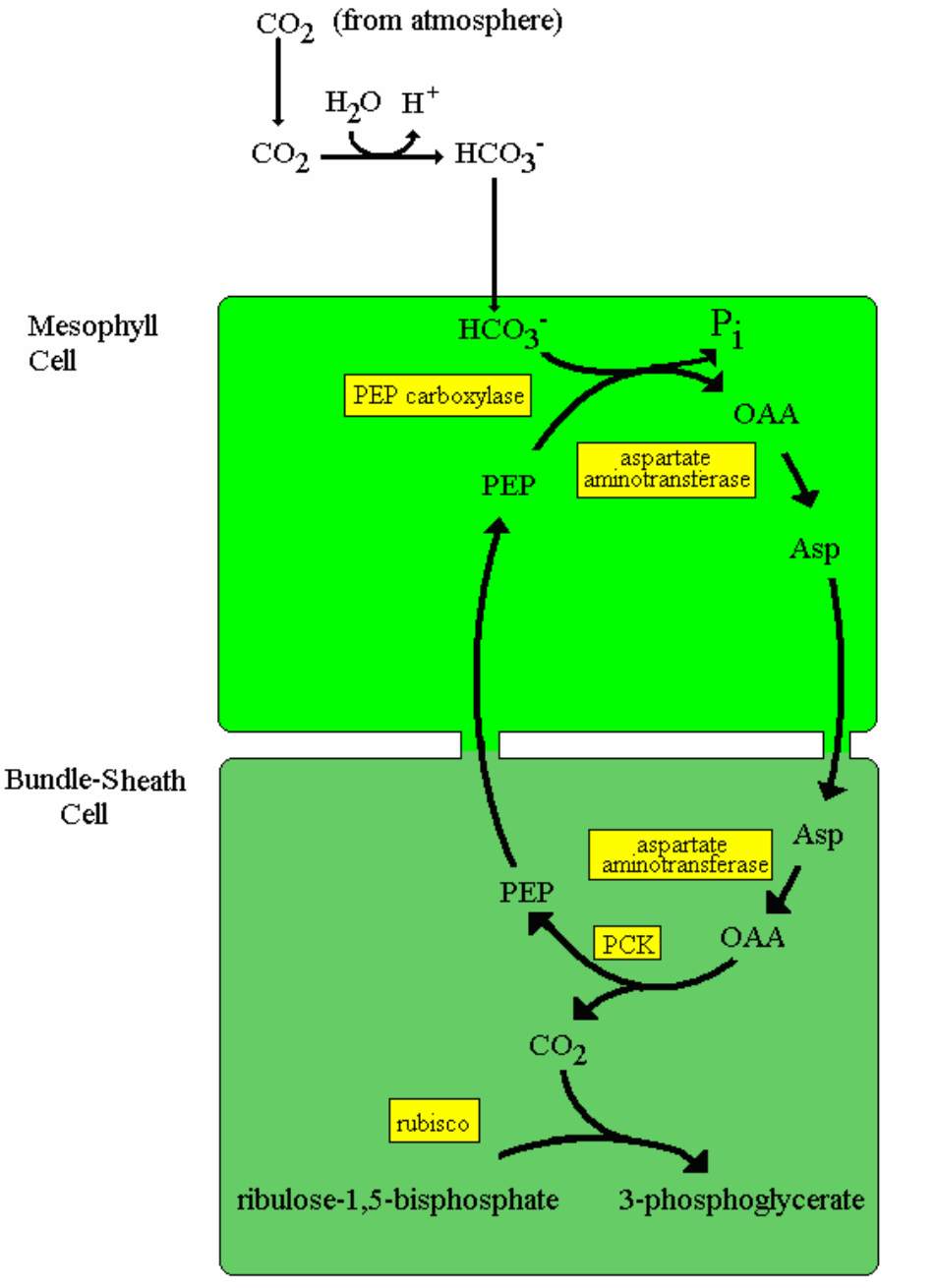

Figure 1.7. One of the pathways used by some types of C_4 plants to concentrate CO_2 in the bundle-sheath cells. Enzymes are shown in yellow boxes. A number of catabolic and anabolic pathways utilize the 3-phosphoglycerate produced.

1.5.2 *Trypanosoma cruzi* PCK

Trypanosoma cruzi is a parasite found in the tropical areas of Latin America that infects humans and causes Chagas disease (Trapani *et al.* 2001). This protozoan infects various tissues throughout the body and without treatment the afflicted person will develop digestive problems, inflammation of arteries and heart tissues. A decade after infection, the damage sustained by the body usually results in illness that incapacitates the affected individual. At this stage of the disease, heart failure due to cardiomyopathy often kills the victim. Presently tens of millions of people are infected, many of whom are impoverished. Since it takes a relatively long time for the disease to progress to fatality and developing a treatment likely would not be financially lucrative, Chagas disease is considered as a 'neglected disease' and is not a research priority for the pharmaceutical industry and governments of developed countries (Pécoul 2004). It would seem that the only way to develop a cure for *T. cruzi* infections would be by developing treatment so inexpensive it could be afforded by even the poorest nations.

T. cruzi PCK has a significantly lower K_m for CO_2 when compared to other closely related PCKs. It has been noted that by having PCK readily reversible at physiological conditions, *T. cruzi* is able to metabolize a wide array of nutrient sources thus increasing the chances of survival during infection (Trapani *et al.* 2001). Since *T. cruzi* uses the ATP-dependent form of PCK and humans use a GTP-dependent form of PCK, the structural differences between the two may lead to a potential drug for treatment of infection. With the exception of active site residues, human PCK is significantly different in terms of amino acid sequence from the *T.*

cruzi form; it may be possible to design a *T. cruzi*-specific PCK inhibitor that will adversely affect its metabolism yet have minimal side effects on the patient (Dunten *et al.* 2002; Trapani *et al.* 2001).

1.6 PCK from Succinate-Producing Microbes

Succinate is a four carbon dicarboxylic acid that is used as the starting material for the production of a large number of industrial chemicals. Succinate is used in the production of detergents, solvents, pharmaceuticals and nutrients. Most if not all of the succinate used by industry is presently derived from petrochemicals because it is the least expensive source. Currently a modest global industrial demand exists for succinate amounting to half a billion dollars (US) a year. If the cost of producing succinate by bacteria could be reduced significantly, bacterially-produced succinate could be used as the starting material for the synthesis of a wider range of other chemicals. The potential market for succinate could expand to a fifteen billion dollar (US) market (Mc Kinlay *et al.* 2005; Zeikus *et al.* 1999).

Production of succinate through fermentation has the potential to be an environmentally friendly process that can replace the fossil fuel consumption while removing CO_2 from the atmosphere. There are established fermentative processes that use agricultural biomass as the starting material for succinate production. In addition to being a 'green' industry, succinate fermentation may expand the potential market for farmers (Zeikus *et al.* 1999). There have been many advancements in the industrial fermentative process that produces succinate. Some of the most significant improvements in succinate production pertain to the isolation

of product, the stage of production that is the most energy-consuming (Lee *et al.* 2006; Zeikus *et al.* 1999).

Another advancement that may make succinate fermentation a viable industrial process involves the coupling of the succinate fermentation process to other fermentative processes. The bio-ethanol industry is considered to be a suitable candidate for integrating with succinate fermentation (Zeikus *et al.* 1999). Many jurisdictions all over the world have legislation or pending legislation mandating a minimum ethanol content in gasoline (CanadianBroadcastingCorporation 2004). The reason for the legislation is to reduce the consumption of gasoline. To accommodate the impending increase in demand for ethanol, many large-scale industrial ethanol fermentation plants have been proposed to be built in the near future (CanadianBroadcastingCorporation 2007). Unfortunately, a significant environmental concern arises with this plan; by having many large-scale plants fermenting sugars to ethanol, there will be a significant increase in production of the greenhouse gas CO_2, Figure 1.8.

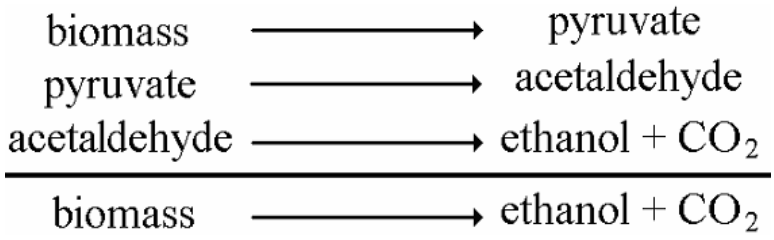

Figure 1.8. Industrial and metabolic steps involved in ethanol production

By coupling succinate and ethanol fermentation together, the CO_2 produced from ethanol production is utilized by succinate-producing bacterium instead of being released into the atmosphere (Zeikus *et al.* 1999).

Other barriers to efficient succinate production through fermentation include the processing of the starting materials. Considerable energy needs to be spent sterilizing and breaking down the biomass into chemical compounds that are usable by microbes. Improving the capacity of succinate production by microbes, and reducing the time required to ferment biomass to succinate is necessary to make the cost of its production competitive with succinate derived from the traditional petrochemical sources. The pathway presented in Figure 1.9 is thought to be responsible for succinate production during anaerobic fermentation by such succinate producing species as *Actinobacillus succinogenes, Anaerobiospirillum succiniciproducens* and *E. coli* (Zeikus *et al.* 1999).

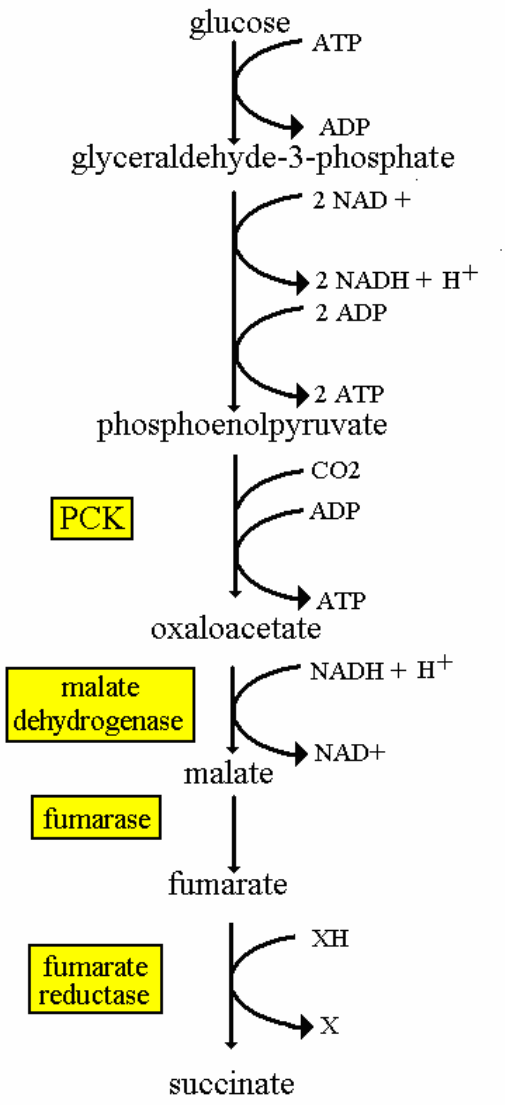

Figure 1.9. Proposed metabolic pathway from succinate production in *A. succinogenes, A. succiniciproducens* and *E. coli*. XH is a reducing agent.

The gram-negative bacterium *Manheimia succiniciproducens* is also capable of fermenting sugars into succinate efficiently. Many of the alternate pathways found in *A. succinogenes, A. succiniciproducens* and *E. coli* that produce other organic acids are not present in *M. succiniciproducens*. Unfortunately *M. succiniciproducens* is not nearly as osmotolerant as *A. succinogenes*; however, it is

able to metabolize a wider range of substrates (Lee *et al.* 2006; Song and Lee 2006). In light of these facts, *M. succiniciproducens* could be a very suitable species for the industrial fermentation of succinate. Initial studies of its metabolism has shown that it is lacking some of the enzymes found in *A. succinogenes, A. succiniciproducens* and *E. coli* that are responsible for the undesirable production of ethanol and acetate. Through genetic modification, it is possible to get very efficient succinate production in *M. succiniciproducens* with virtually no side reaction products. *M. succiniciproducens* has had its genome sequenced, which will potentially be useful when attempting to engineer strains that are more efficient. This species may one day replace *A. succinogenes* as the preferred species used for industrial fermentation of biomass to succinate. In *M. succiniciproducens* PCK has been determined to be the most crucial enzyme involved in succinate production (Lee *et al.* 2006).

A better understanding of the structure and function of PCK may ultimately help to engineer a strain of bacteria that can ferment succinate at a lower production cost than that required to synthesize it from petrochemicals. For some species the carboxylation of PEP appears to be the rate-limiting step in succinate production. By designing a modified form of PCK with an increased rate of CO_2 affixation to PEP, it may be possible to improve yields of succinate made by fermentation (Zeikus *et al.* 1999). Having the ability to enzymaticaly fix CO_2 to a three-carbon molecule efficiently is an ideal way to produce fuels and industrial chemicals in an environmentally and agriculturally friendly fashion.

1.6.1 Overview of *Actinobacillus succinogenes*

At present *A. succinogenes* is the species most likely to be used for biobased succinate production; one of the reasons is that its preferred environment is conducive to efficient production of succinate (Zeikus *et al.* 1999). *A. succinogenes* is a non-motile, osmotolerant gram negative bacterium that was originally found in the rumen of cows. The succinate produced in the rumen is fermented to propionic acid, which is utilized by the cow (Guettler *et al.* 1999).

A thorough study that characterized the succinate-related metabolic pathways was done on *A. succinogenes* to determine what kind of changes to its environment affects the flux through the major fermenting pathways. One significant finding from the study determined that 25 mM is the optimum concentration of the bicarbonate ion that provides the maximum succinate production and growth rate (Mc Kinlay *et al.* 2005).

The crystal structure of *A. succinogenes* PCK has been solved in the native and complexed form (Leduc *et al.* 2005). The PCK-pyruvate-Mn^{2+}-P_i crystal complex reveals that it is still in the open conformation, an interesting observation when compared to the closed conformation *T. cruzi* PCK- P_i assumes. The Mn^{2+} bound to *A. succinogenes* PCK appeared to be is coordinated by seven ligands, forming a slightly distorted pentagonal bipyrimidal geometry, similar to what is observed with Ca^{2+} in the *E. coli* PCK-ATP-Mg^{2+}-pyruvate-Ca^{2+} structure (Sudom *et al.* 2003). In both these structures there is an Asp269 coordinating the metal ion as a bidentate ligand. Due to the smaller size of the ionic radius of Mn^{2+} it is possible that Asp269 is only coordinating it effectively as a monodentate ligand and

so the coordination geometry of Mn^{2+} is a distorted octahedron ((Leduc *et al.* 2005; Sudom *et al.* 2003).

1.6.2 *Anaerobiospirillum succiniciproducens* PCK

A. succiniciproducens is another species that can efficiently convert sugars into succinate. PCK is believed to catalyze the rate limiting step in succinate production. To determine the catalytic roles of the active site residues of PCK, a number of kinetic and mutational studies have been performed on *A. succiniciproducens* PCK (Jabalquinto *et al.* 2002a; Jabalquinto *et al.* 2002b; Laivenieks *et al.* 1997). Initial assays found that *A. succiniciproducens* PCK has a higher V_{max} and lower catalytic efficiency for fixing CO_2 than either *E. coli* or *T. cruzi,* suggesting that the primary role of PCK in *A. succiniciproducens* is for oxaloacetate production (Laivenieks *et al.* 1997). However, as mentioned in section 1.3 later studies have found that when assayed under conditions similar to biological conditions, the K_m for CO_2 decreases significantly (Bazaes *et al.* 2007).

Based on what is known from *E. coli* PCK crystal structures, a number of purported active site residues (His232, Thr255, Asp268 and Asp269) in *A. succiniciproducens* PCK were each mutated and assayed to confirm their catalytic roles (Jabalquinto *et al.* 2002b). When His232 is mutated to glutamine, assays showed that K_m for PEP and Mn^{2+} increases by an order of magnitude. A Thr255Asn mutation significantly decreased affinity for the ADP-manganese complex. Mutating the aspartate at either position 268 or 269 to an asparagine slightly increased the K_m for all of the substrates and cofactors. Both of these latter

mutants exhibited a ten thousand-fold lower V_{max} compared to wild-type PCK. The changes in kinetic properties from the mutations are similar to what is observed when the corresponding residues are mutated in *E. coli* PCK (Novakovski 2001).

Along with *S. cerevisiae* PCK, *A. succiniciproducens* PCK is known to catalyze an oxaloacetate-like and a pyruvate kinase-like side-reaction. It was determined that AMP was a strong activator of the oxaloacetate decarboxylase activity (Jabalquinto *et al.* 1999). It is not known if these additional reactions of PCK normally serve a metabolic function or are just an artifactual side-reaction. However, there is the possibility that the redundant side-reactions of PCK can be useful for survival. If one of these organisms suffers a mutation that abolishes pyruvate kinase or oxaloacetate decarboxylase activity, the redundant side reactions from PCK may be sufficient for the organism to survive. Whatever the roles, if any, are for the side-reactions, they definitely are factors that need to be considered if any metabolic studies on *S. cerevisiae* and *A. succiniciproducens* need to take account of the activities of pyruvate kinase or oxaloacetate decarboxylase.

1.7 Summary

PCK has a crucial metabolic role demonstrated by its ubiquitous presence in all species. For most organisms PCK is essential for gluconeogenesis, whereas for other species it is important for metabolic flexibility. Due to its importance, PCK has been studied extensively for the last half century, and still is today by researchers from around the world. Much of the interest in PCK today is from medicine, agriculture and industry. The findings of the work presented here will be of benefit to all of these areas.

Chapter 2. Materials and Methods

2.1 *A. succiniciproducens* PCK-ATP-Oxalate-Mg^{2+}-Mn^{2+} Complex

2.1.1 Source and Cloning of Genes

The gene for *A. succiniciproducens* PCK, *pckA, was* isolated and prepared by the laboratory of J. Gregory Zeikus, Department of Biochemistry, Michigan State University, E. Lansing, Michigan. The *pckA* gene was isolated from the *A. succiniciproducens* strain ATCC 29305 using the homologous colony hybridization technique. Degenerate oligonucleotide primers designed from peptide sequences were used to find *pckA* from a library made from a digest of the *A. succiniciproducens* genome (Laivenieks *et al.* 1997).

2.1.2 Expression and Purification of Protein

The expression and purification of *A. succiniciproducens* PCK, *pckA* , was performed by the laboratory of J. Gregory Zeikus, Department of Biochemistry, Michigan State University, E. Lansing, Michigan. The *A. succiniciproducens pckA* gene was added to the pProPC1 plasmid (Laivenieks *et al.* 1997) was inserted into *E. coli* PB25 by transformation. The *pckA* gene was intserted in a region of pProPC1 that added a N-terminal 6xHis-tag to itself. Transformed *E. coli* PB25 was grown in LB media (containing 100 μg/ml

ampicillin) at 37 ºC to an OD600 of 0.8 and then induced for 2.5 hours with 0.6 mM isopropyl-β-D-thiogalactopyranoside.

The pelleted cells (3 g. wet wt.) were resuspended in lysis buffer (50 mM Tris-HCl, pH 8.5, 10 mM 2-mercaptoethanol, 1 mM phenylmethanesulfonyl fluoride) and lysed by passing through a French pressure cell (American Instrument Co., Silver Spring, MD, USA). The cell lysate was centrifuged at 30,000 x g for 20 min. and the supernatant was loaded onto a Ni-NTA-agarose column (QIAGEN Inc., Mississauga, ON, Canada). The column was washed with 10 volumes of buffer A (20 mM Tris-HCl, pH 8.5, 100 mM KCl, 10 mM 2-mercaptoethanol, 20 mM imidazole 10% (v/v) glycerol) and 4 volumes of buffer B (20 mM Tris-HCl, pH 8.5, 1.0 M KCl, 10 mM 2-mercaptoethanol, 10% (v/v) glycerol). Bound proteins were eluted with 10 volumes of buffer C (20 mM Tris-HCl (pH 8.5), 100 mM KCl, 100 mM imidazole, 10 mM 2-mercaptoethanol, 10% (v/v) glycerol) and concentrated using ultrafiltration. All operations were performed at 4 °C. Purified enzyme was stored at – 80 °C.

2.1.3 Crystallization Conditions

Crystals of PCK complexed with ATP, oxalate, Mg^{2+} and Mn^{2+} were grown at 22 °C by the hanging drop vapour diffusion method. A 2 µl drop containing 4 mg/ml protein, 25 mM 2-[N-morpholino]ethanosulfonate, pH 6.5, 2.5 mM 1,4-dithiothreitol 0.05, M tri-sodium citrate, pH 5.6, 10 mM ATP, 5 mM oxalate, 5 mM magnesium chloride, 5 mM manganese sulfate, 10% (w/v) polyethylene glycol 4000 and 10% (v/v) isopropyl alcohol was allowed to equilibrate against a 1 ml reservoir of 0.1 M tri-sodium citrate, pH 5.6, 20% (w/v)

polyethylene glycol 4000 and 20% (v/v) isopropyl alcohol. After 6 days a 0.5 mm by 0.2 mm by 0.1 mm crystal was removed and added to a cryoprotectant solution consisting of 0.1 M tri-sodium citrate, pH 5.6, 20% (w/v) polyethylene glycol 4000, 20% (v/v) isopropyl alcohol, 30% (v/v) glycerol and then flash cooled in liquid nitrogen.

2.1.4 Diffraction, Data Collection and Processing

The collection of diffraction data for the ATP-oxalate-Mg^{2+}-Mn^{2+} complex crystal was done at the beamline 14-ID-B at the Advanced Photon Source (Argonne National Laboratories, USA). The crystal was kept at 105 K under a cold stream of nitrogen gas during data collection. Diffraction images in 1° increments were collected with a Mar345 detector using 0.9 Å wavelength radiation. A total of 180 images were each collected for the crystal complex and native crystals.

The software package HKL2000 (Otwinowski and Minor 1996) was used to process the diffraction images of the PCK crystal complex.

2.1.5 Phase Determination, Model Building and Refinement

A molecular replacement solution was found using the coordinates from the *E. coli* PCK model PDB accession number 1AYL. The starting model was divided into two arbitrary domains, roughly corresponding to the N- and C-terminal domains. The sizes of the N- and C-terminal domain fragments were based on the division proposed by Matte et al, 1996. It was predicted that the

asymmetric unit would contain two molecules of PCK. Initially a rotation solution and then a translation solution were found separately for the N- and C-terminal domains of PCK using programs from the AMoRe software package. Then a translation solution for the C-terminal domain relative to the N-terminal domain was found by fixing the originally determined position of the N-terminal domain and rerunning AMoRe (Navaza 1994). The two solutions generated by the two previous steps were combined to form a solution for one complete molecule in the asymmetric unit. The same steps using AMoRe were rerun with the solution for the complete molecule fixed in place and another identical search model of the complete molecule had its rotation and translation solution determined. Once both molecules in the asymmetric unit were found they were combined and subjected to rigid body refinement.

Refinement of the model was done in increasingly higher resolution increments starting at 3 Å resolution. After each cycle of refinement, higher resolution data were added to the next round of calculations in 0.2 Å increments. The CNS software package (Brünger *et al.* 1998) was used in refining the atomic parameters. The software O was used for electron density map visualization and model building (Jones *et al.* 1991). Model building involved density fitting and replacing residues that were different from *E. coli* PCK. Two regions, residues 83-86 and 232-235, in the ATP-oxalate-Mg^{2+}-Mn^{2+} model had to be rebuilt because of a sequence insertion and a deletion respectively. Residues 383 to 395 had to be added to the model manually because this region is not found in any homologous models.

2.1.6 Structure Validation and Protein Data Bank Accession Number

After the model could not be improved by density fitting and refinement, Procheck (CCP4 1994) was used to validate the finished model.

The coordinates and structure factors for the *A. succiniciproducens* PCK complex were deposited in the Protein Data Bank under the accession number 1YTM.

2.2 Substrate-Free *A. succiniciproducens* PCK Structure

2.2.1 Source and Cloning of Genes

The source of *pckA* and the procedures used to obtain purified PCK for determining the crystal structure were the same as described in Section 2.1.1.

2.2.2 Expression and Purification of Protein

The expression and purification of wild-type *A. succiniciproducens* PCK was done in the same fashion as mentioned in section 2.1.2.

2.2.3 Crystallization Conditions

Crystals of substrate-free *A. succiniciproducens* PCK were produced by the hanging drop vapour diffusion method. A 2 μl drop containing 5 mg/ml protein,

20 mM Tris-HCl, pH 7.6, 1 mM EDTA and 15 % (w/v) polyethylene glycol 5000 monomethyl ether was allowed to equilibrate with a 1 ml well solution of 30% polyethylene glycol 5000 monomethyl ether at 22 °C. After six months, a 0.5 mm by 0.5 mm by 0.05 mm crystal formed and was placed in a cryoprotectant solution of 30% (w/v) polyethylene glycol 5000 monomethyl ether and 30% (w/v) glycerol then flash cooled in liquid nitrogen.

2.2.4 Diffraction, Data Collection and Processing

Data collection for native PCK crystals was done on beamline 14-ID-B at the Advanced Photon Source. The crystal was kept at 105 K under a cold stream of nitrogen gas during data collection. A total of 180 diffraction images in 1° increments were collected with a Mar345 detector using 0.9 Å wavelength radiation.

MOSFLM (Leslie 1992) version 6.2.3 was used to process the diffraction images of the crystal of substrate-free PCK.

2.2.5 Phase Determination, Model Building and Refinement

A molecular replacement solution was found using a starting model made from the coordinates of the *A. succiniciproducens* PCK structure determined in section 2.1. The steps taken to determine the molecular replacement solution were done in the same fashion as in section 2.1.

Refinement of the model was done in higher resolution increments starting at 3 Å resolution. After each cycle of refinement model adjustment and

density fitting, higher resolution data were added to the next round of calculations in 0.2 Å increments. The CNS software package (Brünger *et al.* 1998) was used for refinement calculations. Model visualization and building were done with the software O (Jones *et al.* 1991).

2.2.6 Structure Validation and Protein Data Bank Accession Number

After the model could not be improved further by density fitting and refinement, PROCHECK (CCP4 1994) was used to validate the finished model.

The coordinates and structure factors for native *A. succiniciproducens* PCK were deposited in the Protein Data Bank under the accession numbers 1YVY respectively.

2.3 *E. coli* PCK-ATP-Mg^{2+}-CO_2 structure

2.3.1 Source of PCK Gene, Cloning, Expression and Purification of Protein

The *E. coli* PCK used in this study was obtained from the laboratory of Dr. Hughes Goldie, Department of Microbiology, University of Saskatchewan. The protocol used to clone and purify were based on previously determined methods (Goldie and Sanwal 1980a; Sudom *et al.* 2003). Purified PCK was dialyzed extensively against twice-deionized water and freeze-dried.

2.3.2 Crystallization Conditions

Crystals of *E. coli* PCK were grown using the conditions from Tari *et al.,* 1997, except that oxalate was omitted from the crystallization setup. After the crystal was allowed to grow for two weeks, the drop containing crystals was moved to a steel anaerobic growth chamber and left under a 1.5 atm carbon dioxide atmosphere for a week. One hour prior to harvesting, the pressure was increased to 4 atm. Once the chamber was opened the crystals were immediately mixed in 30% glycerol-mother liquor solution and flash cooled in liquid nitrogen.

2.3.3 Diffraction, Data Collection and Processing

Data collection was carried out at the Advance Photon Source BioCARS beamline 14 BM-C. During data collection the crystal was put under a cold stream of nitrogen and kept at 105 K.The detector used was an ADSC Quantum-315. A total of 180 frames in 1˚ increments were collected using X-rays with a wavelength of 0.9 Å. The data collected were processed with the HKL2000 software suite (Otwinowski and Minor 1996).

2.3.4 Phase Determination, Model Building and Refinement

The unmodified coordinates of PCK, ATP and Mg^{2+} were taken from a solved *E. coli* PCK crystal structure, PDB accession number 1AYL, and were used as the starting model for structure determination. Model building was done with

COOT (Emsley and Cowtan 2004) and refinement was initially performed with CNS_SOLVE (Brünger *et al.* 1998) and for the final steps of refinement REFMAC5 was used (Murshudov *et al.* 1997).

2.3.5 Structure Validation and Protein Data Bank Accession Number

Structure validation was done with the program PROCHECK from the CCP4 software suite (CCP4 1994). The coordinates and structure factors were deposited at the PDB. The accession number of the coordinates was assigned as 2OLR.

2.4 *E. coli* PCK-ATP- Mg^{2+}-Mn^{2+}-CO_2-Oxaloacetate Structure

2.4.1 Source of Genes, Cloning, Expression and Purification of Protein

The *E. coli* PCK used in determining this structure was obtained from the laboratory of Dr. Hughes Goldie, Department of Microbiology, University of Saskatchewan. The protocol used to clone and purify were based on previously determined methods (Goldie and Sanwal 1980a; Sudom *et al.* 2003).

2.4.2 Crystallization Conditions

Crystals of wild-type *E. coli* PCK were grown under the condition described by Tari *et al.*, 1997, but without oxalate and ADP was used instead of

ATP. Prior to harvesting, 2 µl of a 1 mM EDTA and saturated solution of oxaloacetate along with 5 µl of glycerol were added to the drop containing the crystal. After 15 minutes the crystal was removed and flash cooled in liquid nitrogen.

2.4.3 Diffraction, Data Collection and Processing

Data collection was done at the Candian Light Source at the Canadian Macromolecular Crystallography Facility (CMCF 1) beamline 08ID-1. A total of 360 frames in 0.5 ° increments were collected. The wavelength of the beam was 1.3317 Å and the detector used was a MAR 225. The collected data were processed by the beamline staff of CMCF-1 using the XDS software package (Kabsch 1993).

2.4.4 Phase Determination, Model Building and Refinement

For refinement the starting model used the coordinates of the protein atoms from the *E. coli* structure 1AYL. Density fitting and the addition of water molecules to the model were performed with the modelling software COOT (Emsley and Cowtan 2004). Refinement was done with the software REFMAC5 (Murshudov *et al.* 1997).

2.4.5 Structure Validation and Protein Data Bank Accession Number

Structure validation was done with the program ProCheck from the CCP4 software suite (CCP4 1994). The structures factors and coordinates were deposited in the PDB and given the accession number of 2PXZ.

2.5 *E. coli* PCK Mutant Lys213Ser.

2.5.1 Source of Genes, Cloning, Expression and Purification of Protein

The *E. coli* mutant K213S PCK used in this study was obtained from the laboratory of Dr. Hughes Goldie, Department of Microbiology, University of Saskatchewan. The protocol used to clone and purify were based on previously determined methods (Novakovski 2001; Goldie and Sanwal 1980).

2.5.2 Crystallization Conditions

K213S PCK-ATP-Mg^{2+}-Mn^{2+} crystals were made by the hanging drop vapour diffusion method. The crystals grew under a 2 µl drop containing 4 mg/ml protein, 20 mM Tris-HCl (pH 7.6), 0.5 mM EDTA, 5 mM ADP, 2.5 mM phosphoenolpyruvate, 2.5 mM $MgCl_2$ and 2.5 mM $MnCl_2$, 0.1 M sodium acetate, 0.05 M sodium cacodylate, pH 6.5, 15% polyethylene glycol 8000 and was allowed to equilibrate with a 1 ml reservoir well containing 0.2 M sodium acetate, 0.1 M sodium cacodylate, pH 6.5 and 30% PEG 8000. The setup was stored at 20 °C and

within a week crystals grew. The crystal used for data collection was rectangular and had the dimensions 0.1 x 0.2 x 0.4 mm. Crystals were placed in a cryoprotectant solution containing 0.2 M sodium acetate, 0.1 M sodium cacodylate, pH 6.5, 30% PEG 8000, 20% glycerol and flash cooled in liquid nitrogen.

2.5.3 Diffraction, Data Collection and Processing

The crystals of K213S PCK-ATP-Mg^{2+}-Mn^{2+} were examined at the APS beamline 14-BM-C. The crystal was diffracted with 0.919 Å wavelength X-rays. Diffraction data were collected with a Quantum Q4 detector in 180 frames in 1° oscillations. Data processing and reduction were done with the DENZO-Scalepack software (Otwinowski and Minor 1996).

2.5.4 Phase Determination, Model Building and Refinement

Using the coordinates from wild-type *E. coli* PCK (PDB accession number 1AYL) the initial phases for the K213S model was determined with the molecular replacement software AMoRe (Navaza 1994). Refinement of the model was performed using the software X-PLOR version 4.1 and CNS_SOLVE (Brünger *et al.* 1998). Density fitting and model refinement were repeated until the value of R_{free} stopped decreasing.

2.5.5 Structure Validation and Protein Data Bank Accession Number

Structure validation was done using PROCHECK(CCP4 1994). The structures factors and coordinates were deposited in the PDB and given the accession number of 2PY7.

2.6 Production of *A. succiniciproducens* PCK Lid Deletion Mutant with Shortened, Δ2x2

A deletion mutant of *A. succiniciproducens* PCK that shortened the lid made by residues 385 to 405 was created by the laboratory of J. Gregory Zeikus, Department of Biochemistry, Michigan State University, E. Lansing, Michigan. The mutant, Δ2x2, had in total four residues (Phe387, Thr388, Thr404 and Phe405) from the lid region deleted. Expression and purification of the mutant form of PCK was performed as described in sections 2.1.1 and 2.1.2.

Δ2x2 was assayed for activity using the methods described by Podkovyrov and Zeikus (Podkovyrov and Zeikus 1993). Δ2x2 was examined by native non-denaturing polyacrylamide gel electrophoresis, PAGE. A 39 ng aliquot of Δ2x2 was loaded to a gel that contained a 4% acrylamide stacking stage that was buffered with 0.125 M Tris-HCl, pH 6.8 and crosslinked with 0.2% tetramethylethylenediamine, TEMED, and 0.1% ammonium persulphate. Also loaded on the stacking gel was 9.8 and 49 ng of wild type *A. succiniciproducens* PCK 9.2. 46 and 184 ng of *A. succiniciproducens* PCK mutant Arg65Ala. The separating portion of the gel composed of 12% acrylamide that was crosslinked in

the same fashion as the stacking portion. The separating portion of the gel was buffered by 1.5 M Tris-HCl, pH 8.8. The gel was run for one hour at 100V and 30A, once the separation was completed the gel was stained with coomasie blue.

2.7 Production of *A. succiniciproducens* PCK Mutant Arg65Ala and Kinetic Assay

The mutant Arg65Ala was created by the laboratory of J. Gregory Zeikus, Department of Biochemistry, Michigan State University, E. Lansing, Michigan. Expression and purification of the mutant form of PCK was performed as described in sections 2.1.1 and 2.1.2.

The mutant R65A was assayed for activity using the methods described by Podkovyrov and Zeikus. Kinetic values were determined with the ENZPACK software package (Biosoft, Ferguson, MO, USA) using the method of Wilkinson (Wilkinson 1980).

Chapter 3. Results

3.1 *A. succiniciproducens* PCK-ATP-Oxalate-Mg^{2+}-Mn^{2+} Structure

After the final round of refinement, the PCK-ATP Mg^{2+}-Mn^{2+}-oxalate model had an R_{work} and R_{free} of 0.214 and 0.256 respectively, Table 3.1. Electron density is not present for the first three and last seventeen residues. The electron densities for a few non-catalytic surface side-chain residues of this structure are also not discernable, likely a result of the side chains being mobile and disordered in the crystal. When the coordinates of the PCK-ATP Mg^{2+}-Mn^{2+}-oxalate structure are subjected to a Ramachandran analysis, almost all of the residues have φ and ψ angles that were in acceptable ranges, with the exception being Tyr477. However this residue is part of a γ-turn motif made up of residues i, i+1 and i+2 (Rose *et al.* 1985) (Pro476, Tyr477 and Phe478, respectively in this case). In a γ-turn, residue i (Pro476) and residue i+2 (Phe478) are hydrogen bonded through the carbonyl group of i and the amide group of i+2. To accommodate this hydrogen bond, the φ and ψ angles in i+1 (Tyr477) must be approximately 75° and – 64° respectively, Figure 3.1.

Table 3.1. Refinement Statistics for *A. succiniciproducens* PCK-ATP-Mg^{2+}-Mn^{2+}-oxalate. Values in parentheses are for the highest resolution shell.

Unit cell	
Space group	$P2_12_12$
a (Å)	194.87
b (Å)	123.22
c (Å)	48.46
α (deg.)	90
β (deg.)	90
γ (deg.)	90
Data collection	
No. molecules in asymm. unit	2
Resolution range (Å)	43.51 – 2.19 (2.28 – 2.19)
No. reflections measured	429 109
No. unique reflections	60 877 (5921)
R_{sym}	0.087 (0.383)
Completeness (%)	99.8 (98.6)
Redundancy	7.1 (4.4)
Mean I/σ(I)	19.2 (2.4)
Refinement statistics	
Resolution range (Å)	10.0 – 2.2 (2.28 - 2.2)
R_{free}	0.256 (0.297)
R_{work}	0.214 (0.254)
Total no. reflections	58 523
No. non-H protein atoms	8 470
No. water molecules	383
Mean B factor protein atoms (Å^2)	31.8
Mean B factor water molecules (Å^2)	32.1
Mean B factor ATP atoms (Å^2)	25.8
Mean B factor oxalate atoms (Å^2)	22.7
Mean B factor Mg^{2+} atoms (Å^2)	12
Mean B factor Mn^{2+} atoms (Å^2)	23
R.m.s. deviations from ideal geometry	
Bond distances (Å)	0.01
Bond angles (deg.)	1.2
Dihedral angles (deg.)	23.3
Improper angles (deg.)	0.77
Ramachandran statistics	
Most favored (%)	87.2
Favored (%)	12.2
Additional allowed (%)	0.4
Disallowed (%)	0.2

$R_{sym} = \Sigma \left| \langle I_{hkl} \rangle - I_{hkl} \right| / \left| I_{hkl} \right|$, where $\langle I_{hkl} \rangle$ is the average intensity over symmetry-related reflections and I_{hkl} is the observed intensity.
$R_{value} = \Sigma \left| \left| F_o \right| - \left| F_c \right| \right| / \Sigma \left| F_o \right|$, where F_o and F_c are the observed and calculated structure factors. For R_{free} the sum is done on the test set reflections (10% of total reflections), for R_{work} on the remaining reflections, and for R_{cryst} on all reflections included in the resolution range.

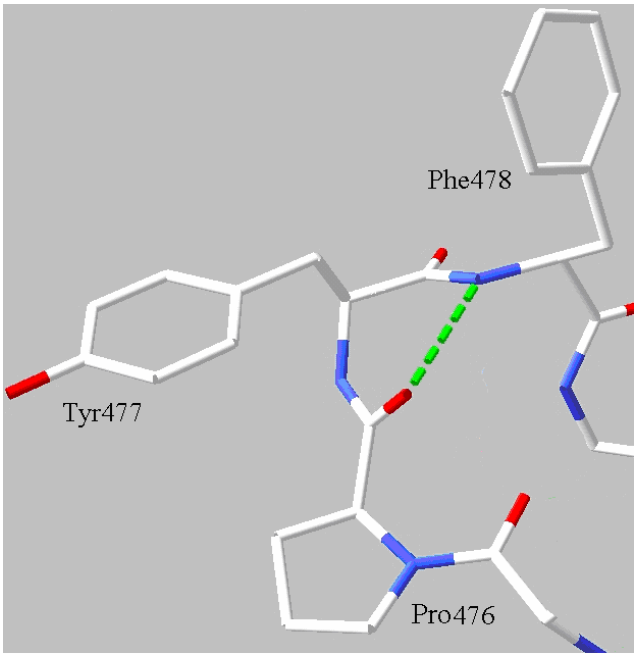

Figure 3.1. Residues Pro476, Tyr477 and Phe478 in the γ-turn motif. The hydrogen bond between the carbonyl group of Pro476 and amide group of Phe478 result in the unusual φ and ψ angles for Tyr477. Image made using DeepView (Guex and Peitsch 1997).

3.1.1 Substrate Binding

In the *A. succiniciproducens* PCK-ATP-Mg^{2+}-Mn^{2+}-oxalate structure, ATP is located in the cleft formed at the interface of the N- and C-terminal domains. As in the case of *E. coli* PCK, the bond between N9 of adenine and the C1' of ribose, χ, puts ATP in the uncommon *syn* conformation, Figure 3.2A. Some van der Waals contacts with the non-polar regions of the adenine ring are made with the side chains of Arg449 and Ile452. The carbonyl group from the peptide backbone of Leu450 and the γ-oxygen of the side-chain of Thr455 are both

hydrogen bonding to the C6 amino group of adenine. Non-bonding contacts are made between the ring oxygen atom of ribose and η1- and η2-nitrogen atoms of Arg449. The ε-nitrogen and ζ-carbon atoms of Arg449 are also making non-bonding contacts with the adenine portion of ATP, Figure 3.2A. Oxalate is observed coordinating Mn^{2+} as a bidentate ligand; an oxygen from the ATP γ-phosphate is also coordinating Mn^{2+}, Figure 3.2B. Two oxygen atoms, one each from the β- and γ-phosphates of ATP are coordinating Mg^{2+}. The β- and γ-phosphate groups of ATP are nearly in an eclipsed conformation with each other, Figure 3.2C. Figure 3.3 shows the interactions made by the P-loop residues, 251-GTGKTT-256, with the phosphate groups of ATP. Also in Figure 3.3, both the η1- and η2-nitrogens from Arg333 are observed hydrogen bonding oxygens 2 and 3 from the γ-phosphate of ATP.

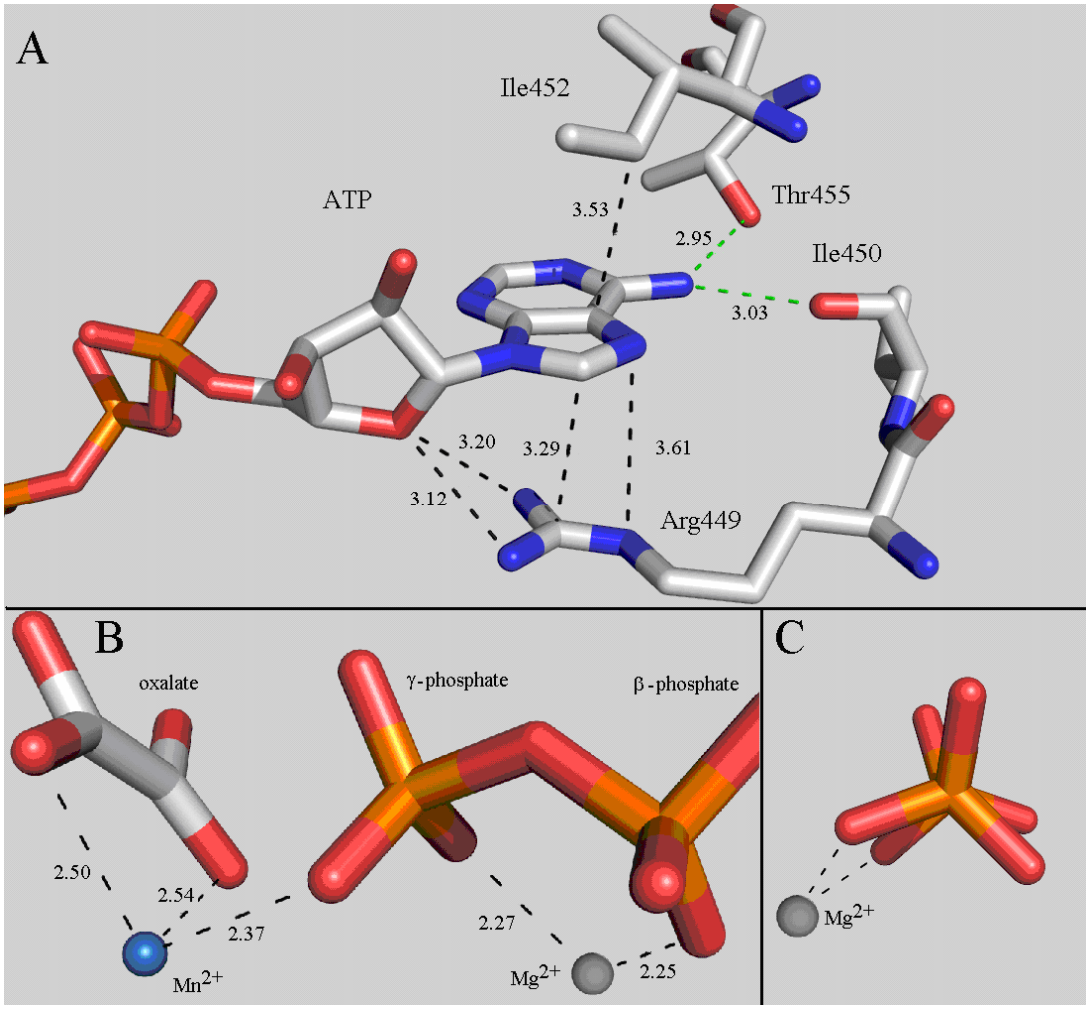

Figure 3.2A. Interactions between ATP with active site residues of PCK. The two hydrogen bonds made by the amine group of C6 from adenine with the carbonyl oxygen of Ile450 and the side chain of Thr455, are shown with green dashes. Arg449 makes a number of van der Waals contacts with adenine and ribose. **3.2B.** Oxalate coordinates Mn^{2+} as a bidentate ligand, an oxygen atom from the ATP γ-phosphate is also coordinating Mn^{2+}. Two oxygen atoms, one from each of the β- and γ-phosphates of ATP are coordinating Mg^{2+}. **3.2C.** View of the nearly eclipsed β- and γ-phosphate groups of ATP. Image made with use of Pymol (DeLano 2002).

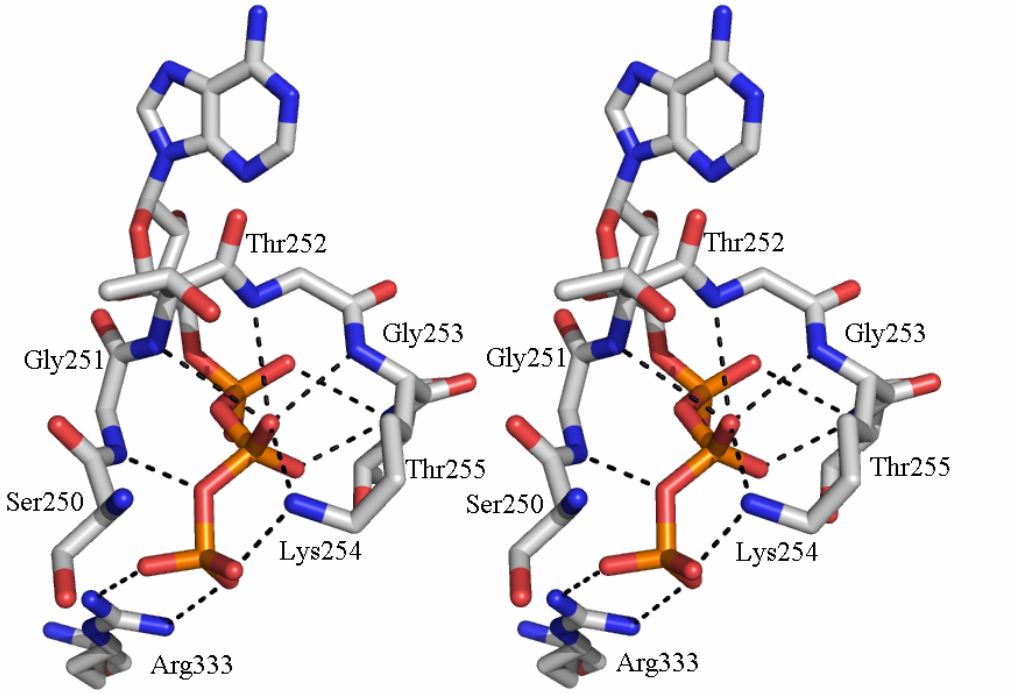

Figure 3.3. Stereo view of the hydrogen bonding network made between the phosphate groups of ATP and the P-loop, residues 250-255, of PCK. As well the hydrogen bonds made between Arg333, bottom of the figure, and two γ-phosphate oxygen atoms of ATP. Black dashed lines represent calculated hydrogen bonds. Image made with use of Pymol (DeLano 2002).

3.1.2 Metal Binding

Both the Mg^{2+} and Mn^{2+} ions are coordinated by ligands in an octahedral fashion. Figure 3.4 illustrates how Mg^{2+} is coordinated by an oxygen atom from the ATP β-phosphate, an oxygen atom of ATP γ-phosphate, γ-oxygen atom of Thr255 and three water molecules. Mn^{2+} is coordinated by an oxygen atom from each of the carboxyl groups of oxalate, a γ-phosphate oxygen atom of ATP, Figure 3.5. As well, an oxygen atom from the carboxylate group of Asp269 and nitrogen atoms from the Lys213 and the His232 side chains coordinate Mn^{2+}.

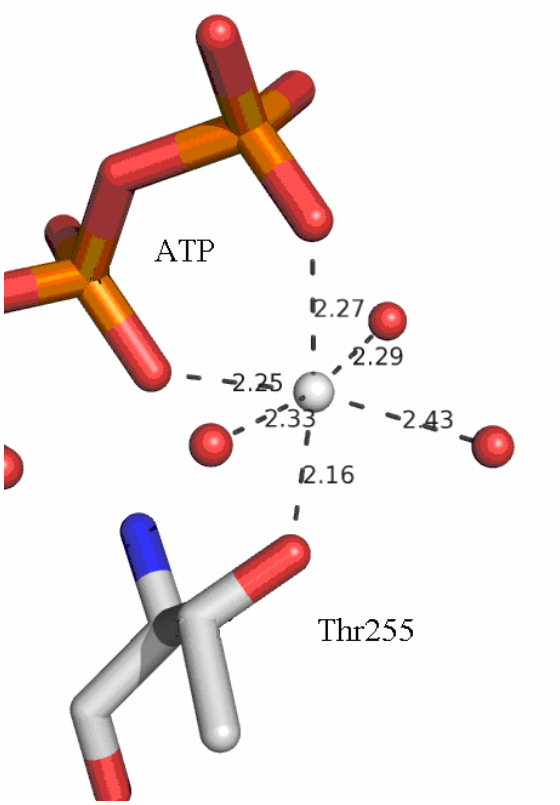

Figure 3.4. Mg^{2+} binding in active site. Red spheres are water molecules. Black dashed lines are coordination bonds. Distances shown are in Angstroms. Image made with use of Pymol (DeLano 2002).

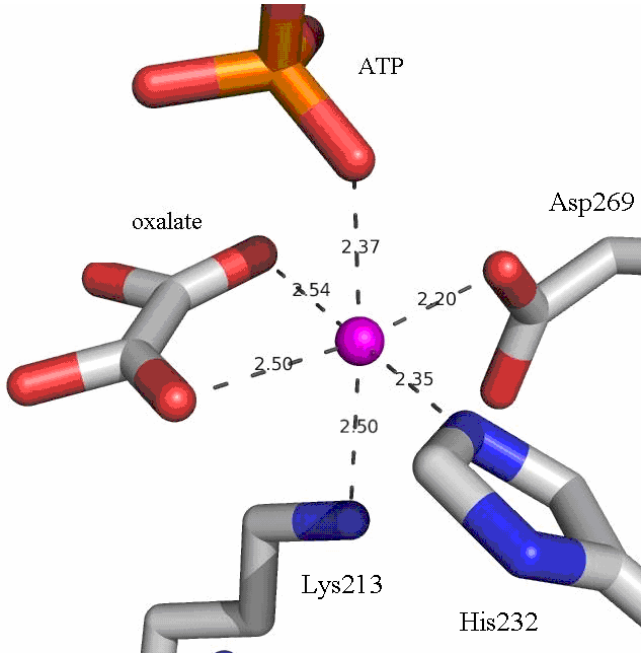

Figure 3.5. The coordination of the Mn^{2+}. Coordination bonds are made by oxalate, γ-phosphate of ATP, Lys213, His232 and Asp269. Black dashed lines are coordination bonds. Distances shown are in Angstroms. Image made with use of Pymol (DeLano 2002).

3.1.3 Domain Movement

When the native and complexed structures of *A. succiniciproducens* PCK are superimposed using the DeepView software (Guex and Peitsch 1997), a large inter domain movement occurs similar to what is observed with *E. coli* PCK (Tari *et al.* 1996). Measurement of the domain movement was done using the DynDom software (Hayward 2004). The angle the N- and C-terminal domains make closing towards each other is 17.5 °, Figure 3.6.

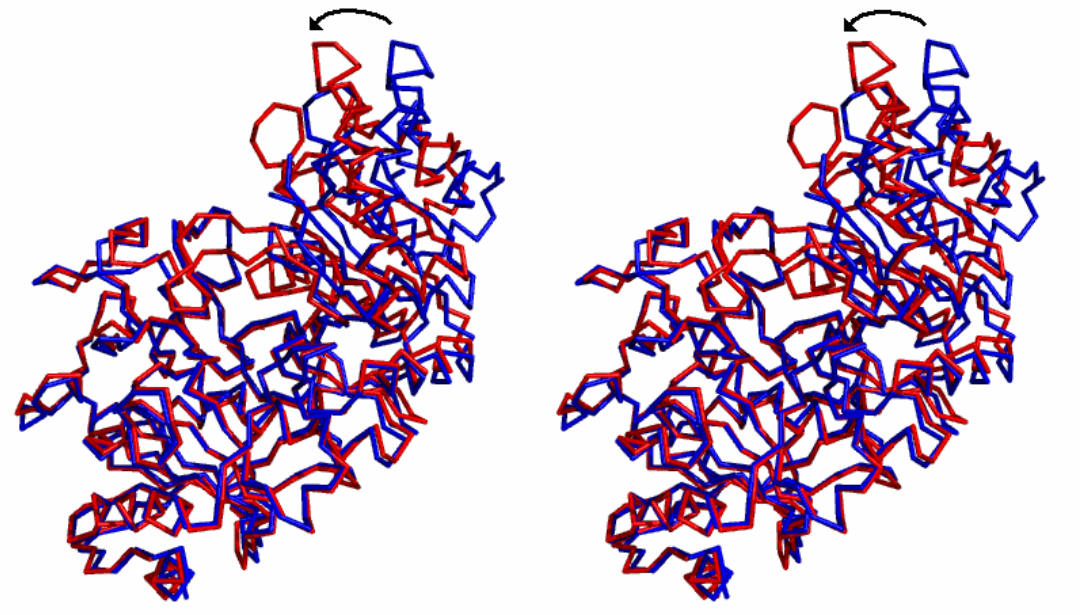

Figure 3.6. Stereoview of the α-carbon trace of the native and substrate bound forms of *A. succiniciproducens* PCK demonstrating the domain movement PCK undergoes upon substrate binding. The region of PCK that is observed to move in this figure is the C-terminal domain. The blue structure is the native form and red is substrate bound PCK. Image made with use of Pymol (DeLano 2002).

3.1.4 Visualization of Previously Disordered Lid/Loop Region (385-405)

There is a sequence of amino acid residues, that is part of the C-terminal portion of PCK that forms a beta-hairpin loop that folds over and covers the active site, Figure 3.7. In all of the crystal structures of PCK that have been determined to date, this loop has always been too mobile or disordered to be resolved in its entirety. In the *A. succiniciproducens* PCK-ATP-oxalate-Mg^{2+}-Mn^{2+} structure, the electron density is resolvable for the entire sequence of amino acid residues in this loop. At the distal end of the loop, polypeptide backbone atoms of residues Thr394

and Arg396 form two hydrogen bonds with the backbone of the active site residue Arg65, Figure 3.8, as would occur between parallel β-strands.

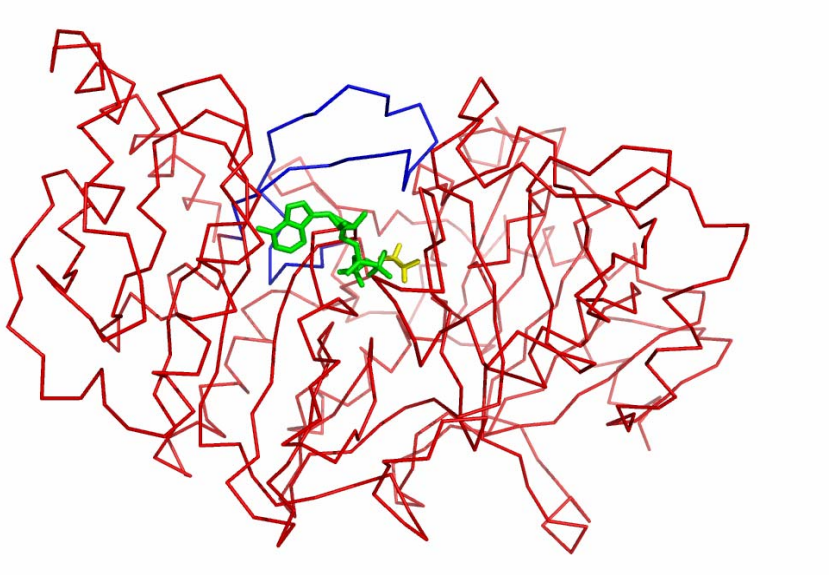

Figure 3.7. A α-carbon trace of *A. succiniciproducens* PCK showing the surface loop made by residues 383 to 395 (in blue) folding over active site. ATP is coloured green and oxalate is yellow. Image made with use of Pymol (DeLano 2002).

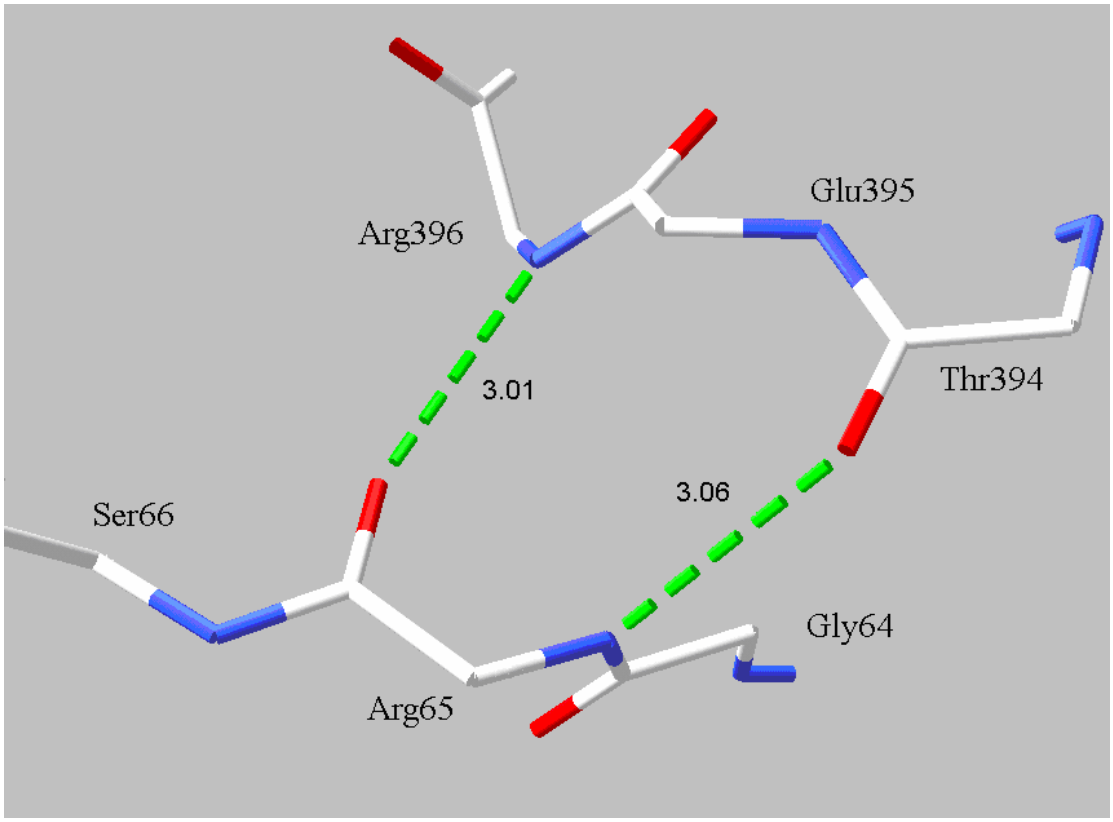

Figure 3.8. Hydrogen bonds between the peptide backbone of Arg65, nitrogen from the backbone of Arg396 and the carbonyl oxygen of Thr394. Distances are in Angstroms. Side chains are omitted for clarity. Image made with use of DeepView (Guex and Peitsch 1997).

3.2 Native *A. succiniciproducens* PCK Structure

As shown by the values in Table 3.2, the overall quality of the native *A. succiniciproducens* PCK model is good. The structure refined to an R_{work} of 0.221 and an R_{free} of 0.263 at a resolution of 2.35 Å.

A Ramachandran plot of the φ and ψ angles from the structure indicates Tyr471 is in a disallowed region. However, as mentioned in section 3.1, the conformation Tyr471 is in is acceptable because it is in the γ-motif. The electron

density for the first 3 and last 17 residues of the structure was not interpretable so they were left out of the model. Additionally a number of surface residue side chains are not visible especially those of lysine residues. There is no resolvable electron density for the surface loop residues 385 to 405.

Table 3.2. Refinement Statistics for Native *A. succiniciproducens* PCK

Values in parentheses are for the highest resolution shell.

Unit cell	
Space group	*C*2
a (Å)	129.66
b (Å)	55.73
c (Å)	139.4
α (deg.)	90
β (deg.)	93.77
γ (deg.)	90
No. molecules in asymm. Unit	2
Resolution range (Å)	10.0-2.35 (2.48-2.35)
No. reflections measured	154 036
No. unique reflections	35 963 (3980)
R_{sym}	0.067 (0.394)
Completeness (%)	98.8 (98.8)
Redundancy	3.5 (3.5)
Mean $I/\sigma(I)$	8.5(1.9)
Refinement statistics	
Resolution range (Å)	10.0-2.35 (2.48-2.35)
R_{free}	0.263 (0.329)
R_{work}	0.221 (0.272)
Total no. reflections	38 295
No. non-H protein atoms	7 627
No. water molecules	195
Mean B factor protein atoms (Å^2)	44.7
Mean B factor water molecules (Å^2)	44.4
R.m.s. deviations from ideal geometry	
Bond distances (Å)	0.02
Bond angles (deg.)	1.8
Dihedral angles (deg.)	60.0
Improper angles (deg.)	3.0
Ramachandran statistics	
Most favored (%)	87.2
Favored (%)	11.7
Additional allowed (%)	0.8
Disallowed (%)	0.3

$R_{sym} = \Sigma \left| \langle I_{hkl} \rangle - I_{hkl} \right| / \left| I_{hkl} \right|$, where $\langle I_{hkl} \rangle$ is the average intensity over symmetry-related reflections and I_{hkl} is the observed intensity.

$R_{value} = \Sigma \left| \left| F_o \right| - \left| F_c \right| \right| / \Sigma \left| F_o \right|$, where F_o and F_c are the observed and calculated structure factors. For R_{free} the sum is done on the test set reflections (10% of total reflections), for R_{work} on the remaining reflections, and for R_{cryst} on all reflections included in the resolution range.

3.3 *E. coli*-ATP-Mg^{2+}-CO_2 structure

Although the *E. coli*-ATP-Mg^{2+}-CO_2 crystal diffracted to a resolution of beyond 1.4 Å, the calculated electron density maps are ambiguous in some crucial areas of the active site. During the data collection and processing, the statistics of the highest resolution shell were in ranges generally considered a good indicator of quality. The electron density in the protein portion of the model was mostly clear. It was possible to resolve minor discrepancies between the model and data; for example, alternate side chain conformations and partial occupancies were easily detected. However, some of the electron density in the active site was ambiguous. After the resolution of the data was cut off at 1.6 Å, the electron density of the active site was fully interpretable. After the last cycle of refinement the R_{work} and R_{free} values of the model were 0.175 and 0.198 respectively, Table 3.3. With the exception of the CO_2 present in the active site, the overall structure is similar to what is observed in other *E. coli* PCK structures (Matte *et al.* 1996; Tari *et al.* 1996; Sudom *et al.* 2001). Only the first five residues of the structure are not visible in the electron density maps.

Table 3.3. Refinement Statistics for *E. coli* PCK-ATP-Mg^{2+}-CO_2 Crystal Structure

Values in parentheses are for the highest resolution shell.

Unit Cell Dimensions:	
Space Group	*C*2
a (Å)	124.86
b (Å)	95.56
c (Å)	46.46
α (deg)	90
β (deg)	96.3
γ (deg)	90
No. molecules in asymmetric unit	1
Resolution Range (Å)	75.8-1.4 (1.45-1.4)
No. reflections measured	934,055
No. unique reflections	105,079 (15056)
R_{sym}	0.078 (0.402)
Completeness (%)	99.3 (97.8)
Redundancy	3.5 (3.35)
Mean *I/s(I)*	9.4 (2.1)
Refinement Statistics:	
Resolution Range (Å)	18.9-1.6 (1.64–1.60)
R_{free}	0.198 (0.199)
R_{work}	0.175 (0.176)
Total no. reflections	71,301
No. non-H protein atoms	4,528
No. water molecules	447
Mean B factor protein atoms ($Å^2$)	13.3
Mean B factor ATP atoms ($Å^2$)	11.2
Mean B factor CO_2 atoms ($Å^2$)	28.3
B factor Mg^{2+} ($Å^2$)	8.3
Mean B factor for water molecules ($Å^2$)	26.3
B factor Cl^- ($Å^2$)	20.5
***R.m.s* deviations from ideal geometry :**	
Bond distance (Å)	0.009
Bond angles (deg)	1.3
Dihedral angles (deg)	25
Improper angles (deg)	2.6
Ramachandran statistics:	
Most favored (%)	91.7
Favored (%)	7.8
Additional allowed (%)	0.2
Disallowed (%)	0.2

$R_{sym} = \Sigma | \langle I_{hkl} \rangle - I_{hkl} | / | I_{hkl} |$, where $\langle I_{hkl} \rangle$ is the average intensity over symmetry-related reflections and I_{hkl} is the observed intensity.

$R_{value} = \Sigma | |F_o| - |F_c| | / \Sigma |F_o|$, where F_o and F_c are the observed and calculated structure factors. For R_{free} the sum is done on the test set reflections (10% of total reflections), for R_{work} on the remaining reflections, and for R_{cryst} on all reflections included in the resolution range.

3.3.1 Binding of CO_2

CO_2 is bound in the active site of the PCK-ATP-Mg^{2+}-CO_2 crystal structure, Figure 3.9. The side chains of Tyr207 and Lys213 are hydrogen bonding with the oxygen atoms of CO_2. There appears to be a second binding site for CO_2 near the active site residue His232. There is also an unexpected chloride ion near the second molecule of CO_2 and the side chain of His232, Figure 3.10. There is a question as to whether the chloride ion and second binding site of CO_2 are biologically significant or not.

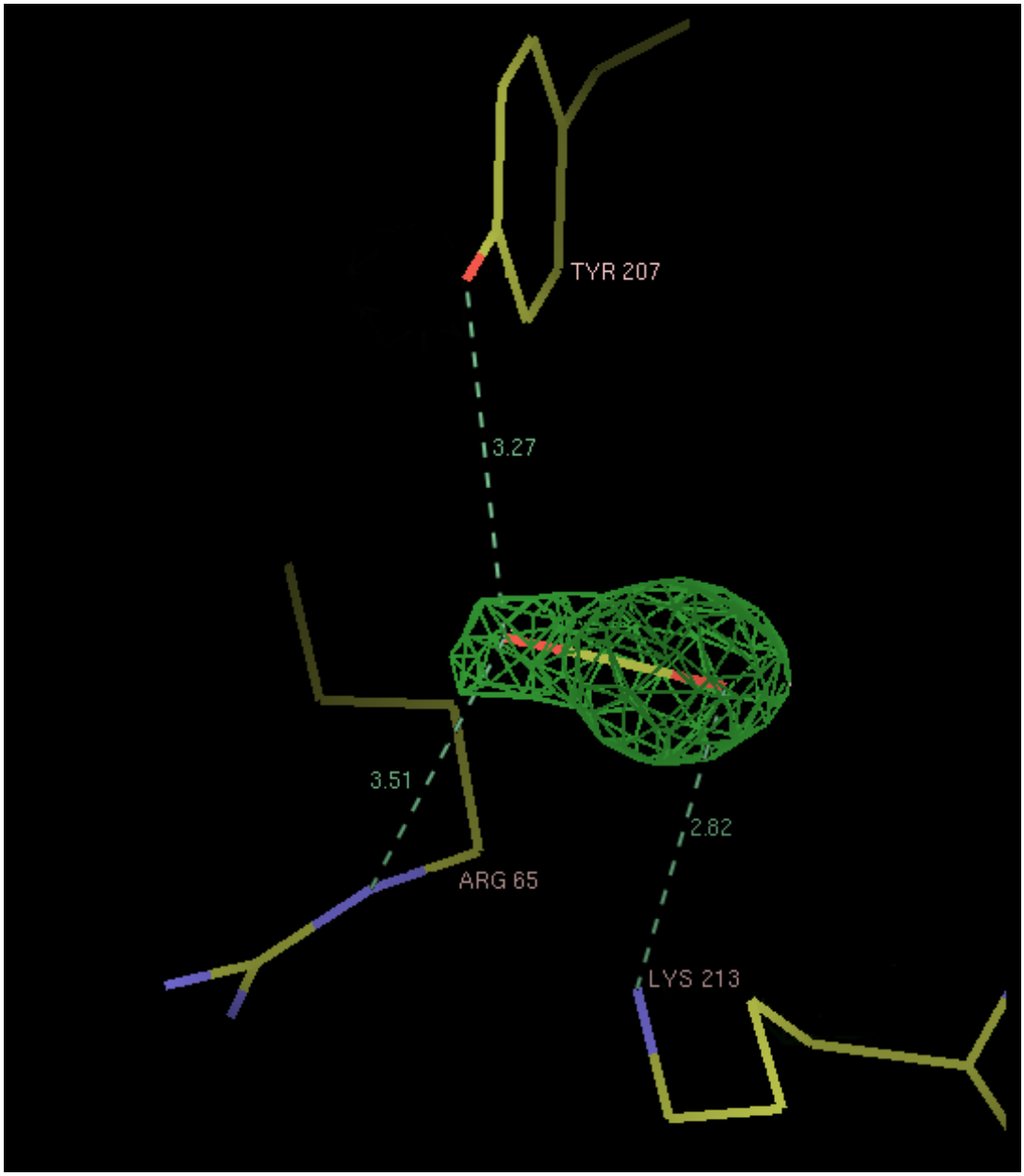

Figure 3.9. Difference electron density map ($|F_o|$-$|F_c|$) contoured at 4σ with a molecule of CO_2 modeled into the electron density. Distances are shown in Angstroms Image made with COOT (Emsley and Cowtan 2004).

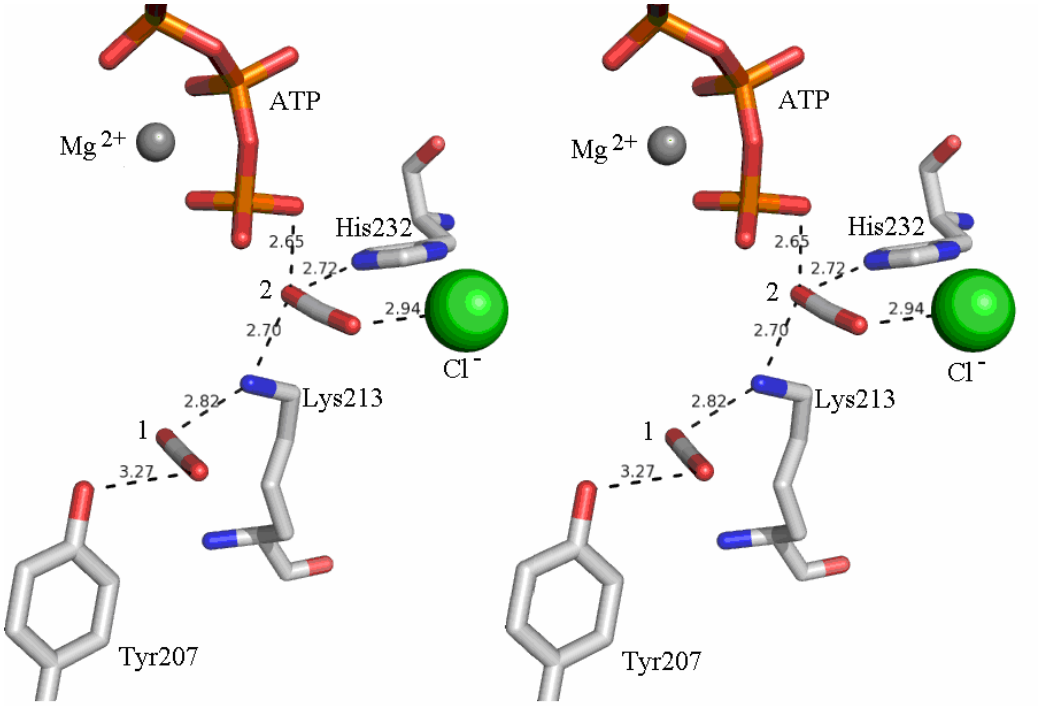

Figure 3.10. The active site of the CO_2-containing crystal structure. One of the CO_2 molecules, 1, is hydrogen bonding with the Lys213 side chain amine group and Tyr207. The other CO_2 molecule, 2, is interacting with His232 and a chloride ion. Distances are shown in Angstroms. Stereo image made with use of Pymol (DeLano 2002).

3.3.2 Disordered Loop/Lid

Although the structure of *E. coli* PCK has been previously determined in this crystal form, i.e. same space group, unit cell dimensions and packing of molecules, the loop/lid made by residues 390-405 have always been too disordered to completely resolve. In this structure, the electron density of the lid is completely visible. Unlike the *A. succiniciproducens* PCK-ATP-Mg^{2+}-Mn^{2+}-oxalate crystal

structure that has the lid folding over the active site while bridging the two domains, the lid in the *E. coli* PCK structure is pointing away from the active site Figure 3.11.

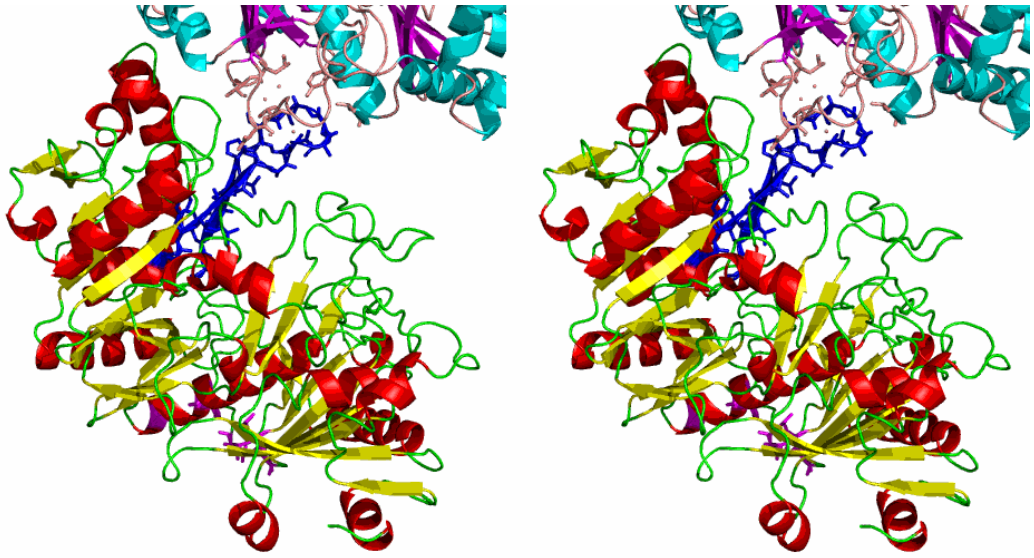

Figure 3.11. Stereo image of the crystal structure of *E. coli* PCK-ATP-Mg^{2+}-CO_2. The lid, including side chains, made up of residues 395-405 is shown in blue interacting with a symmetry related molecule. Red portion of the structure represents α-helices, yellow portions represent β-strands and green portions represent random coil. The symmetry-related structure containins aqua, purple and pink portions which represents α-helices, β-strands and random coil respectively. Image made with use of Pymol (DeLano 2002).

The tip of the lid forms indirect interactions with a symmetry related molecule. The residues Thr394, Gly397 and Thr399 from the lid, interact with Asp76, Thr77, Leu195, Thr196, Tyr221 and Leu225 of the symmetry related

molecule. The interactions between the lid and the symmetry related molecule are mediated through four bridging water molecules, Figure 3.12.

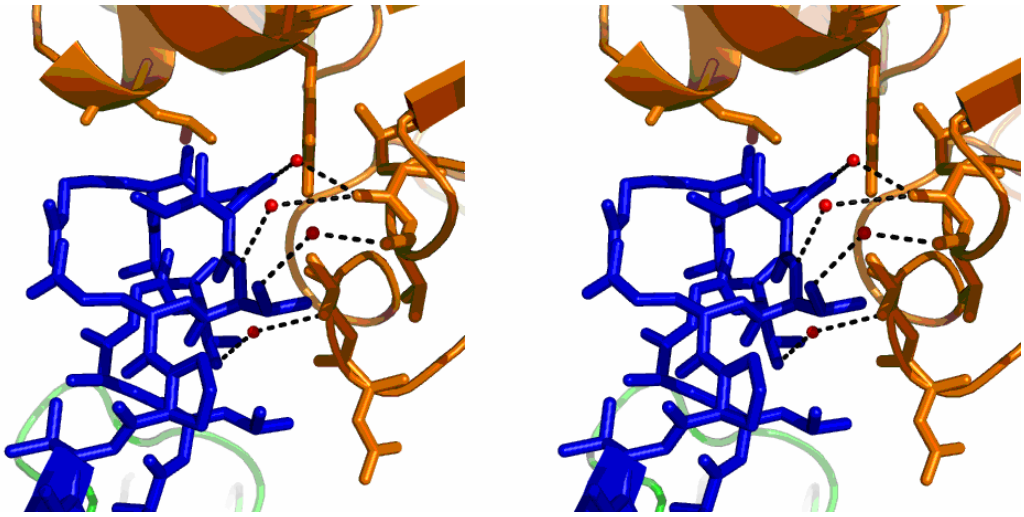

Figure 3.12. Interactions between the lid made by residues 385-405, in blue, with a symmetry related molecule, in orange. Water molecules involved in bridging are shown as red spheres. The water molecules are mediating the interactions between residues Thr394, Gly397 and Thr399 from the lid with Asp76, Thr77, Leu195, Thr196, Tyr221 and Leu225 from the symmetry related molecule. The hydrogen bonds involved in bridging the two molecules are shown as black dashed lines. Stereo image made with Pymol (DeLano 2002).

3.4 *E. coli* –PCK- ATP- Mg^{2+}-Mn^{2+}-CO_2-Oxaloacetate Structure

A crystal complex of *E. coli* PCK-ATP- Mg^{2+}-Mn^{2+}-CO_2-oxaloacetate with a resolution of 2.25 Å was solved. The final stage of density fitting and refinement produced a structure with an R_{work} and R_{free} of 0.216 and 0.248, respectively, Table 3.4. The first ten residues and residues 394-399, part of the lid region, are also not visible in the electron density maps.

Table 3.4. Data Collection and Refinement Statistics for *E. coli* PCK-ATP-Mg^{2+}-Mn^{2+}-CO_2-oxaloacetate

Values in parentheses are for the highest resolution shell.

Unit Cell Dimensions:	
Space Group	*C*2
a (Å)	124.56
b (Å)	94.30
c (Å)	46.35
α (deg)	90
β (deg)	95.54
γ (deg)	90
No. molecules in asymmetric unit	1
Resolution Range (Å)	47.14 - 1.83 (1.92 - 1.83)
No. reflections measured	595228
No. unique reflections	171743 (24303)
R_{sym}	0.085 (0.523)
Completeness (%)	100.0 (100.0)
Redundancy	3.6 (3.5)
Mean *I/s(I)*	13.2 (2.5)
Refinement Statistics:	
Resolution Range (Å)	47.14-2.23 (2.28 - 2.23)
R_{free}	0.248 (0.325)
R_{work}	0.216 (0.255)
Total no. reflections	24889
No. non-H protein atoms	4337
No. water molecules	284
Mean B factor protein atoms ($Å^2$)	20.2
Mean B factor ATP atoms ($Å^2$)	19.6
Mean B factor CO_2 atoms ($Å^2$)	26.3
B factor Mg^{2+} ($Å^2$)	17.5
B factor Mn^{2+} ($Å^2$)	25.1
Mean B factor for water molecules ($Å^2$)	23.7
B factor oxaloacetate atoms ($Å^2$)	33.4
***R.m.s* deviations from ideal geometry:**	
Bond distance (Å)	0.02
Bond angles (deg)	1.9
Dihedral angles (deg)	17.7
Improper angles (deg)	0.3
Ramachandran statistics:	
Most favored (%)	91.4
Favored (%)	7.5
Additional allowed (%)	0.9
Disallowed (%)	0.2

$R_{sym} = \Sigma | \langle I_{hkl} \rangle - I_{hkl} | / | I_{hkl} |$, where $\langle I_{hkl} \rangle$ is the average intensity over symmetry-related reflections and I_{hkl} is the observed intensity.

$R_{value} = \Sigma | |F_o| - |F_c| | / \Sigma |F_o|$, where F_o and F_c are the observed and calculated structure factors. For R_{free} the sum is done on the test set reflections (10% of total reflections), for R_{work} on the remaining reflections, and for R_{cryst} on all reflections included in the resolution range.

3.4.1 Oxaloacetate Binding

The oxaloacetate-containing PCK structure reveals an interesting binding site for oxaloacetate, Figure 3.13. Oxaloacetate was expected to be coordinating the manganese ion, but surprisingly it is over 5 Å away from Mn^{2+}. Oxaloacetate is making at least four direct and three indirect interactions with PCK. The β-carbon from Ser250 forms a hydrophobic contact with the C2 of oxaloacetate. The Leu249 β-carbon is also making a hydrophobic contact with the C2 of oxaloacetate. The third direct interaction is a non-bonding contact between the C1 carboxylate group and the amide nitrogen of Ser250. A fourth direct interaction is a van der Waals contact between the amide nitrogen of Ser250 and the C3 carbon atom. Oxaloacetate is also hydrogen bonding with three water molecules, two are hydrogen bonding with PCK and the other water molecule is coordinating Mn^{2+}. Instead of ADP in the active site, ATP is present which is not too surprising since ATP is known to be an impurity in the ADP. CO_2 is also observed in the structure.

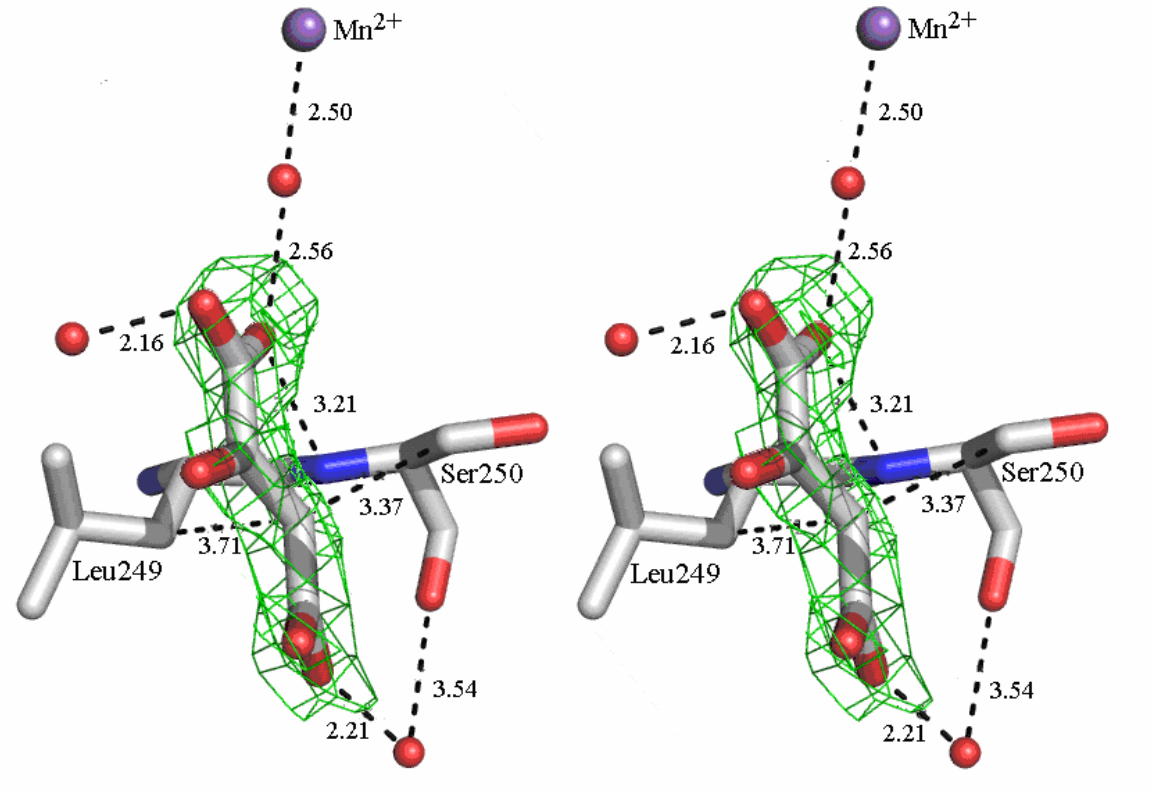

Figure 3.13. Oxaloacetate superimposed onto $|F_O|-|F_C|$ omit density map (contoured at 3.0σ) made from *E. coli* PCK-ATP-Mg^{2+}-Mn^{2+}-oxaloacetate data. Water molecules are shown as red spheres and Mn^{2+} is the purple sphere. Hydrogen bonding and non-bonded contact distances shown in Angstroms. Stereo image made with use of Pymol (DeLano 2002).

3.5 *E. coli* –K213S-PCK-ATP-Mg^{2+}-Mn^{2+} Structure

The K213S-PCK-ATP-Mg^{2+}-Mn^{2+} crystal diffracted to 2.0 Å resolution. After the last round of electron density fitting and model refinement, the final structure had an R_{work} and an R_{free} of 0.191 and 0.229 respectively, Table 3.5. When the atomic coordinates of the K213S-PCK-ATP-Mg^{2+}-Mn^{2+} structure are aligned with the wild-type *E. coli* PCK coordinates using the software DeepView (Guex and Peitsch 1997), with the exception of the region around Mn^{2+} no noticeable differences can be seen. The ATP and Mg^{2+} in the K213S structure are bound in the active site in the same manner as in the wild type crystal structure of *E. coli* PCK. The most significant finding in this structure is that Mn^{2+} is coordinated as a tetrahedral and not an octahedral complex, Figure 3.14. The γ-phosphate of ATP, a water molecule and the side chains of His232 and Asp269 are involved in the coordination of Mn^{2+}. The angles made by the ligands amongst themselves relative to Mn^{2+} are not all near 109.5 ° as would been seen in a ideal tetrahedral geometry. The tetrahedron formed is slightly distorted with the angles made between the water molecule and other ligands greater than 109.5 °, while the bonds made amongst the other ligands are all less than 109.5 °.

Table 3.5. **Data collection and refinement statistics for PCK mutant K213S**. Values in parentheses are for the outer resolution shell.

Data collection	
Space group	*C*2
Unit cell dimensions	
a (Å)	125.71
b (Å)	96.31
c (Å)	46.49
α (deg.)	90°
β (deg.)	96.35°
γ (deg.)	90
No. molecules in asymm. unit	1
Resolution range (Å)	99.0-2.02 (2.28-2.02)
No. reflections measured	89783
No. unique reflections	36560
R_{sym}	0.10 (0.14)
Completeness (%)	85.95 (59.6)
Redundancy	2.95 (1.17)
Mean *I/σ(I)*	13.96 (4.90)
Refinement statistics	
Resolution range (Å)	55.81-2.2 (2.26-2.20)
R_{free}	0.209 (0.233)
R_{work}	0.169 (0.176)
Total no. reflections	24574
No. non-H protein atoms	4561
No. water molecules	403
Mean B factor protein atoms (Å^2)	12.5
Mean B factor water molecules (Å^2)	18.5
Mean B factor ATP (Å^2)	15.5
Mean B factor magnesium ion (Å^2)	4.5
Mean B factor manganese ion (Å^2)	9.3
R.m.s. deviations from ideal geometry	
Bond distances (Å)	0.017
Bond angles (deg.)	1.64
Dihedral angles (deg.)	23.3
Improper angles (deg.)	0.76
Ramachandran statistics	
Most favored (%)	90.2
Favored (%)	9.3
Additional allowed (%)	0.2
Disallowed (%)	0.2

$R_{sym} = \Sigma | \langle I_{hkl} \rangle - I_{hkl} | / | I_{hkl} |$, where $\langle I_{hkl} \rangle$ is the average intensity over symmetry-related reflections and I_{hkl} is the observed intensity.

$R_{value} = \Sigma | | F_o | - | F_c | | / \Sigma | F_o |$, where F_o and F_c are the observed and calculated structure factors. For R_{free} the sum is done on the test set reflections (10% of total reflections), for R_{work} on the remaining reflections, and for R_{cryst} on all reflections included in the resolution range.

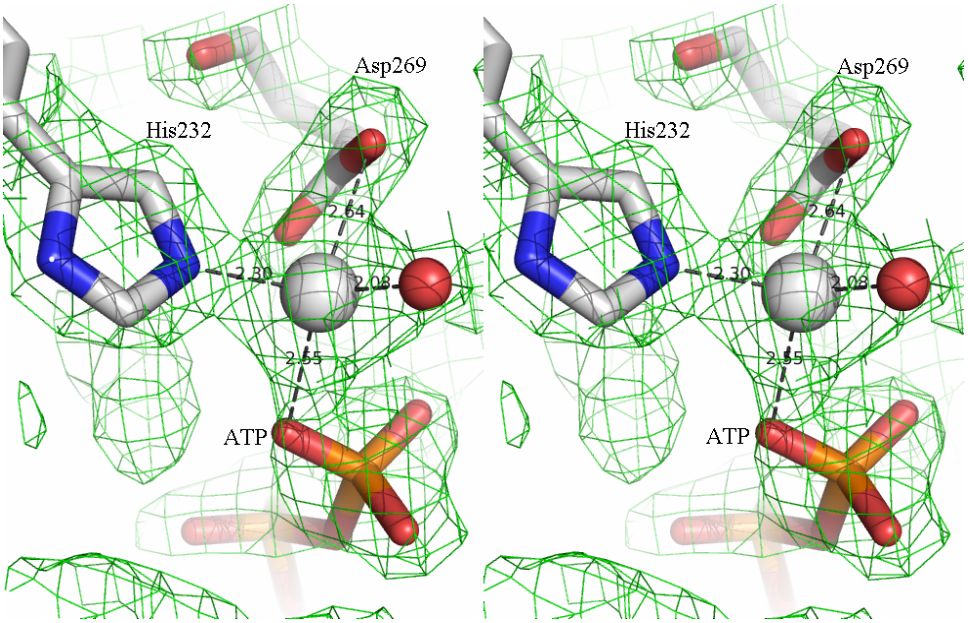

Figure 3.14. The tetrahedral coordination of Mn^{2+} in the *E. coli* K213S-PCK-ATP-Mg^{2+}-Mn^{2+} structure. The 2|Fo|-|Fc| electron density map is contoured at 1.0 σ. Only the atoms involved in coordinating Mn^{2+} are shown for clarity. The grey dashed lines represent coordination bonds and distances are shown in Angstroms. Stereo image made with Pymol (DeLano 2002).

3.6 Kinetic Assay of *Anaerobiospirillum succiniciproducens* PCK Deletion Mutant Δ2x2

Although the deletion mutant with a shortened active site lid, Δ2x2, was able to be expressed and purified, the kinetic assay performed on it could not detect any activity for PCK in the carboxylation reaction.

3.7 Kinetic Assay of the *Anaerobiospirillum succiniciproducens* PCK Mutant Arg65Ala

The assays done on R65A were compared to assays done on wild-type *Anaerobiospirillum succiniciproducens* PCK at the same time, Table 3.6.

Table 3.6. Kinetic Parameters for the Bicarbonate Ion in the Mutational Study on *A. succiniciproducens* PCK.

	K_m (mM)	V_{max} (μmol*min^{-1}*mg^{-1})
Wild Type	15.6 ± 5.1	0.61 ± 0.04
R65A	61.6 ± 34.7	0.011 ± 0.002

Chapter 4. Discussion

4.1 Domain Movement of *A. succiniciproducens* PCK

Although some residues of the calculated electron density map could not be resolved, the native *A. succiniciproducens* PCK crystal structure was able to be used to quantify the movement of the N- and C-terminal domains of PCK towards each other upon substrate binding.

DynDom is software that calculates domain movement in proteins by first defining an interdomain screw axis along the hinge residues that are bridging the domains of the protein. One of the domains is designated as a reference point for measurement. The angle that the other domain makes with the reference domain is calculated relative to the screw axis (Hayward and Lee 2002). Upon binding substrate, DynDom calculated that the domains of *A. succiniciproducens* move towards each other by approximately 17.5°. When the first crystal structure of PCK was solved, it was postulated that PCK had three hinge regions (Matte *et al.* 1996). However, the analysis using DynDom determined that there are five hinge/bending regions involved in domain movement in PCK, Figure 4.1. The bending regions designated as 2 and 4 contain residues that are believed to be involved in catalysis. Lys254, which binds the β- and γ-phosphate groups of ATP, is in bending region 2 (Tari *et al.* 1996). The lid made by residues 385 to 405 is part of bending region 4.

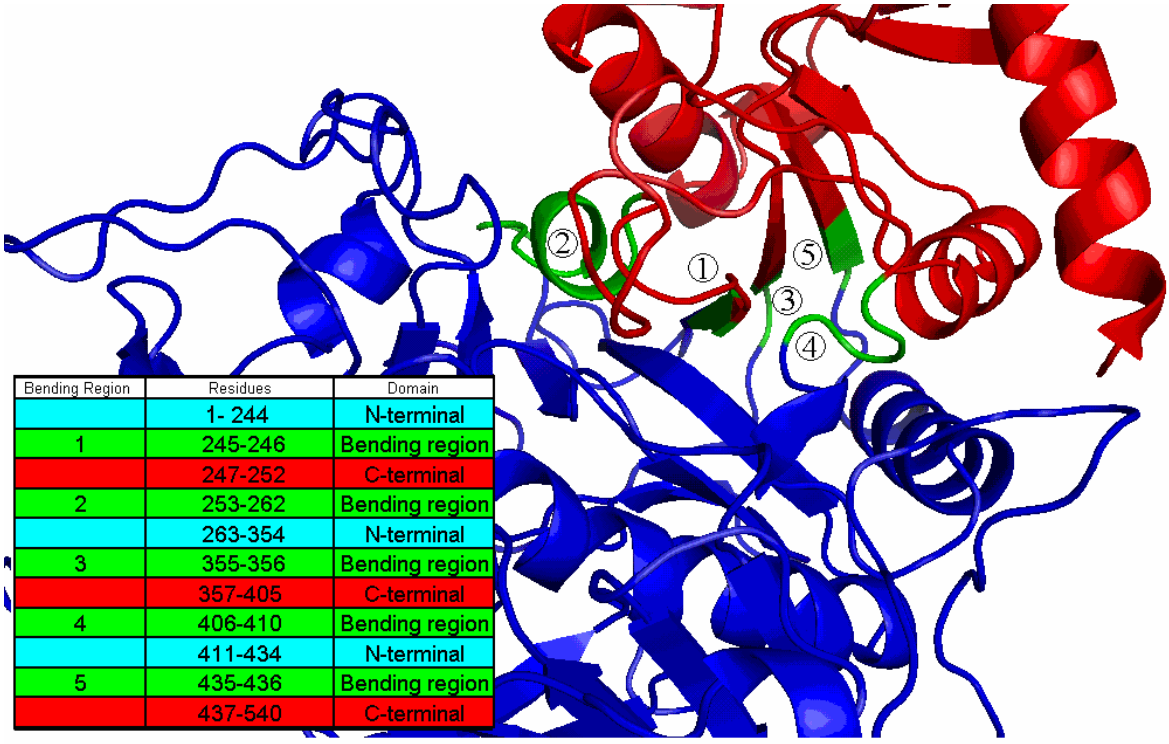

Bending Region	Residues	Domain
	1- 244	N-terminal
1	245-246	Bending region
	247-252	C-terminal
2	253-262	Bending region
	263-354	N-terminal
3	355-356	Bending region
	357-405	C-terminal
4	406-410	Bending region
	411-434	N-terminal
5	435-436	Bending region
	437-540	C-terminal

Figure 4.1. Ribbon diagram of *A. succiniciproducens* PCK illustrating the regions calculated by DynDom to be involved in domain movement. The calculated hinge regions are shown in green. The N-terminal domain is shown in blue and the C-terminal domain is red. Inset table lists the residues involved in domain movement. Image made with use of Pymol (DeLano 2002).

For the N- and C-terminal domains of PCK to move towards each other, at least two distinct sets of interactions between ATP and PCK are believed to be required. The two interactions are thought to occur in sequence. The first set of interactions occur when the phosphate groups of ATP bind in the N-terminal domain, Figure 3.3. The C-terminal domain then moves towards the N-terminal domain, either by random motion or being induced by the phosphate group

interactions with the P-loop. Once the domains come together, Arg449 and Ile452 from the C-terminal domain bind the adenine ring through van der Waal contacts, Figure 3.2 A. Figure 3.2 B illustrates the interactions the phosphate groups of ATP makes with the P-loop for comparison. There is another region of PCK that may be influencing closure but will be addressed in section 4.2.

Evidence that implicates the phosphate groups of ATP in driving domain closure is seen in the *T. cruzi* PCK crystal structure (Tari *et al.* 1996; Trapani *et al.* 2001). *T. cruzi* PCK is found in the closed conformation without any substrates or cofactors present. A sulfate ion from the crystallization buffer is observed in the approximate location where the β-phosphate of ATP is found in *A. succiniciproducens* PCK, Figure 4.2 A. Since ionic sulfate is isomorphous to ionic phosphate, the interactions it makes with PCK are observed to be very similar to the bonding arrangement ATP makes with the P-loop, Figure 4.2 B. It was suggested that the numerous interactions the sulfate/phosphate ion makes in the P-loop are strong enough to induce domain closure. There was no explanation as to how this was achieved and it was conceded the closed domains might also be an artifact due to the crystal packing.

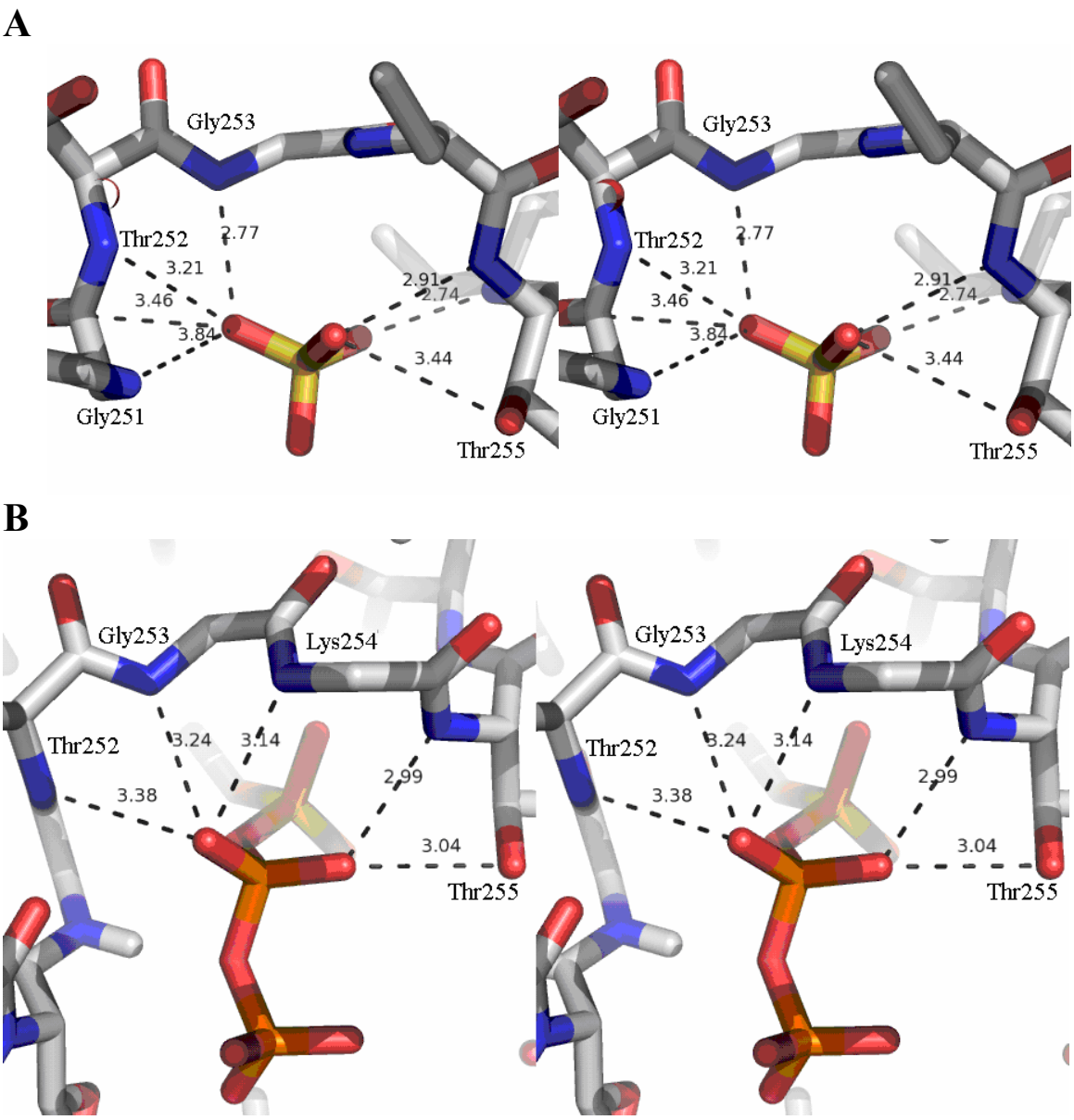

Figure 4.2 A. Interactions SO_4^{2-} makes with the P-loop of *Trypanosoma cruzi*. **B.** The interactions the β-phosphate group ATP makes with the P-loop in the *A. succiniciproducens* ATP-Mg^{2+}-Mn^{2+}-oxalate PCK complex. Distances are shown in Angstroms. Stereo image made with use of Pymol (DeLano 2002).

When the structure of *A. succiniciproducens* PCK-ATP-Mg^{2+}-Mn^{2+}-oxalate is examined in the context of the newly determined hinge regions, it can be

reasoned that the phosphate groups of ATP are likely involved in initiating domain closure. When ATP initially binds PCK, a salt-bridge forms between the β- and γ-phosphate groups of ATP and the side chain of Lys254, a residue that is part of the N-terminal domain. As this interaction forms, the residues 247 to 251 of the P-loop, which are part of the C-terminal domain, move towards the phosphate groups of ATP to form additional hydrogen bonds, Figure 4.3. Though many of the interactions formed between ATP and the P-loop appear to be less than ideal, at least seven interactions between nucleotide and the P-loop are formed. The interactions made are hydrogen bonds, salt bridges and non-bonding contacts, which cumulatively may be enough to induce closure. It is possible that when the P-loop closes around nucleotide, strain is introduced in adjacent C-terminal residues. With the P-loop residues in a different position, some of the bonds in the adjacent C-terminal residues may have to adopt strained angles to maintain their contacts with the P-loop. If the rest of the C-terminal domain is closer to the N-terminal domain this can possibly relieve bond strain on these adjacent residues.

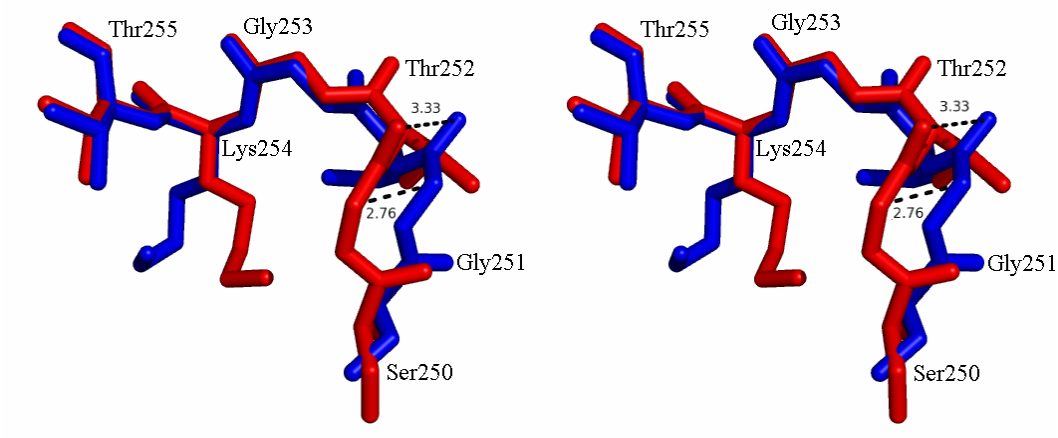

Figure 4.3. ATP induced movement of the P-loop in PCK. Residues 250 to 255 of the P-loop are shown. The blue P-loop is the unbound form of PCK and the red structure is the ATP-bound PCK. The ζ-nitrogen of Lys254 moves approximately 3 Å to form the salt bridge with the β- and γ-phosphate groups of ATP, not shown. Gly251 and Thr252 move approximately 3 Å towards Lys254. Stereo image made with Pymol (DeLano 2002).

In 2004, a study done by Hayward examined a number of proteins known to undergo domain movement upon substrate binding (Hayward 2004). The goal of the study was to determine how substrate binding induces domain movement in a protein. The question of whether domain closure is a result of a diffusion-like process or is induced by the substrate, was addressed. The diffusion-like model is based on the principle that once a substrate binds one domain of the protein, the other domain of the protein would be 'found' by the substrate through random motion and stay closed by interdomain interactions. In the sequential model, domain movement is caused by the ligand binding to one of the domains and causing conformational strain on the protein. To relieve the strain, the other domain must move towards the ligand. The study was able to determine a number of criteria

that are important for domain movement. Hayward concluded that domain movement mostly took the character of the sequential model, though some of the diffusion-like behaviour may occur. The conclusions of the study were based on the examination of five different enzymes that had had their crystal structures determined in multiple conformations. The residues involved in driving domain movement were determined using the DynDom software. If a residue is observed to be interacting with the ligand and is somehow involved in the domain movement, the study designated it as a closure-inducing residue, CIR. All five of the proteins examined were noted to have two or more hinge regions. It is believed that multiple hinges are important for the protein to rotate precisely about the axis made by the domains. Another finding is that at least one of the CIRs make up a part of one of the hinges (Hayward 2004). These two criteria are observed in the domain movement of ATP-dependent PCK. The first is the five calculated hinge regions between the two domains. By being part of the bending region and directly acting with ATP, the active site residue Lys254 is a CIR and is part of the hinge region, also another condition associated with domain movement.

On the other hand, the crystal structure of *A. succinogenes* PCK complexed with Mn^{2+}, phosphate and pyruvate suggests that the adenine ring of ATP drives the domain movement and not the phosphate groups (Leduc *et al.* 2005). The *A. succinogenes* PCK-Mn^{2+}-pyruvate crystal structure has no nucleotide bound but there is a phosphate anion bound in the P-loop region. The structure is still in the open conformation despite making a number of contacts similar to the interactions the P-loop makes with the phosphate group of nucleotides, Figure 4.2 B. As with the *T. cruzi* PCK crystal structure, it must be considered whether this

finding is of biological significance or a result of the environment created by the crystallization conditions.

It should be mentioned that only ATP-dependent PCK has been shown by crystallography to undergo domain movement when it binds with ATP. Crystal structures of human cytoplasmic and chicken mitochondrial GTP-dependent PCK have been solved (Dunten *et al.* 2002; Holyoak *et al.* 2006) with and without substrates bound. The crystal structures suggest that GTP-dependent PCK does not undergo domain movement upon nucleotide binding; all these crystal structures are observed in the closed conformation. The orientation of the N- and C-terminal domains relative to each other is comparable to ATP-dependent PCK in the closed conformation. Although the sequences of ATP-dependent PCK and GTP-dependent PCK are significantly different, the overall topology between the two forms is very similar. The similarity is observed when the structures are aligned using the DALI server, Figure 4.4 (Holm and Sander 1994).

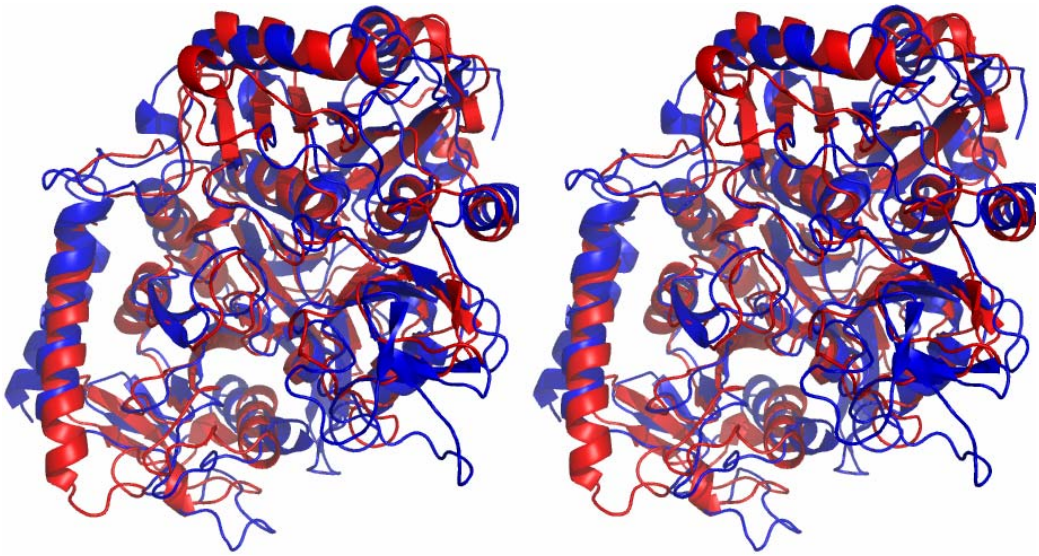

Figure 4.4. Stereo image of ATP-dependent *A. succiniciproducens* PCK (PDB accession number 1YTM), in red, aligned and superimposed with GTP-dependent chicken PCK (PDB accession number 2FAH), in blue. Image made with Pymol (DeLano 2002).

It is therefore acceptable to designate the GTP-dependent PCK conformation as closed based on comparison to ATP-dependent PCK (Dunten *et al.* 2002; Holyoak *et al.* 2006). The findings of the crystallographic studies on GTP-dependent PCK are in contrast with was observed in a fluorescence experiment studying domain movement. By measuring the intrinsic fluorescence of surface tryptophans it was concluded that both ATP-dependent PCK and GTP-dependent PCK undergo conformational change upon substrate binding (Encinas *et al.* 1993).

4.2 *A. succiniciproducens* PCK-ATP-oxalate-Mg^{2+}-Mn^{2+} Structure

The first ten residues are not observed in the electron density maps. The locations, bond lengths and angles made by the substrates and cofactors are found to be in acceptable ranges when compared to the crystal structures of ATP-binding PCK from other species (Tari *et al.* 1996; Leduc *et al.* 2005).

This structure is of good quality and for the first time a region of the structure never before observed is resolved. The region is a lid made up of residues 385 to 405. In most other PCK crystal structures, this region has been too disordered to be visible. In some of the structures, portions of the peptide backbone of the lid are not observed (Trapani *et al.* 2001; Matte *et al.* 1996; Tari *et al.* 1996). In one other crystal structure, the backbone can be observed but the residue side chains cannot be resolved (Sudom *et al.* 2003). One of the reasons why the active site lid can be resolved in the *A. succiniciproducens* PCK-ATP-oxalate-Mg^{2+}-Mn^{2+} structure may be that the crystal packing maintains the lid in the closed conformation over the active site. However, an examination of the structure shows there are no direct interactions between the lid and symmetry related molecules of PCK, so if there is an influence from crystal packing, it is not direct. The one notable difference in crystallization conditions of *A. succiniciproducens* PCK compared to other crystallization conditions was a strict requirement of 20% v/v isopropyl alcohol. Even when the concentration of isopropyl alcohol was raised or lowered one percent, crystals would not grow. Crystal growth however was also resistant to change in concentrations of other reagents in the crystallization setup.

The isopropyl alcohol may be responsible for creating an environment that stabilizes the lid enough to be resolved by crystallography. A visual search of the structure has not found any electron density corresponding to isopropanol, so its role in crystallization is still unclear.

4.2.1 Active Site Lid

For the first time in an ATP-dependent PCK crystal structure, the active site lid made by residues 385 to 405 in the *A. succiniciproducens* PCK-ATP-oxalate-Mg^{2+}-Mn^{2+} is observed in its entirety. The *E. coli* PCK-ATP-Mg^{2+}-Ca^{2+}-pyruvate crystal structure, 1OS1, partially resolves the lid region, but the side chains of Leu391, Thr394, Glu395, Arg396, Ile398, Thr399 and Glu400 are not observed in this structure, so it is difficult to know for certain what interactions the lid is making with the rest of the protein. It is also be noted that the lid from the *E. coli* structure does not extended as far out towards the N-terminal domain as the lid from *A. succiniciproducens* and because of this only the carbonyl group of Gly393 can reach the active site and hydrogen bond with the backbone of Arg65 (Sudom *et al.* 2003). This is in contrast with the situation with *A. succiniciproducens* PCK where peptide backbone atoms of Thr394 and Arg396 are hydrogen bonding with peptide backbone of Arg65.

The active site lid is a β-hairpin turn that is a loop about 20 Å long, that when extended, spans the N- and C-terminal domains of PCK. Between the two strands that make up the lid, there are five anti-parallel β-sheet-like hydrogen bonds between the pairs Phe387 and Phe405, Thr388 and Thr404, Ala389 and Pro403,

Lys390 and Thr402, Leu391 and Pro401. Because of its length, the lid is expected to be very flexible and mobile, which is probably why it has been difficult to resolve in previous crystal structures.

The exact function of the lid is not known for certain; however, three roles have been proposed. The first is for maintaining an environment in the active site that is conducive to catalysis. The second role of the lid may be contributing, along with ATP, to the domain closure of PCK upon substrate binding. Thirdly, an unusual catalytic role is proposed for the lid in section 4.4.3.

The first and most apparent role of the lid is to shield the region around the ATP γ-phosphate and oxaloacetate to enhance catalysis. When the domains fold over the active site during substrate binding the lid sterically forces bulk solvent molecules out of the active site while the ordered water molecules remain bound to PCK and cofactors. The lid effectively covers the region of PCK where catalysis is occurring, thereby preventing any other water molecules from entering the active site

All of the crystal structures of ATP-dependent PCK have ordered water molecules in the active site but none of the proposed reaction mechanisms of PCK have water molecules directly involved. Thus, the lid is probably indirectly enhancing catalysis by eliminating the solvation effect mobile water molecules could have on the reaction intermediates. As mentioned in section 1.4.1.5, it is postulated that the phosphoryl transfer step of the forward reaction of PCK proceeds by having the β-phosphorus atom of ADP undergo a nucleophilic attack by the lone pair electrons from one of the oxygen atoms of the phosphoryl group of PEP. It is known that the reactivity of a nucleophile greatly diminishes in the

presence of a polar protic solvent such as water (McMurry 1992). It can reasonably be concluded that the lid is likely aiding this step of catalysis by maximizing the nucleophilicity of the phosphoryl group of PEP. When PCK catalyzes the reverse reaction, pyruvate in its carbanion form, is thought to be responsible for carbon fixation by nucleophilically attacking CO_2, this mechanism is shown in Figure XX and further discussed in section 4.8. At this step in catalysis, the solvent effect of water would also likely lower the nucleophilicity of the carbanion. For PCK to react in either direction with maximum activity, it most likely needs a solvent-free environment. If PCK does have a strict requirement for this environment, then the importance of the lid is clear; one of its functions is to sequester the substrates and cofactors from bulk solvent to produce an environment that enhances the formation of products.

The second proposed role for the lid is to assist substrate-induced closure of PCK. Thr394 and Arg396, both of which are located on the tip of the lid and are part of the C-terminal domain, are observed hydrogen bonding to the active site residue Arg65 which is on the N-terminal domain. The carbonyl group of Thr394 forms a hydrogen bond with the amide group of Arg65. The amide group of Arg396 also hydrogen bonds with the carbonyl group of Arg65, Figure 3.8. The hydrogen bonding arrangement made between the tip of the lid and Arg65 resembles that observed in parallel β-sheets. The lid is also making another three interactions with other parts of the N-terminal domain. The side chain of the lid residue Arg396 is making two hydrogen bonds with Asp69 and Ser66. There are also hydrophobic interactions made between Phe359 and Pro397, Trp437 and Pro395. The multiple interactions between the lid and the active site demonstrate

the importance of keeping the active site tightly covered by the lid. The hydrogen bonds and hydrophobic interactions formed when the lid approaches the active site may also be encouraging domain closure. Once ATP or ADP binds to PCK, the domains begin to approach each other and, as the two parts of the enzyme close together enough, the hydrogen bonds and hydrophobic interaction the lid can make with the N-terminal domain can readily form and stabilize PCK in the closed conformation.

The importance of this loop is also implied by its conservation of sequence among the ATP-dependent PCKs. The amino acid sequence of the *E. coli* PCK lid, residues 385-405, was used to find similar sequences with the BLAST alignment tool (Altschul *et al.* 1990). The search found over 240 ATP-dependent PCK sequences with the corresponding lid sequence. Along with the strict conservation of active site residues, the sequence that makes up the lid is highly conserved; there are at least thirty-five species that have a lid sequence identical with *E. coli*. Another fifty-five sequences have one to four variances from the *E. coli* sequence, with most of the differences being conservative. Relative to the rest of the amino acids that make up PCK the lid sequence is very significantly more conserved. When the rest of the amino acid sequences from the thirty-five species that have the identical lid sequence are compared, the overall sequence identity is 90 to 75%.

In one of the crystal structures of chicken mitochondrial PCK presented by Holyoak and coworkers a lid that closely that resembles the lid found in the *A. succiniciproducens* PCK-ATP-Mg^{2+}-Mn^{2+}-oxalate structure is observed. (Holyoak *et al.* 2006). There is no sequence homology or similarity between the two forms of

PCK, yet the shape of the lid takes up is similar, Figure 4.5, and both lids are observed to be hydrogen bonding with an active site arginine. When the sequence of the lid from the GTP-dependent form is used to find similar sequences using the BLAST alignment tool (Altschul *et al.* 1997), it was found that lid sequence is completely conserved in at least twenty four species that use the GTP-dependent form of PCK. By observing the lid in the GTP-dependent form PCK taking the same shape and interacting with the same active site residue as the ATP-dependent form it can be argued the function of the lid in critical for the enzyme's function.

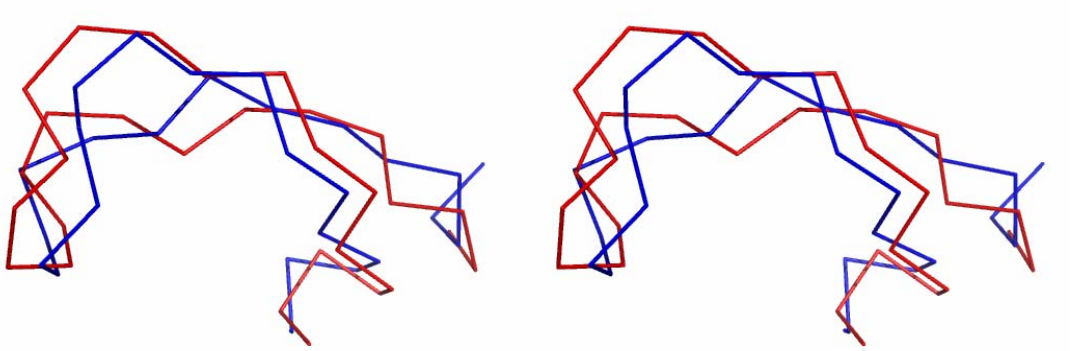

Figure 4.5. Stereo image of aligned α-carbon trace of the lids from ATP-dependent *A. succiniciproducens* PCK (PDB accession number 1YTM), in red, and GTP-dependent chicken PCK (PDB accession number 2FAH), in blue. Image made with Pymol (DeLano 2002).

The third predicted role for the loop involves catalysis and is discussed in section 4.4.2.

4.2.1.1 Truncation of the Active Site Lid

The importance of the lid was further demonstrated by creating a double deletion mutant of *A. succiniciproducens* PCK, Δ2x2, that shortened the lid by the length of two amino acids. The residues deleted were specifically chosen to minimize disruptions that affect the formation of the β-hairpin and preserve the alternating orientation of the peptide backbone. The locations of the deletions were chosen because the residues deleted contained the least amount of interactions with the rest of the PCK molecule, Figure 4.6.

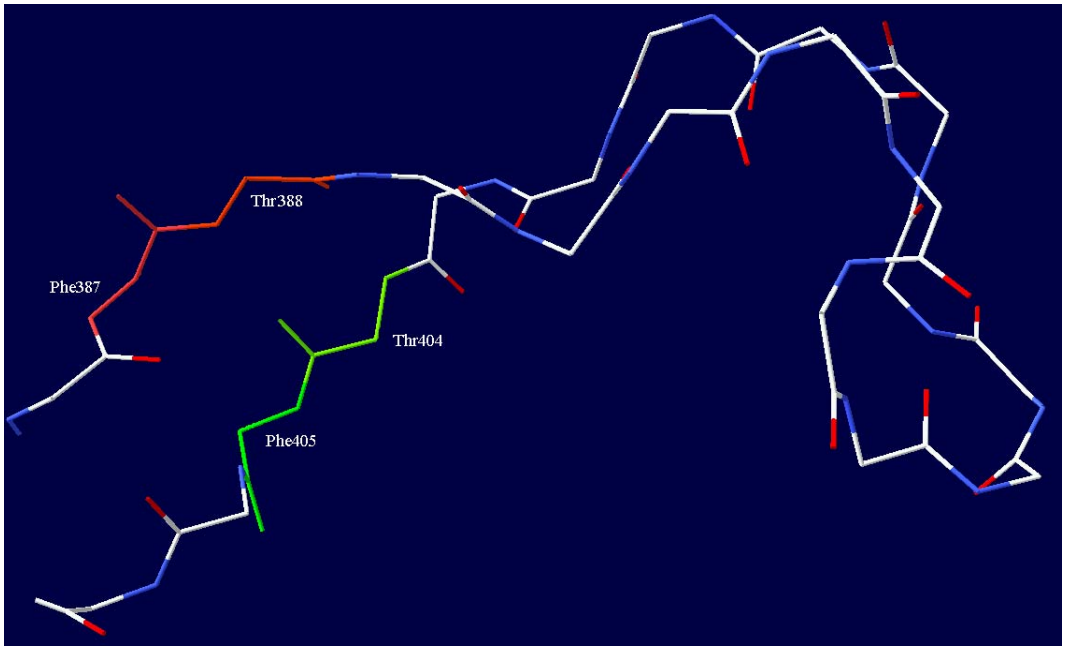

Figure 4.6. Image of lid made by residues 385 to 405. Only the peptide backbone is shown for clarity. Residues deleted in the Δ2x2 mutant, Phe397 and Thr388 in red, Thr404 and Phe405 in green, are shown. Image made with DeepView (Guex and Peitsch 1997).

When assayed as described by Laivenieks et al. (Laivenieks *et al.* 1997), all detectable activity Δ2x2 was abolished. The complete inactivation of Δ2x2 was unexpected since the lid is not believed to directly interact with substrates. To determine if the deletion mutant was misfolding, Δ2x2, R60A (a functional *A. succiniciproducens* PCK mutant) and wild type *A. succiniciproducens* PCK were examined by non-denaturing polyacrylamide gel electrophoresis, PAGE. Since wild type and R60A PCK are known to be functional, the band patterns that formed in the native PAGE gel are used as the reference for proper folding. The lane containing Δ2x2 exhibited a banding pattern very close to what is observed with wild type PCK, implying that Δ2x2 is properly folded, Figure 4.7. However, the results from the non-denaturing PAGE are not enough evidence to suggest Δ2x2 is folding correctly. The results from performing the non-denaturing PAGE can only demonstrate if a protein is drastically misfolding, subtle changes in folding must be determined some other way. Suggestions for further experimental investigation of Δ2x2 are given in section 5.1.

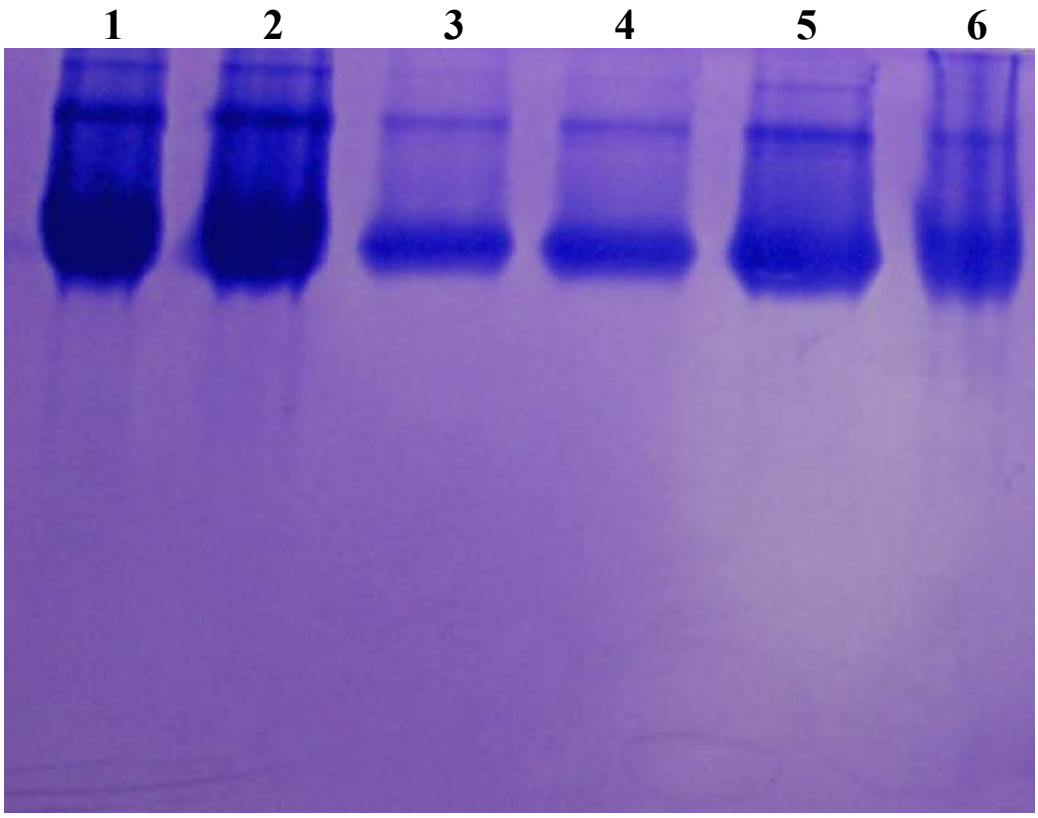

Figure 4.7. Native PAGE analysis of *A. succiniciproducens* PCK. Lanes 1 and 2 contain 9.8 and 49 ng of wild type PCK respectively, lanes 3,4 and 5 contain 9.2, 46 and 154 ng of R60A respectively, lane 6 39 ng of Δ2x2.

If Δ2x2 is assumed to be folding correctly, there is a question as to why activity is completely abolished. The lack of activity may be because the domains of PCK cannot close together properly without being able to form the hydrogen bonds and hydrophobic interactions made between the lid and the N-terminal domain. If domain closure cannot occur properly this may result in the substrates not being brought close enough to the appropriate active site residues to react. Another possible cause for the loss of activity is that the shortened lid prevents complete domain closure. If the two domains of PCK are unable to close together, bulk solvent has access to the active site, which could be preventing catalysis. There

is also the possibility that Δ2x2 is folding incorrectly but its migration band from the native PAGE study remains similar to that of wild type enzyme.

4.2.2 Potential Interactions between the Active Site Lid and the C-Terminal Domain

In the *E. coli*-ATP-Mg^{2+}-CO_2 crystal structure, which will be further discussed in section 4.3, the residues that make up part of the lid are completely resolvable in the electron density map. Unlike the lid observed in *A. succiniciproducens* PCK, the lid is not bridging the N- and C-terminal portions of PCK and covering the active site, but is extended straight and pointing away from the active site, Figure 3.11. It also appears that the lid is held in its position by interacting with a symmetry related molecule through four bridging water molecules. Due to the fact that interactions are between the lid and a symmetry related molecule in the crystal, it is likely that the lid does not occupy the observed position for any significant amount of time in solution.

The lid is notably nearby an α-helix from the C-terminal domain made up of the residues 505 to 521, Figure 4.8. If the lid is moved over slightly towards this helix, there are least four attractive interactions that could occur between the lid and C-terminal end of PCK. If these interactions are made, the lid would stay in close contact with the C-terminal domain. Although the interactions look favourable it is not certain if the lid can actually completely fold on this C-terminal region of PCK.

It is also not known if the lid's potential interactions with the C-terminal helix have any significance for catalysis. It is possible that the purpose of the lid-helix interaction is to keep the lid from randomly moving around before the substrates bind, to minimize the chances that the lid will block substrates attempting to bind in the active site. Once the substrates bind, the induced closure of the domains possibly pulls the lid from the C-terminal domain and have it fold over the active site and interact with the N-terminal domain.

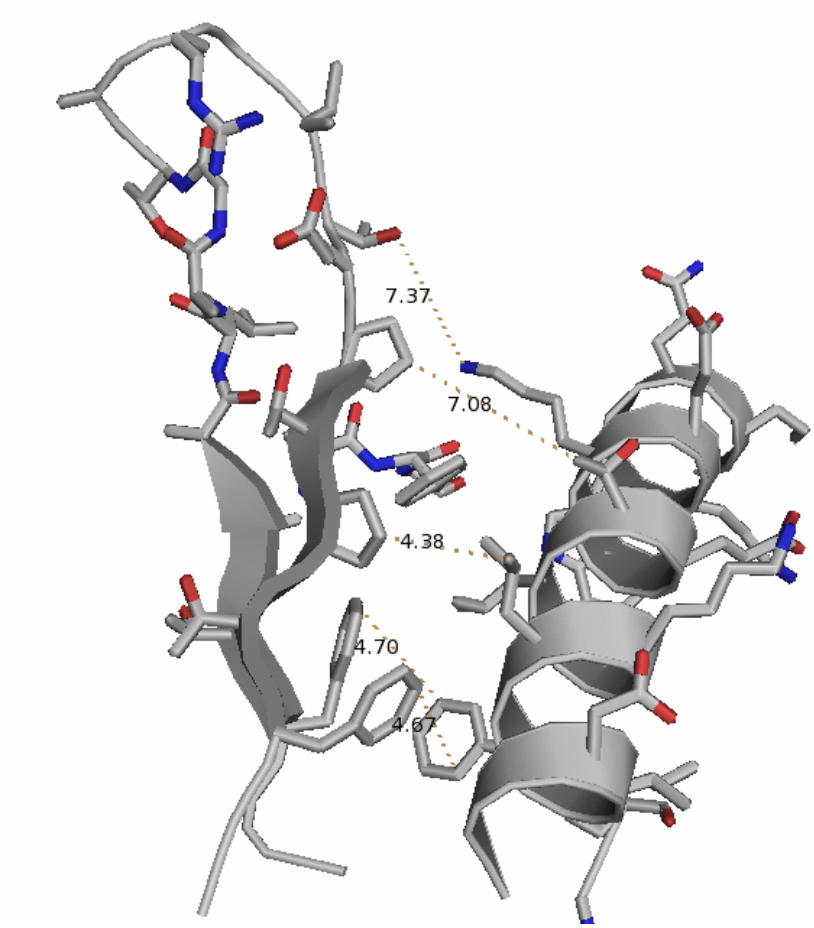

Figure 4.8. Lid made by residues 385-405 from *E. coli* PCK. The lid is pointing away from the N-terminal domain and adjacent to the C-terminal helix made up of residues 505 to 521. Distances are shown in Angstroms. Image made with Pymol (DeLano 2002).

Similar lids/loops are observed in other enzymes but none are comparable in function to the lid of ATP-dependent PCK.

The P-loop of GTP-dependent PCK also acts as a mobile active site loop that is possibly used for the regulation of catalysis. In a series of chicken mitochondrial PCK crystal structures, the conformation of the GTP-binding P-loop is observed to vary with the oxidation state of its environment. When PCK is in an oxidating environment, the cysteine of the P-loop becomes deprotonated, which causes the rearrangement of the P-loop so the side chain sulfur atom of Cys288 can coordinate Mn^{2+}. The new conformation of the P-loop distorts, preventing GTP from binding. Moreover, it results in Mn^{2+} changing coordination state. Instead of being octahedrally coordinated Mn^{2+} becomes tetrahedrally coordinated. When the metabolic conditions in the cell change and the environment in the mitochondria becomes reducing, the cysteine become protonated and the conformation of the P-loop reverts to a shape that allows for GTP/GDP binding. The coordination number of Mn^{2+} then returns to six. Once Mn^{2+} is coordinated octahedrally, the substrates can position themselves properly and react (Holyoak *et al.* 2006). These findings suggest that the activity of PCK is regulated by the amount of oxidizing or reducing agents present in the environment. This conclusion is in agreement with a study that determined gluconeogenesis in rat liver cells is stimulated when subjected to a reducing environment (Arinze *et al.* 1973).

A crystallographic study of yeast triosephosphate isomerase, TIM, has shown that a mobile active site loop is covering the active site. Crystal structures of TIM solved in the open and closed conformation indicate that the lid must be open

for substrate to bind and product to be released. The secondary structure of the lid is a random coil, and unlike the lid of ATP-dependent PCK; the overall length of the lid from TIM is shorter than its width giving it more of a 'flap' appearance. When the substrate, dihydroxyacetone phosphate or glyceraldehyde-3-phosphate, is bound to the active site, it is completely covered by the lid. For catalysis to occur, the lid needs to close over the active site and cover the substrate. An NMR experiment has determined that the time it takes for the loop to open and close is partially rate limiting for the forward and reverse reactions catalyzed by TIM (Rozovsky and McDermott 2001). The function of the lid is similar to what is proposed for to ATP-dependent PCK, the lid in TIM encourages catalysis by isolating substrates.

The active site lid from human pancreatic lipase is long and narrow like that occurring in ATP-dependent PCK, but instead of being made up of a β-hairpin turn, the loop is made up of a helix-turn-helix motif. One of the functions of the lid is to 'gate' the hydrophobic portion of the active site from the solvent so that only the hydrophobic portion of its substrate can bind (Cherukuvada *et al.* 2005). Another study on lipase created a mutant with a lid shortened through a deletion mutation. It was determined that the activity of the enzyme becomes substantially reduced but not abolished like what occurs for the Δ2x2 mutant of *A. succiniciproducens* PCK. Other kinetic features of the lipase are also abolished, demonstrating the importance of the active site lid (Jennens and Lowe 1994).

4.3 *E. coli*-PCK-ATP-Mg^{2+}-CO_2 Structure

The *E. coli*-PCK-ATP-Mg^{2+}-CO_2 crystal structure, PCK2, proved valuable for a number of reasons. First, the crystal diffracted to a resolution of 1.6 Å; thus, most of the structure, especially the active site, can accurately be resolved. The second reason, is that this is the second crystal structure of ATP-dependent PCK that has the lid made by residues 385-405 completely resolvable. The importance of this lid has been discussed in the previous section. Thirdly, the technique of subjecting the crystal to a high-pressure atmosphere of CO_2 to create the PCK2 structure was successful. Another reason this structure is of value is that is that it directly confirms that there is a binding site on the enzyme for the CO_2 molecule.

To create a crystal of PCK complexed with gaseous CO_2, a lesser used technique was employed. CO_2 was incorporated into the protein crystal structure using a high-pressure CO_2 atmosphere. The advantage of this technique is that it directly incorporates CO_2 in the structure. If an indirect approach, such as using the bicarbonate ion to furnish CO_2 is employed, there are more variables in the crystallization steps to consider. Issues affecting the bicarbonate ion such as pH, concentration and side reactions could make it more difficult to grow a crystal. It should be noted however that a CO_2-containing crystal of *E. coli* PCK, PCK1, was grown using the bicarbonate ion (Cotelesage *et al.* 2007). Other gases such as oxygen (Sjögren and Hajdi 2001), nitric oxide (Copeland *et al.* 2003) and xenon (Sauer *et al.* 1997) have been added to protein crystals by subjecting the crystals to high pressures of the respective gases. However, xenon is the only gas that is

routinely added to crystals. Xenon is employed to create heavy-atom derivatives of crystals for phasing (Sauer *et al.* 1997).

The location of CO_2 in PCK2 is very close to where CO_2 is located in PCK1 (Cotelesage *et al.* 2007). PCK2 and PCK1 both have the same unit cell and space group. The one exception is the length of the *b* axis, which in PCK2 is shorter by almost 5 Å. *E. coli* PCK has already been solved in this crystal form a few times and the length of the *b* axis in all the other structures is closer to that of PCK1 (Tari *et al.* 1997; Sudom *et al.* 2001). The shortened axis length can possibly be attributed to crystal dehydration. The initial stages of protein crystal dehydration will often result in one of the unit cell dimensions decreasing (Perutz 1946).

The most significant difference between the crystal structures of PCK1 and PCK2 is the orientation of the CO_2, which, relative to each other is approximately 75 °. The different orientation of CO_2 is because Mn^{2+} is not present in the PCK2 structure. In PCK1 Lys213 is held in place due to it coordinating Mn^{2+}, while in PCK2 the amine portion of the side chain of Lys213 is free to point in the opposite direction and hydrogen bond with an oxygen atom from one end of the CO_2 molecule. The hydrogen bond between the oxygen atom from the other end of CO_2 and Tyr207 is present in PCK2 and PCK1, Figure 4.9.

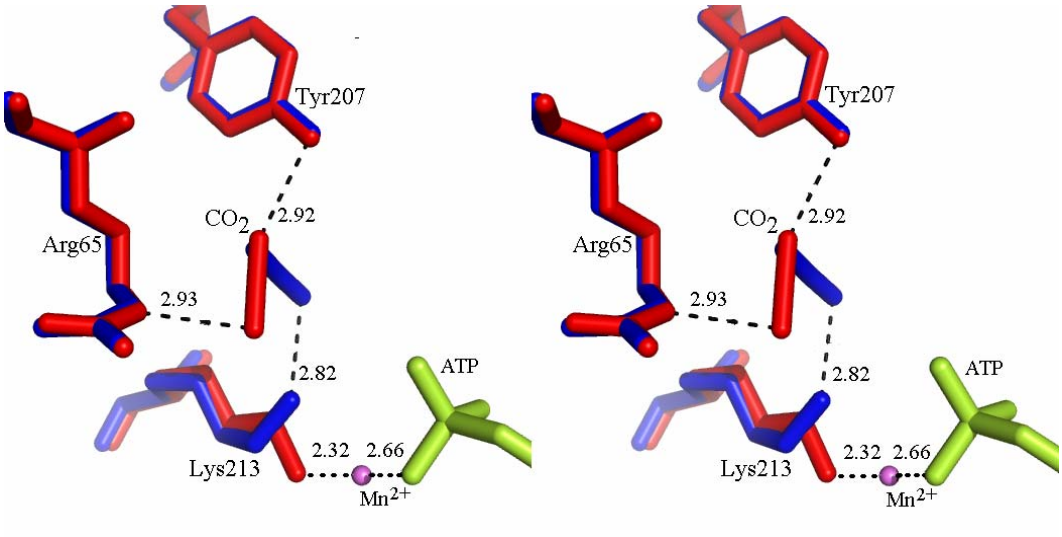

Figure 4.9. The active sites of the PCK-ATP-Mg^{2+}- CO_2 crystal structure, PCK2, shown in blue, and PCK-ATP-Mg^{2+}-Mn^{2+}-CO_2 crystal structure, PCK1, shown in red, superimposed. CO_2 in PCK1 is hydrogen bonded to the side chains of Arg65 and Tyr207. CO_2 in PCK2 is hydrogen bonded to the side chains of Tyr207 and Lys213. ATP, shown in green, is observed in both structures. Mn^{2+} is only present in PCK1; the side chain of Lys213 of PCK1 is coordinating Mn^{2+}. Stereo image made with use of Pymol (DeLano 2002).

The difference in the orientation of CO_2 between PCK2 and PCK1 may explain in part the ability of Mn^{2+} to activate the reaction rate of PCK. When PCK catalyzes the forward reaction without Mn^{2+} present, the decreased rate of decarboxylation may be because the side chain amine group of Lys213 makes the labile carboxylate group of oxaloacetate a poorer leaving group. If the amine group of Lys213 is orientated towards the carboxylate group of oxaloacetate instead of coordinating Mn^{2+}, the side chain of Lys213 may be disrupting the electronic

environment created by the side chains of Arg65 and Tyr207 needed to encourage the decarboxylation of oxaloacetate.

In the case of the reverse reaction catalyzed by PCK, when Mn^{2+} is not present, the crystal structures indicate that CO_2 is oriented differently in the active site. By being orientated differently, CO_2 is not ideally located to be affixed to *enol* pyruvate/PEP. There is also the possibility that the different hydrogen bonds made between PCK and CO_2 are also polarizing CO_2 in a manner that makes it less susceptible to the nucleophilic attack required to covalently attach it to *enol* pyruvate/PEP. The carboxylation reaction mechanism of PCK is further discussed in section 4.7.

For PCK to have a binding site for CO_2 is unusual, CO_2 binding sites are believed to be relatively rare in enzymes (O'Leary 1992). A study analyzing the effect of a R65Q mutation demonstrates that the K_m for CO_2 does not significantly change (Cotelesage *et al.* 2007). This mutation implies that CO_2 is making a hydrogen bond with the ε-nitrogen of Arg65 binding CO_2. Glutamine contains an ε-nitrogen atom that is the same number of atoms away from its α-carbon like the ε-nitrogen of arginine. The results of the kinetic study shown in section 3.7 show that when Arg65 is mutated to alanine in *A. succiniciproducens* PCK the K_m for CO_2 increases four-fold. These results also reaffirm the role that the ε-nitrogen in Arg65 has in CO_2 binding.

The proposed reaction mechanism for the reverse reaction of PCK in section 4.8 postulates that the conversion of PEP into oxaloacetate requires the reaction intermediate pyruvate to be in a reactive and short lived carbanion form. To compensate for the unstable intermediate, PCK holds CO_2 in a location where

the carbanion forms so it can immediately react as opposed to waiting for a random collision with an unbound CO_2. More on reaction mechanisms will be discussed further in section 4.8.

There are only a few published crystal structures that contain CO_2. Some of the solved structures containing CO_2 include: deacetoxycephalosporin C synthase (DAOCS), pyruvate:ferredoxin oxidoreductase (PFOR) and uroporphyrinogen decarboxylase (UD). In the DAOCS crystal structure one oxygen atom of CO_2 is hydrogen bonded in the active site to an arginine residue and a water molecule (Lee *et al.* 2001). The crystal structure of UD shows one of the oxygen atoms of CO_2 is hydrogen bonded by an arginine residue and water molecule (Phillips *et al.* 2003). In the PFOR crystal structure one of the oxygen atoms is hydrogen-bonding to an asparagine residue, while the other oxygen atom is hydrogen bonded to the side chains of both a threonine and a lysine residue (Chabrière *et al.* 2001). The common interaction between CO_2 and the protein is that CO_2 makes hydrogen bonds with a basic amino acid side chain.

The probable reason for CO_2 hydrogen bonding with a basic side chain is to polarize CO_2 by drawing electrons to its oxygen atoms making its carbon atom more electron deficient. In the case of carboxylation reactions, a more electrophilic carbon atom has increased reactivity towards a nucleophilic attack. It should be noted that only PCK and PFOR each physiologically function as a decarboxylase/carboxylase. DAOCS and UR are presumed to each function only as a decarboxylase (O'Leary 1992). The effect a basic amino acid side chain has in context of a decarboxylation reaction may be by disrupting the resonance-stabilized form of the carboxyl group of the substrate. The carboxylate group of the reacting

molecule is made unstable by disrupting delocalization of its electrons and therefore destabilizing the resonant structure making it higher in energy, less stable and therefore a better leaving group.

4.4 *E. coli* –PCK-ATP-oxaloacetate-CO_2-Mg^{2+}-Mn^{2+}

It has been a challenge to produce a crystal structure of ATP-dependent PCK complexed with oxaloacetate. Many unsuccessful attempts have been made to co-crystallize PCK with oxaloacetate. A number of attempts have also been made to soak oxaloacetate solutions into a PCK crystal. Soaking crystals in conservative volumes and concentrations of oxaloacetate have not worked in the past. Adding larger volumes and concentrations of oxaloacetate somehow severely reduced the ability of the crystal to diffract and in some cases, it just outright destroyed the crystal (unpublished results by the author). Considering the relative ease it has taken to produce well diffracting *E. coli* PCK crystals complexed with other substrates and analogues, it is unusual that after thousands of attempts it has not been possible to incorporate oxaloacetate into a PCK crystal. A search of the Protein Data Bank (Berman *et al.* 2000) determined that oxaloacetate has been successfully co-crystallized in five different proteins. None of the methods in the supporting literature makes mention of any extraordinary procedures required to incorporate oxaloacetate into the crystal. In at least two of the structures, oxaloacetate is cocrystallized with the protein of interest (Hall *et al.* 2004; Karpusas *et al.* 1990). The other structures incorporated oxaloacetate by simply soaking oxaloacetate into pre-grown crystals (Auerbach *et al.* 1997; Huang *et al.* 2005; Kim *et al.* 1999).

There may be number of reasons as to why it is so difficult to produce a well-diffracting crystal of PCK complexed with oxaloacetate. It is known that in the presence of divalent metals and especially under acidic conditions oxaloacetate is prone to spontaneous decarboxylation to pyruvate (Krebs 1942). The findings by Krebs demonstrate that the range of crystallization conditions under which oxaloacetate is limited. Obviously, PCK cannot be co-crystallized with oxaloacetate and ATP, as it would just react to form PEP. There have been attempts to crystallize PCK in the presence of ADP with the hope that oxaloacetate would bind in the active site but not be able to react. It has been found that all grades of ADP used in the crystallization attempts contain ATP as an impurity (unpublished work from Hughes Goldie, Department of Microbiology, University if Saskatchewan). Thus, the attempts to crystallize PCK with oxaloacetate, ADP and a divalent metal have failed probably because crystallization environment becomes a heterogeneous mixture of substrates and analogues involved in a complicated equilibrium. PCK in this environment will be continuously catalyzing the forward and reverse reaction and therefore continuously undergoing substrate-induced domain movement. It is this lack of conformational homogeneity that may be the reason PCK is not crystallizing (Giegé *et al.* 1995). Another issue with PCK that could be preventing crystallization may be because it can catalyze the decarboxylation of oxaloacetate with and without ATP present. This nucleotide-free side reaction has been observed in *E. coli* (Hou *et al.* 1995), yeast (Cannata and Stoppani 1963) and *A. succiniciproducens* PCK (Jabalquinto *et al.* 1999). This unintended side reaction may be creating conditions not conducive to crystal growth. The obvious alternative is to attempt to crystallize PCK only with oxaloacetate as a substrate. Attempts

using this approach have not been successful; even if a structure were to be obtained, the biological significance would be in question because it is likely that many of the catalytically important interactions oxaloacetate makes with PCK involve a divalent metal.

Further searches of the Protein Data Bank (Berman *et al.* 2000) found twenty-four protein crystal structures complexed with oxaloacetate. Of the twenty-four, nine structures are of chicken citrate synthase. No divalent metals were present in the crystal structures of citrate synthase as they are not needed for catalysis (Karpusas *et al.* 1990). Six more making a total of fifteen of the twenty-four oxaloacetate containing structures were solved from crystals grown without divalent metal ions present in the crystallization conditions. Nine more of the structures were solved from crystals grown in the presence of metal of which seven contain a divalent metal. The pH range the crystals grew in was 4.7 to 8.2; the majority of the metal-containing structures were solved from crystals grown at a pH above 7. This is in agreement with the finding that oxaloacetate is more stable at higher pHs (Krebs 1942).

4.4.1 Location of Substrates

The PCK-ATP-Mg^{2+}-Mn^{2+}-CO_2-oxaloacetate crystal structure reveals a non-catalytic second binding site for oxaloacetate, Figure 3.13. Interestingly oxaloacetate is observed at an unexpected location just beyond the active site. Instead of coordinating Mg^{2+} as expected (Tari *et al.* 1997), oxaloacetate is 5 Å away. The non-hydrogen atoms of oxaloacetate in the structure have an occupancy of 0.7. The reason for the lower occupancy of oxaloacetate may be because of the

techniques used to add it to the crystal. The only way to successfully incorporate oxaloacetate into the PCK crystal was to soak an existing crystal in a saturated solution of oxaloacetate, remove the crystal from the solution and flash cool it. It was found that there was only a very short window of time to successfully bind oxaloacetate into PCK. The crystals that were soaked for less than 15 minutes did not contain oxaloacetate and the ones soaked for any longer were damaged and did not diffract X-rays well enough for structure determination.

There are four direct interactions oxaloacetate makes with PCK. There are two hydrophobic contacts between the C3 methylene group of oxaloacetate and the β-carbon methylene groups of Leu249 and Ser 250. The amide nitrogen of Leu249 makes a hydrogen bond with the carboxylate group of C1 and a van der Waals contact with C2. Oxaloacetate is also hydrogen bonding with three ordered water molecules, one of which is coordinated to Mn^{2+}, the other two are hydrogen bonded to PCK residues, Figure 3.13. The importance of the ordered water molecules in PCK will be further discussed in section 4.6. Although not observed in this structure, another weak hydrogen bond between PCK and oxaloacetate can potentially form if the side chain of Ser250 is rotated 90 ° towards the C1 carboxylate group of oxaloacetate.

The location of CO_2 in this structure is the same region observed in PCK1. However, due to the resolution of the structure, the volume of the electron density in the region between Arg65 and Tyr207 is larger than the expected size of CO_2 and therefore makes determining the precise orientation impossible. However, it is likely that hydrogen bonds occur with Arg65 and with Tyr207, similar to the

interactions found in the PCK1 structure. It may be because of the CO_2 bound in the active site of PCK that oxaloacetate is observed in a non-catalytic second binding site. CO_2 could be physically blocking oxaloacetate from binding in the active site and therefore forcing it to bind in the pocket made by Leu249 and Ser250 and three ordered water molecules.

Instead of ADP being found in the active site, ATP was found which was not too unexpected because ATP is known to be an impurity in most grades of ADP.

4.4.2 Conformation of Oxaloacetate

The conformations oxaloacetate adopts in the twenty-four protein-oxaloacetate crystal structures were compared. The torsion angles made by atoms C1-C2-C3-C4 of oxaloacetate were measured and compared with the modeling software COOT (Emsley and Cowtan 2004). With the exception of one structure examined, oxaloacetate took only two conformations. The first type was observed in fourteen structures while the second type was seen in the other nine. The first major conformation of oxaloacetate has the torsion angle of 96 ± 14˚. The second conformation taken by oxaloacetate has the torsion angle of 175 ± 6˚, figure 4.10. It should be kept in mind that the in this conformation oxaloacetate may be in the enol tautomer form. In the PCK-ATP-Mg^{2+}-Mn^{2+}-CO_2-oxaloacetate structure presented

here, oxaloacetate has a torsion angle of 162 °, which puts it in the second conformation group.

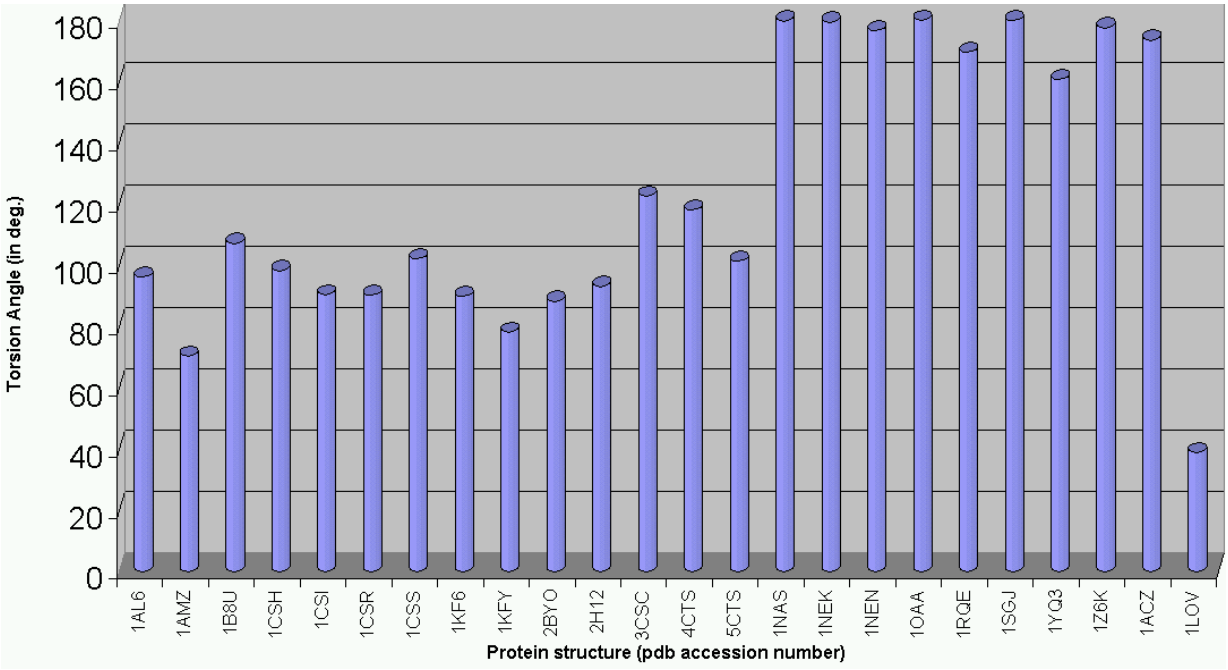

Figure 4.10. Torsion Bond Angles of Oxaloacetate Found in Protein Crystal Structures. Torsion angle of oxaloacetate defined by atoms C1-C2-C3-C4.

4.4.3 Role of Lid (residues 380-405) in Positioning Oxaloacetate

In the calculated electron density maps of the *E. coli* PCK-ATP-Mg^{2+}-Mn^{2+}-CO_2-oxaloacetate crystal structure, the portion of the lid made by residues 394-399 cannot be resolved. However, this crystal complex was grown in the same experimental setup as the PCK-ATP-Mg^{2+}-CO_2 crystals examined in section 3.3. Thus, it can be confidently assumed that the lid in this structure is not folded over the active site. Another reason oxaloacetate is observed in an unexpected location in

this crystal structure may be because the lid region formed by residues 385 to 405 is not folded over the active site. When the *E. coli* PCK-ATP-Mg^{2+}-Mn^{2+}-CO_2-oxaloacetate structure is superimposed with the nearly identical *A. succiniciproducens* PCK ATP-Mg^{2+}-Mn^{2+}-oxalate crystal structure, some possible steric conflict with oxaloacetate and the side chain from the lid on residue Lys390 is observed, Figure 4.11.

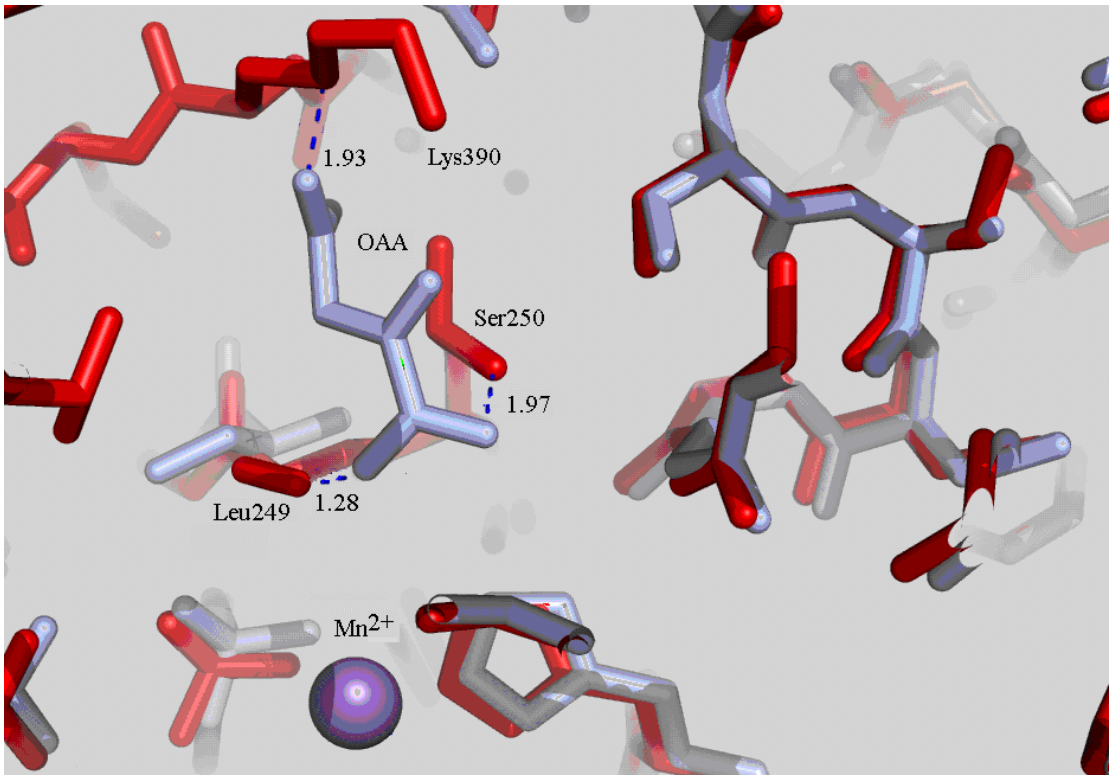

Figure 4.11. *E. coli* PCK-ATP-Mg^{2+}-Mn^{2+}-CO^2-oxaloacetate (purple) superimposed with *A. succiniciproducens* PCK-ATP-Mg^{2+}-Mn^{2+}-oxalate (red). Residues from *A. succiniciproducens* PCK that are close to oxaloacetate (OAA) are labeled (distances are shown in Angstroms). Image made with use of Pymol (DeLano 2002).

In light of these observations, a novel function for the lid and the non-catalytic binding site of oxaloacetate is proposed. The lid may be directing oxaloacetate to the active site. When oxaloacetate initially binds to PCK, it is at the observed non-catalytic binding site where it waits for ATP to bind. Then when ATP binds, domain closure brings the lid over to the N-terminal domain which pushes oxaloacetate towards the active site. It is unclear what purpose this sort of mechanism serves. One possibility is that the second non-catalytic binding site may be to increase the affinity PCK has for oxaloacetate. Some forms of xylanse (Black *et al.* 1995) and esterase (Ferreira *et al.* 1993) are known to have non-catalytic binding sites. For both these enzymes, it is thought that the function of the non-catalytic binding sites is to increase their affinity for substrates.

Another possible function for the non-catalytic binding site in PCK may be for properly aligning oxaloacetate in the active site. There is at least one example of an enzyme that utilizes a second non-catalytic binding in a similar manner (Birdsall *et al.* 1996). Thymidylate synthase, TS, catalyzes the conversion of deoxyuridyl monophosphate, dUMP to deoxythymidylate monophosphate, dTMP. During the conversion 5,10-methylene-5,6,7,8-tetrahydrofolate, CH2THF, donates one of its methyl groups to dUMP to form dTMP. Through a series of crystal structures, it was concluded that when CH2THF initially binds TS, it binds in a non-catalytic binding site, presumably to align itself properly relative to the already bound dUMP. Then TS undergoes a conformational change that results in CH2THF being moved to the active site where it can transfer its methyl group to dUMP. The C-terminal end of TS is near the non-catalytic binding site and it is thought that the last residue of the C-terminal end is involved in moving the CH2THF out of the

active site, possibly by steric crowding. A mutational study was done on TS that removed the last two residues of its C-terminal end (Perry *et al.* 1999). It was observed that when the last residue of the C-terminal end were removed TS was rendered inactive.

It is proposed that steric crowding is responsible for positioning a substrate in chicken mitochondrial PCK (Holyoak *et al.* 2006). When the crystal structure of chicken mitochondrial PCK-PEP-Mn^{2+} complex is superimposed on the crystal structure of chicken mitochondrial PCK complexed with GDP and Mn^{2+}, it is observed that PEP is too far away to react with ADP. The crystal structures show the side chain of Tyr254 can adopt two conformations. One of the conformations would have steric clashes with PEP bound in the location found in the crystal structure. It has been proposed that after the substrates bind PCK, the side chain of Tyr254 pushes bound PEP out of its binding site and puts it in a location in the active site where it can react (Holyoak *et al.* 2006).

4.5 *E. coli* K213S PCK-ATP-Mg^{2+}-Mn^{2+} Structure

The crystal structure of the K213S mutant PCK was essentially the same as all other ATP-dependent PCK crystal structures. The location of substrates, cofactors, many of the ordered water molecules and most active site residue side chains are found in expected locations. Mn^{2+} is found in its usual location but instead of being coordinated octahedrally as observed in all the other ATP-

dependent PCK crystal structures, it is coordinated in a tetrahedral fashion. Mn^{2+} is observed to coordinate tetrahedrally in at least one GTP-dependent PCK crystal structure (Holyoak *et al.* 2006). Tetrahedrally coordinated inorganic Mn^{2+} complexes are known to exist, though they are not as common as octahedral Mn^{2+} compounds (Cotton and Wilkinson 1980).

The reason that Mn^{2+} undergoes tetrahedral coordination in K213S is likely due to Lys213 being absent from the structure. It would make sense to presume that when the lone pair electrons from the ζ-nitrogen of Lys213 are not coordinating Mn^{2+}, there is extra space for the lone pair electrons from the other two coordinating side chains and γ-phosphate oxygen of ATP to rearrange to maximize the distances amongst themselves. However, when the K213S crystal structure is superimposed over a wild type Mn^{2+}-containing PCK crystal structure the bond distances and angles His232, Asp269 and the ATP γ-phosphate make with Mn^{2+} appear unchanged. The only coordinating water molecule is on the other side of Mn^{2+}, equidistant from the other three lone pair of electrons from His232, Asp269 and the ATP γ-phosphate, resulting in a somewhat distorted tetrahedral shape. The angle subtended by the water molecule, Mn^{2+} and His232 is 110˚ as expected in a tetrahedron. The angles the coordinating water molecule and Mn^{2+} make with Asp269 and the γ-phosphate of ATP are 128˚ and 118˚ respectively. The coordination bond lengths for the four ligands are all between 2.05 to 2.22 Å. The bond distances and bond angles compare favourably to what is observed in the chicken mitochondrial PCK structure (Holyoak *et al.* 2006).

Crystal field theory is used in inorganic chemistry to explain the coordination geometry of coordination complexes (Cotton and Wilkinson 1980). This theory may explain why the K213S PCK mutant has its Mn^{2+}coordination geometry change from octahedral to tetrahedral. In K213S, the region around Mn^{2+} there is one fewer set of lone pair electrons due the absence of the Lys213 side chain; it is plausible that water molecules in this area are not ordered enough to coordinate Mn^{2+} in place of Lys213. Then the only remaining coordinating water molecule reorients to form a tetrahedral arrangement with the other ligands around Mn^{2+}. The main assumption of the crystal field theory is that the ligands that are coordinating the metal are treated as point negative charges. Then depending on the number of ligands coordinating the metal atom, the d-orbitals of the metal will split to stabilize the compound. Orbital splitting is the phenomenon when the five, equal in terms of energy, d-orbitals are divided into groups of higher and lower energy. The total energy of the orbitals, however, remains the same. The orbitals that are pointing towards the ligands become higher by a certain amount of energy, while the orbitals not facing the ligands are lowered in energy by the same amount.

When there are only four lone pairs of electrons around Mn^{2+}, the lowest energy state that can be attained by the complex is the tetrahedral geometry. In the K213S PCK mutant this is achieved by breaking the degeneracy of the d-orbitals of Mn^{2+}. The two lower energy orbitals, d_z^2 and d_x^2-$_y^2$ wind up pointing away from the four ligands, minimizing the energy sufficiently to stabilize the complex. This is opposite to what occurs with octahedral complexes. The lowest energy the orbitals can be an arranged in an octahedral complex is by designating d_{xy}, d_{yx} and d_{zx} as the

lower energy orbitals because they are farthest away from the six orthogonally oriented point negative charges (Cotton *et al.* 1987).

If the reasoning for the stable tetrahedral arrangement of Mn^{2+} in K213S is taken as correct, the inhibitory nature Mn^{2+} has on the K213S PCK mutant in kinetic assays can be rationalized. When oxaloacetate binds, only one of its carbonyl oxygen atoms can coordinate Mn^{2+}. In this situation, Mn^{2+} cannot assist with catalysis because the oxaloacetate coordinating will not be able to be positioned properly in the active site to react and form PEP. Since only one of the oxygen atoms from oxaloacetate can coordinate Mn^{2+}, there are many possible ways for oxaloacetate to orient itself in the active site. Since the bulky side chain of Lys213 is absent, oxaloacetate will have even more freedom to orient itself in the active site. It was possible to manually model in oxaloacetate into at least two potentially stable binding sites without being properly oriented near catalytic residues, Figure 4.12. It is known that the reactivity of enzyme-bound enolate molecules involved in carboxylation reaction increases when it is coordinating a divalent metal (O'Leary 1992). The metal is involved in stabilizing the anion intermediate by drawing and consequently delocalizing electrons away from the high energy transition state intermediates required for catalysis. In the case of the K213S PCK mutant, this effect cannot occur sufficiently because only one part of oxaloacetate is interacting with Mn^{2+}.

From the work presented here, it appears that Mn^{2+} is inhibiting activity in the K213S PCK mutant by altering how oxaloacetate interacts with PCK in at least two possible ways. One is by disrupting the precise alignment of oxaloacetate

required for catalysis due to the tetrahedral shape of the Mn^{2+} complex it forms. The other reason for inhibition is by the reduction or elimination of the electron withdrawing effects Mn^{2+} has on oxaloacetate when it is a mondentate ligand, which may make it less reactive.

It should be mentioned that without Mn^{2+} present, assays have determined that the K213S mutant has the same amount of kinetic activity as Mn^{2+}-free wild-type PCK. Furthermore, under these conditions, the K_m the K213S PCK mutant has for the ATP-Mg^{2+} complex is one fourth of what is observed with wild-type PCK (Novakovski 2001). The possible reason for the decrease in K_m is that some of the electron withdrawing effect Mn^{2+} would have on the γ-phosphate of ATP are now absent. The extra negative charge on ATP results in tighter binding with its positively-charged environment in the active site.

The abolition of the oxaloacetate decarboxylase-like activity in the K213S PCK mutant also suggests that oxaloacetate binding is somehow disrupted (Novakovski 2001). For the oxaloacetate decarboxylase-like reaction to occur, oxaloacetate is required to bind in the active site normally. The same interactions and reaction mechanism pertaining to decarboxylation are expected to occur; the only real difference this reaction has with the forward reaction of PCK is that no phosphoryl group transfer occurs. The lack of oxaloacetate decarboxylase-like activity in K213S suggests that oxaloacetate is not able to bind properly. It was also determined in the same study that the mutants H232Q and D269N lacked oxaloacetate decarboxylase-like activity as well. The His232 and D269 residues directly interact with Mn^{2+}; leading to the conclusion that both mutations are also

disrupting Mn^{2+} binding, which results in the loss of oxaloacetate decarboxylase-like activity.

A

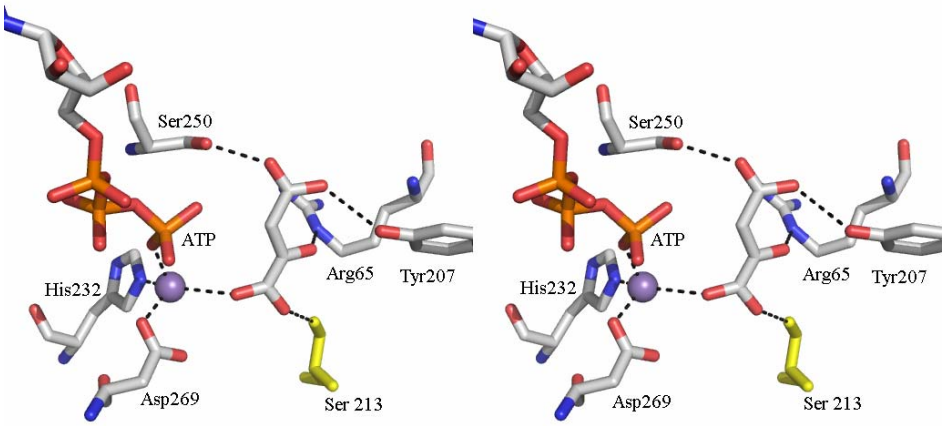

B

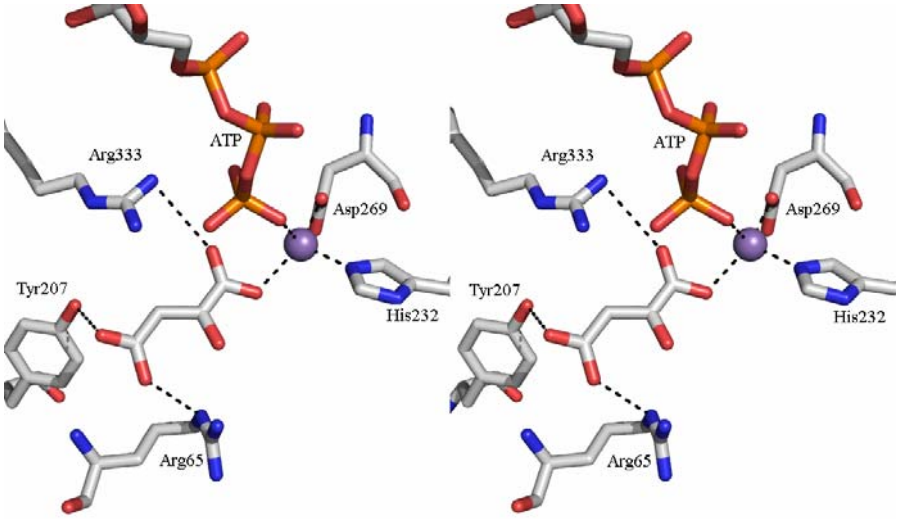

Figure 4.12. Potential alternative binding sites for oxaloacetate in the K213S PCK mutant when Mn^{2+} is tetrahedrally coordinated. **A**. One of the hydrogen bonds oxaloacetate forms is with the Ser213. In this orientation, oxaloacetate is positioned too far away from ATP for the phosphoryl transfer step. **B.** In this orientation, the carbonyl group of C2 is not in line with the γ-phosphate. Stereo images made with Pymol (DeLano 2002).

4.6 Survey of Ordered Water Molecules

It is fortunate that many crystal structures from four species of ATP-dependent PCK have been solved. This has allowed for a systematic comparison between them to determine if there are any common structural features amongst them. To understand better the roles ordered water molecules play in PCK, all the known ATP-dependent PCK crystal structures were superimposed with the DeepView software (Guex and Peitsch 1997) and examined. Four structures were left out of the survey as they were in the open conformation and would be difficult to properly superimpose, but they themselves were compared in the same fashion. In total nine structures in the closed conformation were overlapped and examined. There are seven structures from *E. coli*, and one each from *A. succiniciproducens* and *T. cruzi* (PDB accession numbers: 1AYL, 1AQ2, 1KC3, 1K3D, 2PY7, 2PXZ, 2OLR, 1YTM, 1II2)(Cotelesage *et al.* 2005; Cotelesage *et al.* 2007; Sudom *et al.* 2001; Tari *et al.* 1997; Tari *et al.* 1996; Trapani *et al.* 2001). The combined structures were visually inspected to determine which water molecules are common between the various species and complexes. The criteria for deciding whether a particular water molecule was structurally or catalytically important in PCK occured when all species had a water molecule at the same position. To be considered part of the cluster a water molecule has to be less than 1 Å from the cluster made by water molecules from the other structures, Figure 4.13.

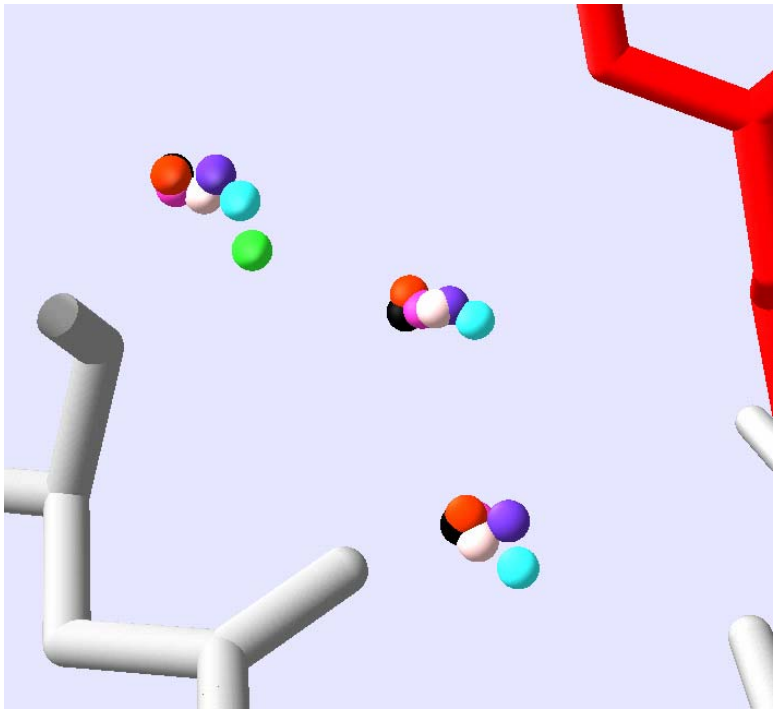

Figure 4.13. An example of three ordered water molecules that are conserved in *E. coli, T. cruzi* and *A. succiniciproducens* PCK. To determined which water molecules are ordered and conserved, nine ATP-dependent PCK crystal structures were superimposed and the models were searched for clusters of water molecules. Each colour of sphere represents a water molecule from a particular structure. For clarity, the protein atoms from only one structure are shown. Image made with DeepView (Guex and Peitsch 1997).

Some of the water molecules in the crystal structures are already known to be conserved because they are directly interacting with substrates or cofactors. In most of the PCK structures containing both Mg^{2+} and Mn^{2+}, the two metals are coordinated in part by water molecules. There are also a number of conserved non-

catalytic water molecules that are near active site residues. It was found that there are about seventy-five water molecules present in all the crystal structures of PCK in the closed conformation. Of the seventy-five waters, only eighteen were on the surface. Many of the ordered water moleclues have clear roles in maintaining the protein structure by interacting with and properly positioning secondary structural elements. A common interaction made by the waters is to bridge two secondary structural elements through hydrogen bonds. Hydrogen bonds are observed to form between the peptide backbone amide and carbonyl oxygen, as well with residue side chains. It was observed that *E. coli* and *A. succiniciproducens* PCK have more conserved water molecules between themselves than *T. cruzi* has between either of them. Since *E. coli* and *A. succiniciproducens* PCK are closer in amino acid sequence (67 % identity) than is *T. cruzi* (42 % identity to *E. coli*), it is expected that there is a correlation based on sequence similarities.

An example of how ordered water molecules contribute to the structure of PCK can be observed in a pocket made by Tyr29, Ala54 and Ala308. In the pocket, there are three water molecules that are interacting with secondary structural elements of PCK. One of the water molecules is interacting with the N-terminal end of the α-helix made by residues 29 to 38. Another water molecule is held between two β-sheets made by residues 54-60 and 307-312. A third water molecule is bridging the two above-mentioned water moleclues. The three water molecules are shielded from bulk solvent by the side chains of Tyr33, Val55 and Arg306, Figure 4.14. Like this example, many of the other ordered water molecules conserved in all the PCK crystal structures seem to have a role in maintaining tertiary structure.

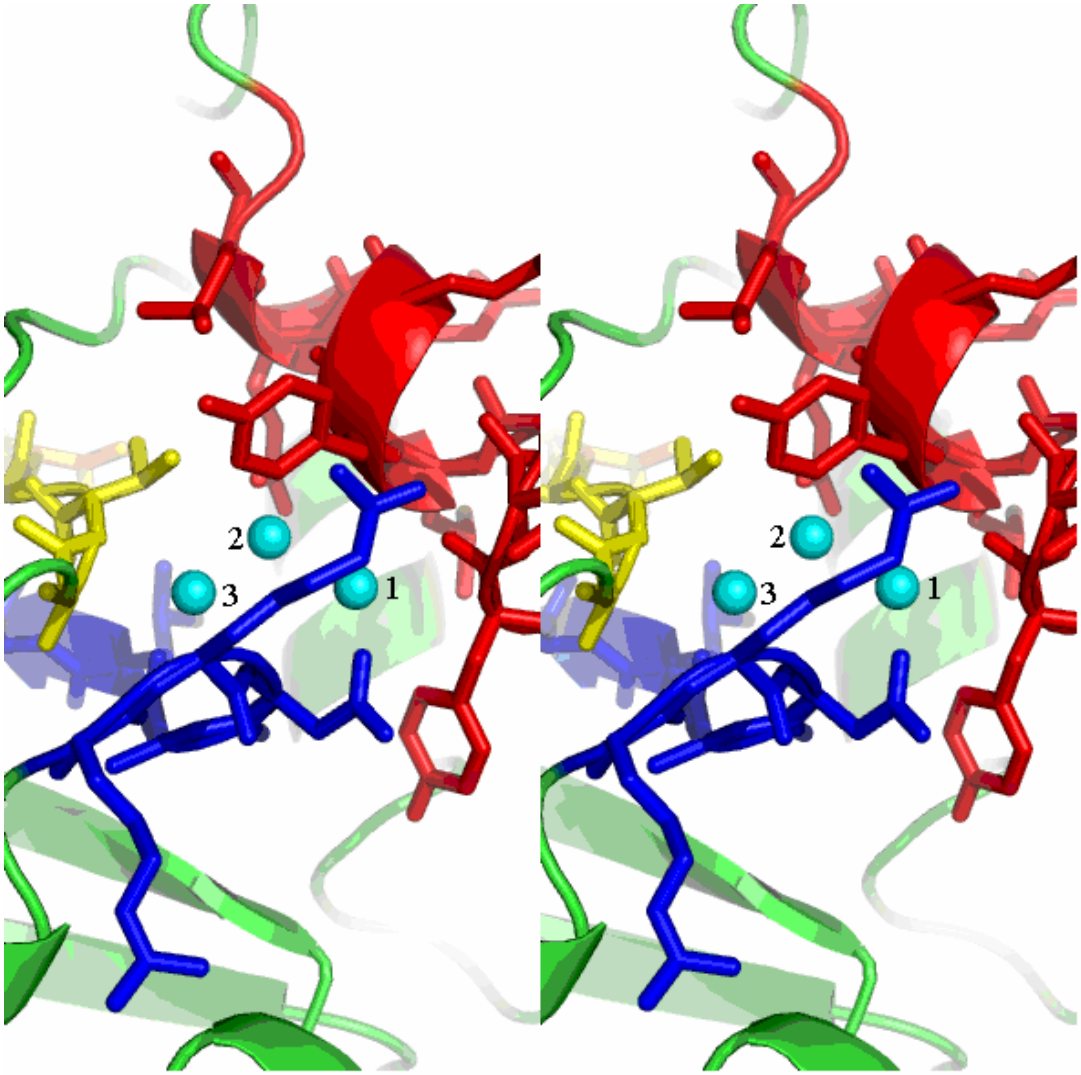

Figure 4.14. An example of conserved ordered water molecules conserved in ATP-dependent PCK. The three water molecules, shown as blue spheres, are all observed in PCK crystal structures from *E. coli, A. succiniciproducens* and *T. cruzi*. Two water molecules, 1 and 2, are interacting with the N-terminal end of the α-helix made of residues 29 to 38, in red. Another water molecule, 3, is held between two β-strands made by residues 54-60, in yellow and 307-312, in blue. Stereo image made with Pymol (DeLano 2002).

The same survey was done on the four PCK structures in the open conformation (1OEN, 1YVY, 1YGG, 1YLH)(Cotelesage *et al.* 2005; Leduc *et al.* 2005; Matte *et al.* 1996). Although all four of the structures superimposed well, there were about fifty water molecules that were conserved in all the structures. Most of them were found buried in the protein away from the surface, likely important for maintaining protein structure. When both surveys of the open and closed forms of PCK are compared, there are about 30 waters molecules conserved throughout all the structures. All of the common water molecules are found below the surface of PCK and presumably have a function in maintaining the tertiary structure of PCK.

The conclusions from the ordered water molecule survey are comparable to other surveys done with other types of proteins. For example, a number of crystal structures from the legume lectin family have been examined. Of the eleven structures made up from five different species it was found many water molecules have roles in stabilizing secondary structural elements. Similar to the study of ATP-dependent PCK, the closer any two sequences were in identity, the more water molecules were found to be conserved in both structures (Loris *et al.* 1994). Another study examining multiple crystal structures of ribonucleases from different sources have also observed many conserved water molecules between species (Loris *et al.* 1999). A study on elastase crystal structures from the same species examined a number of structures containing various solvents as a substitution for water. It is thought that by replacing water in the crystals with other solvents, all the water molecules in the structure that are bulk solvent would be replaced by the new solvent. Therefore, any water molecules that remains are more likely to be an

integral part of the protein tertiary structure. If the solvent is varied for a number of crystals, there would be a strong case for designating all the water molecules that remain conserved throughout all the structures as integral to the protein structure. A total of eleven structures were examined; all crystals were grown in different organic solvents; some solvents used include benzene, ethanol and acetone. Thirty nine water molecules were found to be conserved throughout all of the structures. Sixteen water molecules were buried in elastase and inaccessible by the bulk solvent, the rest of the waters were on the surface (Mattos and Ringe 2001). The findings from this study are comparable to what was determined in the survey done on ATP-dependent PCK. Elastase is roughly half the size of PCK and proportionally it has roughly half as many ordered water moleclues. The criteria in the PCK survey that considered a water molecule as being conserved were the same as that in the elastase study. Water molecules were required to be in all the structures examined and all water molecules had to be within 1 Å of the cluster. The notable differences between the two studies are that with PCK, only crystals with an aqueous environment were used and there were more than one species examined. Despite the differences, both approaches to studying the solvent structure of proteins give comparable results.

4.6.1 Ordered Waters in the Oxaloacetate Binding Site

To validate the proposed role for the lid in section 4.4.2, there must be confidence that the second non-catalytic binding site for oxaloacetate is biologically valid. Due to the weak interactions between PCK and oxaloacetate, it is difficult to decide if the binding site of oxaloacetate is biologically relevant. One way to rationalize the binding site is by considering how many interactions are present and whether they are arranged in a manner that minimizes the chance of non-specific binding.

In the case of the observed second oxaloacetate binding site of PCK, there are at least five interactions. Four interactions are directly with PCK atoms but the other one is with an ordered water molecule, Figure 3.13. The water molecule is observed to be conserved in all seven of the *E. coli* PCK crystal structures examined. There are two other water molecules bound by oxaloacetate but they are each only observed to be conserved in two of the crystal structures examined. Despite most of the interactions being weak it could be argued that there are sufficient specific interactions between oxaloacetate and PCK to suggest this is a true binding site. When the proposed function of the second oxaloacetate binding site is considered, it would be expected that this binding site inteacts with oxaloacetate weakly so the lid can dislodge it readily.

4.7 Role of Helix Dipole (residues 209-227) in Carboxylation/Decarboxylation

The use of a helix dipole to contribute electric charges in the active sites of proteins is routinely observed (Hol 1985). Triosephosphate isomerase for example has an active site histidine that uses a positive charge generated by a helix dipole to lower its pK_a. Glyceraldehyde 3-phosphate dehydrogenase also uses the positive charge from a helix dipole to stabilize the anionic form of an active site cysteine.

In nucleotide-binding proteins, a positive charge is often encountered at the amino end of an α-helix that is near the binding site of the phosphate groups of nucleotides (Matte *et al.* 1998). The reason for having the positive charge near the phosphate groups of nucleotides is to neutralize the negative charges of the phosphate group. By counteracting the large number of negative charges in the phosphate groups, nucleotides are more likely to undergo phosphoryl group transfers. In ATP-dependent PCK, a positive charge is believed to form at the N-terminal end of an α-helix made up of residues 254 to 259, to assist in neutralizing the cluster of negative charges from phosphate groups of ATP and to minimize the electrostatic repulsion between the enolate pyruvate hydroxyl group and phosphorus atom of the ATP γ-phosphate. In the case of the reverse reaction, the repulsion between ADP and PEP is minimized so the two molecules can be brought together to react (Tari *et al.* 1997). The observation of this and other positive charges around the phosphoryl groups of ATP demonstrate the importance of counter balancing the negative charges on the phosphates in order to facilitate catalysis.

In PCK there is another α-helix made up by residues 209-227 that may have an important role in catalysis. The amino end of the helix is near the region in

the active site where carboxylation/decarboxylation occurs. Based on the proposed reaction mechanisms of PCK, discussed in the next section, a positive charge in this region would be beneficial for catalysis in both directions.

It is known that partial electric charges can build up on the ends of an α-helix, but often it is only a small fraction of a full charge. It must be considered whether this helix dipole made by helix 209-227 is sufficiently strong enough to generate a significant charge. A study examining the structural and environmental factors in proteins that determine dipole strength confirm that the location of the helix made by residues 209-227 in PCK is ideal for creating a strong helix dipole (Sengupta *et al.* 2005). The study determined that the more exposed an α-helix is to solvent, the more its electric dipole was reduced. However, if one end of the helix is exposed to solvent and the other end is not, the dipole can be strong and generate a larger charge. The α-helix made up of residues 209-227 has its carboxyl end exposed to the surface while the amino end is buried in the active site away from water. It is reasonable to assume the N-terminal end of the α-helix made up of residues 209-227 has at least a +0.5 charge, although theoretically a helix dipole can generate a charge as high as +/- 0.7 (Sengupta *et al.* 2005).

The predicted location of the dipole-generated positive charge is near Gly209. In the CO_2-containing PCK crystal structures, the location of CO_2 is about 4 Å from Gly209, leading to the conclusion that the positive charge is assisting both the forward and reverse reaction of PCK, Figure 4.15.

During the forward reaction of PCK, the dipole may be assisting decarboxylation by disrupting the arrangement of the delocalized electrons of the resonance stabilized carboxylate group. This in turn makes the carboxylate group

unstable and more favourable to dissociate from the rest of the molecule. A similar situation has been observed with the enzyme transcarboxylase 12S, an enzyme that catalyses the conversion of methylmalonyl-CoA and pyruvate to propionyl-CoA and oxaloacetate. Evidence from one of its crystal structures suggests that a positive charge from a helix dipole is assisting the decarboxylation of oxaloacetate (Hall *et al.* 2003).

The reverse reaction of PCK benefits from the positive charge in this region by helping stabilize the unstable carbanion form of pyruvate, so it can nucleophilicly attack CO_2 to form oxaloacetate. This reaction mechanism will be further discussed in section 4.8.

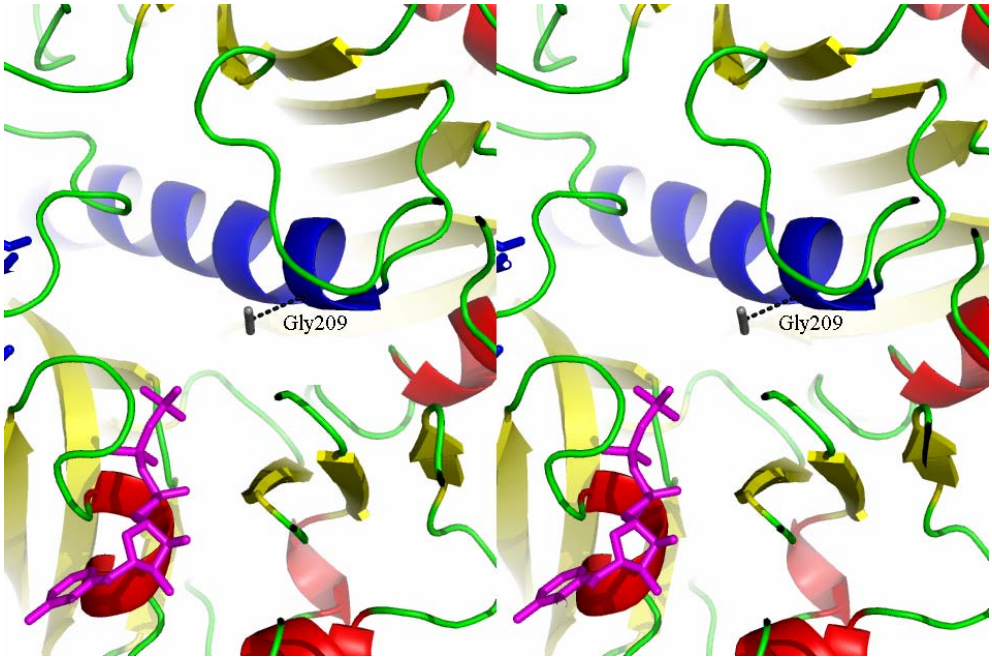

Figure 4.15. Stereogram of the PCK2 crystal structure from section 3.4 demonstrating the region around the α-helix made up by residues 209-227, shown in blue. The location of CO_2, in grey, is observed to be approximately 4 Angstroms from Gly209, which is roughly where the positive charge from the α-helix dipole is believed to be. The dashed line is between the carbon atom of CO_2 and the α-carbon of Gly209. ATP, in purple, is shown for reference. Stereo image made with use of Pymol (DeLano 2002).

4.8 Proposed Reaction Mechanism for Oxaloacetate Formation

Based on previously determined crystal structures and the work presented here, a mechanism for the conversion of PEP into oxaloacetate is proposed, Figure 4.16. When the PEP and ADP bind in the active site of PCK, the β-phosphate of ADP is close to the phosphate group of PEP. Then the lone pair of

electrons from one of the β-oxygens of ADP nucleophilicly attack the phosphorus atom of PEP forming a transition state pentacoordinated phosphorus atom.

The lone pair of electrons from one of the oxygens atoms equatorially bound to the transition state phosphorus atom can migrate to its phosphorus-oxygen bond to form a double bond. The electrons from the phosphorus-oxygen bond that bridges the two molecules migrate from the phosphate group of PEP to form the enolate form of pyruvate and ATP. One of the resonant forms of pyruvate contains a carbanion carbon at C3. The lone pair of electrons from the carbanion can attack the nearby bound carbon dioxide. The newly formed oxaloacetate and ADP then dissociate from the enzyme.

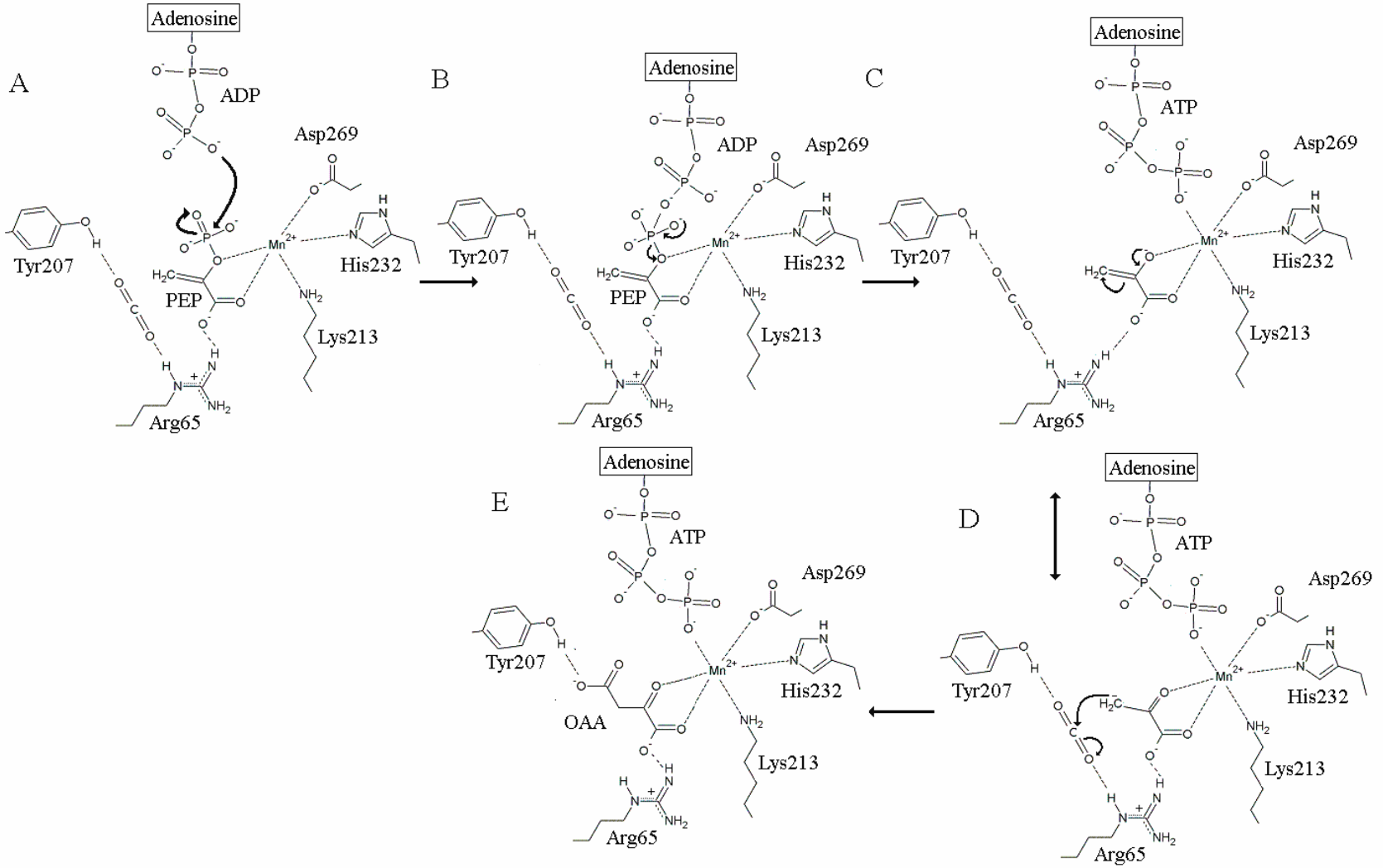

Figure 4.16. Proposed mechanism for the conversion of PEP, ADP and carbon dioxide to oxaloacetate and ATP. A. Lone pair electrons from β-phosphate oxygen of ADP attack phosphate from PEP in S_N2-like manner forming a high energy complex. B. The phosphate transfer is completed. C. The enolate of pyruvate forms. D. The carbanion from the resonant keto form of pyruvate combines with nearby carbon dioxide by nucleophillic addition. E. The newly formed ATP and oxaloacetate can dissociate from the enzyme.

4.8.1 Comparison to Other Carboxylases

There is relatively little knowledge regarding carboxylases that directly affix CO_2 to substrates (O'Leary 1992). At least four CO_2–containing protein crystal structures have been reported in literature. Of these PCK and PFOR are thought to catalyze a carboxylation and decarboxylation reaction. The other two, UR and DOACS appear to function only as decarboxylases (Lee *et al.* 2001; Phillips *et al.* 2003; Chabrière *et al.* 2001). The common feature found in all of the CO_2 binding sites is a basic residue hydrogen bonding with CO_2. The role the basic residue has in decarboxylation appears to be in destabilizing the leaving carboxylate group. It is not certain however if the basic residue has a function in carboxylation reactions, though a hydrogen bond between a basic amino acid side chain and CO_2 may be polarizing CO_2 to make it more susceptible to a nucleophilic attack. To understand better how an enzyme can directly use CO_2, more structural elements important for carboxylation reactions will need be discovered. However, a literature search finds that there still has been very little research done on carboxylases that use CO_2 directly. However, in the last decade two other carboxylating enzymes believed to employ a similar reaction mechanism as PCK have been examined.

Acetone carboxylase catalyses the conversion of acetone and CO_2 to form acetoacetate [6] (Sluis and Ensign 1997).

$$\text{ATP} + \text{acetone} + CO_2 \longrightarrow \text{acetoacetate} + \text{AMP} + 2\ P_i \qquad [6]$$

Although it has not been extensively researched, a study on acetone decarboxylase from *Xanthobacter autotrophicus* has determined some useful

kinetic information. It is a 360 kDa hexamer made up of three different types of subunits. The K_ms for ATP, CO_2 and acetone are 0.12 mM, 4.17 mM and 7.80 μM respectively; V_{max} is 0.49 U / mg (Sluis and Ensign 1997). The K_ms for CO_2 and ATP are lower than what is observed for the substrates involved in the reverse reaction of *A. succiniciproducens* PCK, but V_{max} for acetone decarboxylase is over a hundred times lower compared to that of *A. succiniciproducens* PCK (Laivenieks *et al.* 1997). Although Mn^{2+} is essential for the carboxylation reaction, when Mn^{2+} is not present in the assay, acetone decarboxylase is still able catalyze the breakdown of ATP, especially in the presence of acetone.

Acetone is probably interacting with Mn^{2+} in the active site in a manner that encourages deprotonation of one of its methyl groups. To initiate carbanion formation the acetone-Mn^{2+} complex is also likely required to be phosphorylated by ATP. By forming a phosphorylated acetone-Mn^{2+} complex, the pK_a of the methyl group hydrogens may be lowered significantly to allow for deprotonation under biological conditions. Thus, the lowered pK_a increases the rate of carbanion formation; once formed, the carbanion will nucleophilicly attack CO_2 to form acetoacetate. No crystal structure of acetone decarboxylase has been published, but preliminary crystallization conditions have been reported (Nocek *et al.* 2004).

Phenol carboxylase from *Pseudomonas* strain K 172 is another enzyme known to directly affix CO_2 to a substrate. The reaction phenol carboxylase catalyzes, affixes CO_2 to phenylphosphate to form 4-hydroxybenzoate [7] (Lack and Fuchs 1992).

$$\text{phenylphosphate} + CO_2 \longrightarrow \text{4-hydroxybenzoate} + P_i \qquad [7]$$

A study characterizing phenyl carboxylase, determined its molecular mass to be 280 kDa. The K_ms for CO_2 and phenylphosphate are 1.5 mM and 0.2 mM respectively. Compared to *A. succiniciproducens* PCK and acetone decarboxylase, the K_m for CO_2 in phenol carboxylase is quite low; however its V_{max} is the lowest of the three at 0.012 U / mg. Like PCK and acetone decarboxylase, phenol carboxylase requires Mn^{2+} for activity.

The proposed reaction mechanism for the conversion of phenylphosphate to 4-hydroxybenzoate occurs as follows. By an unknown interaction with Mn^{2+} the pK_a of the C1 hydrogen of phenylphosphate is lowered. After the proton from the C1 of phenylphosphate dissociates, the carbanion that forms will nucleophilicly attack a nearby CO_2 to form 4-hydroxybenzoate (Lack and Fuchs 1992).

Unfortunately, not much is known about acetone carboxylase and phenylphosphate carboxylase structurally. It has not been established if there are binding sites for CO_2 on these enzymes. Nor is it known if these enzymes have any of their key active site residues determined. Like PCK, the presumed reaction mechanisms all use phosphorylation and the coordination of Mn^{2+} to encourage carbanion formation. It would be very interesting to see what structural aspects the two enzymes employ to enhance the carboxylation reaction and compare them to PCK.

Chapter 5. Conclusions and Proposed Future Work

With all the crystal structures presented here, significant new unique findings have added to the knowledge and understanding of ATP-dependent PCK. Some original assumptions concerning PCK structurally and functionally have been confirmed and new phenomena have been determined. By using the findings from the crystal structures presented in this thesis, a reaction mechanism for the reverse reaction (CO_2-fixing direction) has been proposed.

5.1. Lid Made by Residues 385-405

The findings from the two *A. succiniciproducens* PCK crystal structures have demonstrated the catalytic importance of a mobile surface loop. A simple visual inspection of the structures shows the importance of isolating the substrates from the bulk solvent to ensure proper reaction conditions. The lid is also implicated in domain closure of PCK, but at present, it is not clear if the lid induces the domain movement or has a role to assist in keeping the domains together once PCK is in the closed confirmation.

The double deletion mutant that shortened the lid of *A. succiniciproducens* PCK, Δ2x2, completely abolishes activity demonstrating that the lid is important and possibly essential for activity. The conservation of the lid sequence amongst ATP-dependent and GTP-dependent PCKs furthers demonstrates

its importance. Though there is evidence that Δ2x2 is folding correctly and the lack of activity is due to the shortened lid, more studies need to be performed on the mutant to ensure that it is in fact folded correctly. Circular dichroism could be used to compare the relative amounts of secondary structure between Δ2x2 and wild type PCK. Another way to determine if Δ2x2 is folding correctly is by raising an antibody specific for wild type *A. succiniciproducens* PCK and determining if it can cross react with the mutant. Ruling out misfolding, will reaffirm the importance of the lid. Another experiment that could ultimately confirm the complete inactivation of PCK involves transforming the Δ2x2 gene into a PCK-deficient strain of *E. coli* that cannot grow on gluconeogenic substances. If there is a minor amount of activity in Δ2x2 that was not detectible by assay, the transformed strain should be able to survive on gluconeogenic media. An experiment of this type is likely possible as *E. coli* has successfully been transformed with PCK and phosphoenolpyruvate carboxylase from *A. succinogenes* for experimental purposes (Kim *et al.* 2003).

5.2. CO_2 Binding to PCK

Determining the CO_2 binding site in PCK is a very important finding. Much of the interest in PCK revolves around the carboxylation/decarboxylation step of catalysis. For industrial production of succinate through fermentation, there is interest in increasing the carboxylation rate of PCK, as it is believed to be one of the rate-limiting steps in succinate formation. By determining the location of CO_2 in PCK, a plausible reaction mechanism for the carboxylation step can be proposed.

One of the steps in the reaction involves the carbanion form of pyruvate. If this step is rate limiting, a mutant of PCK that is modified in the region around the CO_2 binding site may enhance the reaction rate. A mutant of this sort may be able to enhance catalysis through carbanion stabilization. Adding nearby positive charges to encourage the formation and stabilization of the carbanion may be one approach. Another way to increase the rate of carboxylation in PCK is to make CO_2 more reactive. One approach to increasing the rate of carboxylation in PCK may be by increasing the electrophilicity of the CO_2 carbon atom. It may be possible to achieve this by strengthening the hydrogen bond between CO_2 and PCK, which would further polarize CO_2, and make it more susceptible to nucleophilic attack. Arg65 probably could not be altered because of the additional interactions it forms with oxaloacetate. Tyr207 is then the only residue that could be mutated. Perhaps replacing Tyr207 with and arginine or lysine residue could alter CO_2 binding favourably. Another approach could be to introduce a non-standard or synthetic amino acid at position 207. A tyrosine analogue that is able to form a stronger hydrogen bond with CO_2 may be a suitable replacement.

5.3. Oxaloacetate, Lid and Non-Catalytic Second Binding Site

The proposed mechanical role for the lid and second binding site of oxaloacetate in PCK is unique. In order to determine if the second binding site of oxaloacetate is biologically relevant, a mutational study altering residues Leu249 and Ser250 would need to be performed. An investigation into the role of Lys390 with regards to the mechanical function of the lid would also be required. If

mutating Lys390 to an amino acid that is lacking a large side chain has a negative effect on the rate of catalysis, this would add evidence to the proposed role of the lid. If the proposed role were correct, then appropriate mutants of Leu249 and Ser250 would result in an increase in K_m for oxaloacetate. If the abovementioned mutations negatively affect the function of the second non-catalytic oxaloacetate binding site and the mechanical role of the lid, it may be possible this mutant would be useful for the succinate industry. By impeding the forward reaction of PCK, the products of the reverse reaction are more likely to continue to be metabolized, to eventually form succinate.

5.4. K213S PCK Mutant

The observed inhibition Mn^{2+} has on K213S is unusual and was not predicted. The crystal structure of K213S complexed with Mn^{2+} appears to offer an explanation for the inhibition. The coordination geometry of Mn^{2+} is tetrahedral in K213S which alters the way oxaloacetate binds, which in turn reduces its reactivity.

References

Aich, S., F. Imabayashi and L. T. J. Delbaere (2003). "Expression, Purification, and Characterization of a Bacterial GTP-Dependent PEP Carboxykinase." Protein Expression and Purification **31**: 298-304.

Aich, S, L. T. J. Delbaere (2007). "Phylogenetic Study of the Evolution of PEP Carboxykinase" Evolutionary Bioinformatics. In Press.

Altschul, S. F., W. Gish, W. Miller, E. W. Myers and D. J. Lipman (1990). "Basic Local Alignment Search Tool." Journal of Molecular Biology **215**: 403-410.

Altschul, S. F., T. L. Madden, A. A. Schäffer, J. Zhang, Z. Zhang, W. Miller and D. J. Lipman (1997). "Gapped BLAST and PSI-BLAST: A New Generation of Protein Database Search Programs." Nucleic Acids Research **25**: 3389-3402.

Arinze, I. J., A. J. Garber and R. W. Hanson (1973). "The Regulation of Gluconeogensis in Mamalian Liver. The Role of Mitochondrial Phosphoenolpyruvate Carboxykinase." Journal of Biological Chemistry **248**: 2266-2274.

Arnelle, D. R. and M. H. O'Leary (1992). "Binding of Carbon Dioxide to Phosphoenolpyruvate Carboxykinase Deduced from Carbon Kinetic Isotope Effects?" Biochemistry **31**: 4363-4368.

Auerbach, G., A. Herrmann, M. Gütlich, M. Fischer, U. Jacob, A. Bacher and R. Huber (1997). "The 1.25 Å Crystal Structure of Sepiapterin Reductase Reveals its Binding Mode to Pterins and Brain Neurotransmitters." The EMBO Journal **16**: 7219-7230.

Bazaes, S., M. Toncio, M. Laivenieks, J. G. Zeikus and E. Cardemil (2007). "Comparative Kinetic Effects of Mn(II), Mg(II) and the ATP/ADP Ratio on Phosphoenolpyruvate Carboxykinase from *Anaerobiospirillum succiniciproducens and saccharomyces cerevisiae*." The Protein Journal. **26**: 265-9

Berman, H. M., J. Westbrook, Z. Feng, G. Gillilang, T. N. Bhat, H. Weissig, I. N. Shidyalov and P. E. E. Bourne (2000). "The Protein Data Bank." Nucleic Acids Research **28**: 235-242.

Birdsall, D. L., J. Finer-Moore and R. M. Stroud (1996). "Entropy in Bi-Substrate Enzymes: Proposed Role of an Alternate Site in Chaperoning Substrate into, and Products out of, Thymidylate Synthase." Journal of Molecular Biology **255**: 522-535.

Black, G. W., G. P. Hazlewood, S. J. Millward-Sadler, J. I. Laurie and H. J. Gilbert (1995). "A Modular Xylanase Containing a Novel Non-Catalytic Xylan-Specific Binding Domain." Biochemical Journal **307**: 191-195.

Brünger, A. T., P. D. Adams, G. M. Clore, W. L. Delano, P. Gros, R. W. Grosse-Kunstleve, J.-S. Jiang, J. Kuszewski, N. Nilges, N. S. Pannu, R. J. Read, L. M. Rice, T. Simonson and G. L. Warren (1998). "CRYSTALLOGRAPHY NMR SYSTEM (CNS): A New Software System For Macromolecular Structure Determination." Acta Crystallographica D **54**: 905-921.

Canadian Broadcasting Corporation (2004). "Ontario to Require 5% Ethanol in Gas by 2007." www.cbc.ca\canada\story\2004\11126\ethanol-gas-ontario-041126.html.

Canadian Broadcasting Corporation (2007). "Ethanol A Clean Cocktail for Your Car?" www.cbc.ca/news/background/energy/ethanol.html.

Cannata, J. J. B. and A. O. M. Stoppani (1963). "Phosphopyruvate Carboxylase from Bakers' Yeast." Journal of Biological Chemistry **238**: 1919-1927.

CCP4 (1994). "The CCP4 Suite: Programs for Protein Crystallography." Acta Crystallographica D **50**: 760-763.
Chabrière, E., X. Vernede, B. Guigliarelli, M. Charon, C. Hatchikian and J. Fontecilla-Camps (2001). "Crystal Structure of the Free Radical Intermediate of Pyruvate:Ferredoxin Oxidoreductase." Science **294**: 2559-2563.
Cheek, S., K. Ginalski, H. Zhang and N. V. Grishin (2005). "A Comprehensive Update of the Sequence and Structure Classification of Kinases." BMC Structural Biology **5**.
Cheek, S., H. Zhang and N. V. Grishin (2002). "Sequence and Classification of Kinases." Journal of Molecular Biology **320**: 855-881.
Chen, Z., R. P. Walker, R. M. Acheson and R. C. Leegood (2002). "Phosphoenolpyruvate Carboxykinase Assayed at Physiological Concentrations of Metal Ions Has a High Affinity for CO_2." Plant Physiology **128**: 160-164.
Cheng, K.-C. and T. Nowak (1989). "Arginine Residues at the Active Site of Avian Liver Phosphoenolpyruvate Carboxykinase." Journal of Biological Chemistry **264**: 3317-3324.
Cherukuvada, S. L., A. S. N. Seshasayee, K. Raghunathan, S. Anishetty and G. Pennathur (2005). "Evidence of a Double-Lid Movement in *Pseudomonas aeruginosa* Lipase: Insights from Molecular Dynamics Simulations." PLoS Computational Biology **1**: 182-189.
Cooper, T. G., T. T. Tchen, H. G. Wood and C. R. Benedict (1968). "The Carboxylation of Phosphoenolpyruvate and Pyruvate." Journal of Biological Chemistry **243**: 3857-3863.
Copeland, D. M., A. H. West and G. B. Richter-Addo (2003). "Crystal Structures of Ferrous Horse Heart Myoglobin Complexed With Nitric Oxide and Nitrosoethane." PROTEINS: Structure, Function, and Genetics **53**: 182-192.
Cotelesage, J. H., L. Prasad, J. G. Zeikus, M. Laivenieks and L. T. J. Delbaere (2005). "Crystal Structure of *Anaerobiospirillum succiniciproducens* PEP Carboxykinase Reveals an Important Active Site Loop." International Journal of Biochemistry & Cell Biology **37**: 1829-1837.
Cotelesage, J. J. H., J. Puttick, H. Goldie, B. Rajabi, B. A. A. Novakoski and L. T. J. Delbaere (2007). "How Does an Enzyme Recognize CO_2?" International Journal of Biochemistry & Cell Biology.
Cotton, F. A. and G. Wilkinson (1980). "Advaced Inorganic Chemistry *A Comprehensive Text*." 4th Edition. John Wiley and Sons, New York.
DeLano, W. L. (2002). "The PyMOL Molecular Graphics System." DeLano Scientific. www.delanoscientific.com
Delbaere, L.-T.-J., A.-M. Sudom, L. Prasad, Y. Leduc and H. Goldie (2004). "Structure/Function Studies of Phosphoryl Transfer by Phosphoenolpyruvate Carboxykinase." Biochimica et Biophysica Acta-Protiens and Proteonomics.**1697**:271-278.
Dunten, P., C. Belunis, R. Crowther, K. Hollfelder, U. Kammlott, W. Levin, H. Michel, G. Ramsey, A. Swain, D. Weber and S. Wertheimer (2002). "Crystal Structure of Human Cytosolic Phosphoenolpyruvate Carboxykinase Reveals a New GTP-binding Site." Journal of Molecular Biology **216**: 257-264.
Emsley, P. and K. Cowtan (2004). "COOT: Model-Building Tools for Molecular Graphics." Acta Crystallographica D **60**: 2126-2132.
Encinas, M. V., M. C. Rojas, H. Goldie and E. Cardemil (1993). "Comparative Steady-State Fuorescence Studies of Cytosolic Rat Liver (GTP), *Saccharomyces*

cerevisiae (ATP) and *Escherichia coli* (ATP) Phosphoenolpyruvate Carboxykinases." Biochimica et Biophysica Acta **1162**: 195-202.

Ferreira, L. M. A., T. M. Wood, G. Williamson, C. Faulds, G. P. Hazlewood, G. W. Black and H. J. Gilbert (1993). "A Modular Esterase from *Pseudomonas fluorescens* subsp. *cellulosa* Contains a Non-Catalytic Cellulose-Binding Domain." Biochemical Journal **294**: 349-355.

Friedlander, T. P., J. C. Regier, C. Mitter and D. L. Wagner (1996). "A Nuclear Gene for Higher Level Phylogenetics: Phosphoenolpyruvate Carboxykinase Tracks Mesozoic-Age Divergences Within Lepidoptera (Insecta)." Molecular Biology and Evolution **13**: 591-604.

Galinier, A., J. Lavergne, C. Geourjon, S. Fieulaine, S. Nessler and J. Jault (2002). "A New Family of Phosphotransferases with a P-loop Motif." The Journal of Biological Chemistry **277**: 11362-11367.

Giegé, R., J. Drenth, A. Ducruix, A. MaPherson and W. Saenger (1995). "Crystallogenesis of Biological Macromolecules. Biological, Microgravity, and other Physico-Chemical Aspects." Progress in Crystal Growth and Characterization **30**: 237-281.

Goldie, H. (1984). "Genetic and Physiological Characterization of *Escherichia coli* Phosphoenolpyruvate Carboxykinase Locus: Studies with *pck-lacZ* fusions." Journal of Bacteriology **159**: 832-836.

Goldie, H. and B. D. Sanwal (1980a). "Allosteric Control by Calcium and Mechanism of Desensitization of Phosphoenolpyruvate Carboxykinase of *Escherichia coli*." Journal of Biological Chemistry **255**: 1399-1405.

Goldie, H. and B. D. Sanwal (1980b). "Genetic and Physiological Characterization of *Escherichia coli* Mutants Deficient in Phosphoenolpyruvate Carboxykinase Activity." Journal of Bacteriology **141**: 1115-1121.

Guerra-Giraldez, C., L. Quijada and C. E. Clayton (2002). "Compartmentation of Enzymes in a Microbody, the Glycosome, is Essential in *Trypanosoma brucei*." Journal of Cell Science **115**: 2651-2658.

Guettler, M. V., D. Rumler and M. K. Jain (1999). "*Actinobacillus succinogenes* sp. nov., a Novel Succinic-Acid-Producing Strain from the Bovine Rumen." International Journal of Systematic Bacteriology **49**: 207-216.

Guex, N. and M. C. Peitsch (1997). "SWISS-MODEL and the Swiss-PdbViewer: An Environment for Comparative Protein Modeling." Electrophoresis(18): 2714-2723.

Hall, P. R., R. Zheng, L. Antony, M. Pusztai-Carey, P. R. Carey and V. C. Yee (2004). "Transcarboxylase 5S Structures: Assembly and Catalytic Mechanism of a Multienzyme Complex Subunit." The EMBO Journal **23**: 3621-3631.

Hansen, E. J. and Y. M. Patel (1994). "Phosphoenolpyruvate Carboxykinase (GTP): the Gene and the Enzyme." Advances in Enzymololgy and Related Areas of Molecular Biology **69**: 203-281.

Hayward, S. (2004). "Identification of Specific Interactions that Drive Ligand-induced Closure in Five Enzymes with Classic Domain Movements." Journal of Molecular Biology **339**: 1001-1021.

Hayward, S. and R. Lee (2002). "Improvements in the Analysis of Domain Motions in Proteins from Conformational Change: DynDom version 1.50." Journal of Molecular Graphics and Modeling **21**: 181-183.

Holm, L. and C. Sander (1994). "Searching Protein Structure Databases has Come of Age." Proteins **19**: 165-173.

Holyoak, T., S. M. Sullivan and T. Nowak (2006). "Structural Insights into the Mechanism of PEPCK Catalysis." Biochemistry **45**: 8254-8263.

Hou, S., Y. Chao and J. Liao (1995). "A Mutant Phosphoenolpyruvate Carboxykinase in *Escherichiacoli* Conferring Oxaloacetate Decarboxylase Activity." Journal of Bacteriology **177**: 1620-1623.

Huang, L.-s., G. Sun, D. Cobessi, A. C. Wang, J. T. Shen, E. Y. Tung, V. E. Anderson and E. A. Berry (2005). "3-Nitropropionic Acid Is a Suicide Inhibitor of Mitochondrial Respiration That, Upon Oxidation by Complex II, Forms a Covalent Adduct with a Catalytic Base Arginine in the Active Site of the Enzyme." Journal of Biological Chemistry **281**: 5965-5972.

Jabalquinto, A. M., M. Laivenieks, M. Cabezas, J. G. Zeikus and E. Cardemil (2002a). "The Effect of Active Site Mutations in the Oxaloacetate Decarboxylase and Pyruvate Kinase-like Activities of *Anaerobiospirillum succiniciproducens* Phosphoenolpyruvate Carboxykinase." Journal of Protein Chemistry **21**: 443-445.

Jabalquinto, A. M., M. Laivenieks, N. F. D. Gonzalez, A. Yevenes, M. V. Encinas, J. G. Zeikus and E. Cardemil (2002b). "Evaluation by Site-Directed Mutagenesis of Active Site Amino Acid Residues of *Anaerobiospirillum succiniciproducens* Phosphoenolpyruvate Carboxykinase." Journal of Protein Chemistry **21**: 393-400.

Jabalquinto, A. M., M. Laivenieks, J. G. Zeikus and E. Cardemil (1999). "Characterization of the Oxaloacetate Decarboxylase and Pyruvate Kinase-Like Activities of *Saccharomyces cerevisiae* and *Anaerobiospirillum succiniciproducens* Phosphoenolpyruvate Carboxykinases." Journal of Protein Chemistry **18**: 659-664.

Jennens, M. L. and M. E. Lowe (1994). "A Surface Loop Covering the Active Site of Human Pancreatic Lipase Influences Interfacial Activiation and Lipid Binding." Journal of Biological Chemistry **269**: 25470-25474.

Jones, T. A., J. Y. Zou and S. W. Cowan (1991). "Improved Methods for Building Protein Models in Electron Density Maps and the Location of Errors in these Models." Acta Crystallographica A **47**: 110-119.

Kabsch, W. (1993). "Automatic Processing of Rotation Diffraction Data from Crystals of Initially Unknown Symmetry and Cell Constants." Journal of Applied Crystallography **26**: 795-800.

Karpusas, M., B. Branchaud and S. J. Remington (1990). "Proposed Mechanism for the Condensation Reaction of Citrate Synthase: 1.9-Å Strcutre of the Ternary Complex with Oxaloacetate and Carboxymethyl Coenzyme A." Biochemistry **29**: 2213-2219.

Kim, P., M. Laivenieks, C. Vieille and J. G. Zeikus (2003). "Effect of Overexpression of *Actinobacillus succinogenes* Phosphoenolpyruvate Carboxykinase on Succinate Production in *Escherichia coli*." Applied and Environmental Microbiology **70**: 1238-1241.

Kim, S.-Y., K. Y. Hwang, S.-H. Kim, H.-C. Sung, Y. S. Han and Y. Cho (1999). "Structural Basis for Cold Adaptation Sequence, Biochemical Properties, and Crystal Structure of Malate Dehydrogenase From a Psychrophile *AquaspirillIum Arcticum*." Journal of Biological Chemistry **274**: 11761-11767.

Krebs, A. and W. A. Bridger (1980). "The Kinetic Properties of Phosphoenolpyruvate Carboxykinase of *Escherichia coli*." The Canadian Journal of Biochemistry **58**: 309-318.

Krebs, H. A. (1942). "The Effect of Inorganic Salts on the Ketone Decomposition of Oxaloacetic Acid." Biochemical Journal **36**: 303-305.

Lack, A. and G. Fuchs (1992). "Carboxylation of Phenylphosphate by Phenol Carboxylase, an Enzyme System of Anaerobic Phenol Metabolism." Journal of Bacteriology **174**: 3629-3636.

Laivenieks, M., C. Vielle and J. G. Zeikus (1997). "Cloning, Sequencing, and Overexpression of the *Anaerobisopirillum succiniciproducens* Phosphoenolpyruvate Carboxykinase (pckA) Gene." Applied and Environmental Microbiology **63**: 2273-2280.

Leduc, Y. A., L. Prasad, M. Laivenieks, J. G. Zeikus and L. T. J. Delbaere (2005). "Structure of PEP Carboxykinase from Succinate-Producing *Actinobacillus succiniogenes*: A New Conserved Active-Site Motif." Acta Crystallographica D **62**: 903-912.

Lee, H. J., M. D. Lloyd, K. Harlos, I. J. Clifton, J. E. Baldwin and C. J. Schofiled (2001). "Kinetic and Crystallographic Studies on Deacetoxycephalosporin C Synthase (DAOCS)." Journal of Molecular Biology **308**: 937.

Lee, S. J., H. Song and S. Y. Lee (2006). "Genome-Based Metabolic Engineering of *Mannheimia succiniciproducens* for Succinic Acid Production." Applied and Environmental Microbiology **72**: 1939-1948.

Leslie, A. G. W. (1992). "Recent Changes to the MOSFLM Package for Processing Film and Image Plate Data." Joint CCP4 + ESF-EAMCB Newsletter on Protein Crystallography. **26**.

Liao, J. C., Y. Chao and R. Patnaik (1994). "Alteration of the Biochemical Valves in the Central Metabolism of *Escherichia coli*." Annals New York Academy of Sciences. 21-34.

Loris, R., U. Langhorst, S. De Vos, K. Decanniere, J. Bouckaert, D. Maes, T. R. Transue and J. Steyaert (1999). "Conserved Water Molecules in a Large Family of Microbial Ribonucleases." PROTEINS: Structure, Function, and Genetics **36**:117-134.

Loris, R., P. P. G. Stas and L. Wyns (1994). "The Importance of Bound Water for the Sequence-Structure Relationship Within the Legume Lectin Family." Journal of Biological Chemistry **269**: 26722-26733.

Matte, A. (1996). Crystallographic Studies of *Escherichia coli* Phosphoenolpyruvate Carboxykinase. Biochemistry. Saskatoon, University of Saskatchewan. **Ph.D. Thesis**.

Matte, A., H. Goldie, R. M. Sweet and L. T. J. Delbaere (1996). "Crystal Structure of *Escherichia coli* Phosphoenolpyruvate Carboxykinase: A New Structural Family with the P-loop Nucleoside Triphosphate Hydrolase Fold." Journal of Molecular Biology **256**: 126-143.

Matte, A., L. W. Tari and L. T. J. Delbaere (1998). "How do Kinases Transfer Phosphoryl Groups?" Structure **6**:413-419.

Matte, A., L. W. Tari, H. Goldie and L. T. J. Delbaere (1997). "Structure and Mechanism of Phosphoenolpyruvate Carboxykinase." Journal of Biological Chemistry **272**: 8105-8108.

Mattos, C. and D. Ringe (2001). "Solvent Structure." International Tables of Crystallography Volume F: 807.
Mc Kinlay, J. B., J. G. Zeikus and C. Vieille (2005). "Insights into *Actinobacillus succinogenes* Fermentative Metabolism in a Chemically Defined Growth Medium." Applied and Environmental Microbiology **71**: 6651-6656.
McMurry, J. (1992). "Organic Chemistry." 3rd Edition, Brooks/Cole, New York.
Murshudov, G., A. Vagin and E. Dodson (1997). "Refinement of Macromolecular Structures by the Maximum-Likelihood Method." Acta Crystallographica D **53**: 240-255.
Navaza, J. (1994). "AMoRe: an Automated Package for Molecular Replacement." Acta Cryst. A **50**: 157-163.
Nocek, B., J. Boyd, S. A. Ensign and J. W. Peters (2004). "Crystallization and Preliminary X-ray Analysis of an Acetone Carboxylase from *Xanthobacter autotrophicus* strain Py2." Acta Crystallographica Section D-Biological Chemistry **60**: 385-387.
Novakovski, A. A. (2001). Mutations Which Alter Substrate and Metal Ion Kinetics of *Escherichia coli* Phosphoenolpyruvate Carboxykinase. Microbiology. Saskatoon, University of Saskatchewan. **Masters Thesis**.
O'Leary, M. H. (1992). "Catalytic Strategies in Enzymatic Carboxylation and Decarboxylation." The Enzymes **20**: 235-266.
Oberholzer, A. E., P. Schneider, C. Bachler, U. Baumann and B. Erni (2006). "Crystal Structure of the Nucleotide-Binding Subunit DHAL of the *Escherichia coli* Dihydroxyacetone Kinase." Journal of Molecular Biology **359**: 539-.
Otwinowski, Z. and V. Minor (1996). "Processing of X-ray Diffraction Data Collected in Oscillation Mode." Methods in Enzymology **276**: 307-326.
Pécoul, B. (2004). "New Drugs for Neglected Disease: From Pipeline to Patients." PLoS Medicine **1**: 19-22.
Perry, K. M., C. W. Carreras, L. C. Chang, D. V. Santi and R. M. Stroud (1999). "Structures of Thymidylate Synthase with a C-terminal Deletion: Role of the C-terminus in Alignment of 2'-Deoxyuridine 5'-Monophosphate and 5,10-Methylenetetrahydrofolate." Biochemistry **32**: 7116-7125.
Perutz, M. F. (1946). "Th Composition and Swelling Properties of Haemoglobin Crystals." Transactions of the Faraday Society **42B**: 187.
Phillips, J. D., F. G. Whitby, J. P. Kushner and C. P. Hill (2003). "Structural Basis for Tetrapyrrole Coordination by Uroporphyrinogen Decarboxylase." The EMBO Journal **23**: 6225-6233.
Podkovyrov, S. M. and J. G. Zeikus (1993). "Purification and Characterization of Phosphoenolpyruvate Carboxykinase, a Catabolic Carbon Dioxide Fixing Enzyme, from *Anaerobiospirillum succiniciproducens*." Journal of General Microbiology **139**: 223-228.
Rohrer, S. P., H. J. Saz and T. Nowak (1986). "Purification and Characterization of Phosphoenolpyruvate Carboxykinase from the Parasitic Helminth *Ascaris suum*." Journal of Biological Chemistry **261**: 13049-13055.
Rose, G. D., L. M. Gierasch and J. A. Smith (1985). "Turns in Peptides and Proteins." Advances in Protein Chemistry **37**: 1-109.
Saenger, W. (1984). Principles of Nucleic Acid Structure, Springer-Verlag.
Samuelov, N. S., R. Lamed, S. Lowe and J. G. Zeikus (1991). "Influence of Carbon Dioxide Bicarbonate Levels and pH On Growth Succinate Production and

Enzyme Activities of *Anaerobiospirillum succiniciproducens*." Applied and Environmental Microbiology **57**: 3013-3019.
Sauer, O., A. Schmidt and C. Kratky (1997). "Freeze-Trapping Isomorphous Xenon Derivatives of Protein Crystals." Journal of Applied Crystallography **30**: 476-486.
Schulz, G. E., E. Schiltz, A. G. Tomasselli, R. Frank, M. Brune and A. Wittinghofer (1986). "Structural Relationships in the Adenylate Kinase Family." European Journal of Biochemistry **161**: 127-132.
Sjögren, T. and J. Hajdi (2001). "Structure of the Bound Dioxygen Species in the Cytochrome Oxidase Reactionof Cytochrome cd_1 Nitrate Reductase." Journal of Biological Chemistry **276**: 13072-13076.
Sluis, M. K. and S. A. Ensign (1997). "Purification and Characterization of Acetone Carboxylase from *Xanthobacter* strain Py2." Proceedings of the National Academy of Sciences **94**: 8456-8461.
Sommer, J. M., T. T. Nguyen and C. C. Wang (1994). "Phosphoenolpyruvate Carboxykinase of *Trypanosoma brucei* is Targeted to the Glycosomes by a C-Terminal Sequence." Biochemistry **350**: 125-129.
Song, H. and Y. L. Lee (2006). "Production of Succinic Acid by Bacterial Fermentation." Enzyme and Microbial Technology **39**: 352-361.
Sudom, A., R. Walters, L. Pastushok, D. Goldie, L. Prasad, L. T. J. Delbaere and H. Goldie (2003). "Mechanisms of Activation of Phosphoenolpyruvate Carboxykinase from *Escherichia coli* by Ca^{2+} and of Desensitization by Trypsin." Journal of Bacteriology **185**: 4233-4242.
Sudom, A. M., L. Prasad, H. Goldie and L. T. J. Delbaere (2001). "The Phosphoryl-Transfer Mechanism of *Escherichia coli* Phosphoenolpyruvate Carboxykinase from the use of AlF_3." Journal of Molecular Biology **314**: 83-92.
Tari, L. W., A. Matte, H. Goldie and L. T. J. Delbaere (1997). "Mg^{2+}-Mn^{2+} Clusters in Enzyme-Catalyzed Phosphoryl-Transfer Reactions." Nature Structural Biology **4**: 990-994.
Tari, L. W., A. Matte, U. Pugazhenthi, H. Goldie and L. T. J. Delbaere (1996). "Snapshot of an Enzyme Reaction Intermediate in the Structure of the ATP-Mg^{2+}-Oxalate Ternary Complex of *Escherichia coli* PEP Carboxykinase." Nature Structural Biology **3**: 355-363.
Trapani, S., J. Linss, S. Goldenberg, H. Fischer, A. F. Craievich and G. Oliva. (2001). "Crystal Structure of the Dimeric Phosphoenolpyruvate Carboxykinase (PEPCK) from *Trypanosoma cruzi* at 2 Å Resolution." Journal of Molecular Biology **313**: 1059-1072.
Traut, T. (1994). "The Functions and Consensus of Nine Types of Peptide Segments That Form Different Types of Nucleotide Binding Sites." European Journal of Biochemistry **222**: 9-19.
Urbina, J. A. and L. Avilan (1989). "The Kinetic Mechanism of Phosph*enol*pyruvate Carboxykinase from *Panicum maximum*." Phytochemistry **28**: 1349-1353.
Utter, M. F. and H. M. Kolenbrander (1972). "Formation of Oxaloacetate by CO_2 Fixation on Phosphoenolpyruvate." The Enzymes **6**: 117-168.
Utter, M. F. and K. Kurahashi (1953). "Mechanism of Action of Oxaloacetate Carboxylase from the Liver." Journal of American Chemical Society **75**: 758.
Walker, R. P., Z.-H. Chen, R. M. Acheson and R. C. Leegood (2002). "Effects of Phosphorylation on Phospho*enol*pyruvate Carboxykinase from the C4 Plant Guinea Grass." Plant Physiology **128**: 165-172.

Walker, R. P. and R. C. Leegood (1996). "Phosphorylation of Phosphoenolpyruvate Carboxykinase in Plants." Biochemistry Journal **317**: 653-658.

Wiese, T. J., D. O. Lambeth and P. D. Ray (1991). "The Intracellular Distribution and Activities of Phosphoenolpyruvate Carboxykinase Isozymes in Various Tissues of Several Mammals and Birds." Comparative Biochemistry and Physiology **100B**: 297-302.

Wilkinson, F. (1980). "Chemical Kinetics and Reaction Mechanisms." Van Nostrand Reinhold Co., New York.

Wingler, A., R. P. Walker, Z.-H. Chen and R. C. Leegood (1999). "Phosphoenolpyruvate Carboxykinase Is Involved in the Decarboxylation of Aspartate in the Bundle Sheath of Maize." Plant Physiology **120**: 539-545.

Yu, R. C., P. I. Hanson, R. Jahn and A. T. Brünger (1998). "Structure of the ATP-Dependent Oligomerization Domain of N-ethylmalemide Sensitive Factor Complexed with ATP." Nature Structural Biology **5**: 803-811.

Zeikus, J. G., M. K. Jain and P. Elankovan (1999). "Biotechnology of Succinic Acid Production and Markets for Derived Industrial Products." Applied Microbiology and Biotechnology **51**: 545-552.

Zhou, T., M. Daugherty, N. V. Grishin, A. L. Osterman and H. Zhang (2000). "Structure and Mechanism of Homoserine Kinase: Prototype for the GHMP Kinase Superfamily." Structure **8**: 1247-1257.